Energy Storage Requirement Modeling of Mobile Robots for Intralogistics

Zur Erlangung des akademischen Grades eines

DOKTORS DER INGENIEURWISSENSCHAFTEN
(Dr.-Ing.)

von der KIT-Fakultät für Maschinenbau des
Karlsruher Instituts für Technologie (KIT)

angenommene

DISSERTATION

von

M.Eng. Marvin Sperling
geb. in Celle

Tag der mündlichen Prüfung:	10.07.2025
Hauptreferent:	Prof. Dr.-Ing. Kai Furmans
Korreferent:	Prof. Dr.-Ing. Ludger Overmeyer

Man sollte alles so einfach wie möglich machen, aber nicht einfacher.
Albert Einstein

Kurzfassung

Intralogistische Prozesse werden in der Industrie vermehrt mit Hilfe von flexiblen, fahrerlosen Transportsystemen automatisiert. Um ihre Flexibilität hinsichtlich der freien Navigation und einem Minimum an fest installierter Peripherie zu wahren, werden fahrerlose Transportfahrzeuge (FTF) mit Energiespeichersystemen ausgestattet, die einen regelmäßigen Ladeprozess benötigen. Die Flotten werden vermehrt heterogen, welches systemunabhängige Untersuchungen in der Wissenschaft bedarf. Eine Literaturrecherche hat ergeben, dass Materialfluss und Layout einen signifikanten Einfluss auf den Energiebedarf eines FTF haben, welcher sich zugleich auf den Energiespeicherbedarf auswirkt. Weiterhin konnte weder ein Dimensionierungsverfahren für Energiespeichersysteme von FTF, noch ein ganzheitliches Modell identifiziert werden, mit dem der Leistungsbedarf, Energiebedarf, oder Energiespeicherbedarf von FTF im Betrieb bestimmt werden kann. In dieser Arbeit wird untersucht, welche Informationen Materialfluss- und Layoutdaten für energetische Betrachtungen von FTF aufweisen müssen (Forschungsfrage (RQ) 1) und wie der Leistungsbedarf von FTF unter Berücksichtigung von Systemspezifikationen und Materialfluss- und Layoutdaten modelliert werden kann (RQ 2). Weiterhin wird untersucht, wie der Energiespeicherbedarf für FTF unter Berücksichtigung von Fahrzeugspezifikationen, Materialfluss- und Layoutdaten, Ladeinfrastruktursystemverteilung und Ladestrategie ermittelt werden kann (RQ 3). Eine Einflussanalyse hat ergeben, dass die Beschreibung von Materialfluss- und Layoutdaten mit Matrizen ausreichende Informationen zur Untersuchung von Energiebedarfsbetrachtung von FTF beinhalten. Zur Beantwortung der ersten Forschungsfrage wurde weiterhin eine Taxonomie ausgearbeitet, um unterschiedliche Materialfluss- und Layoutdaten klassifizieren zu können, welche mit einem erstellten Datensatz, bestehend aus 72 unterschiedlichen

Materialfluss- und Layoutdaten exemplarisch angewandt wurde. Zur Modellierung des Leistungs- und Energiebedarfs hat die Literaturrecherche zustandsbasierte Ansätze aufgezeigt. Daraufhin wurde ein zustandsbasiertes Modell mit insgesamt zehn unterschiedlichen Zuständen entwickelt, welches mit realen Versuchen von über 368 Betriebsstunden an zwei verschiedenen industriell eingesetzten FTF validiert wurde. Es wurde gezeigt, dass das Modell den Leistungsbedarf von FTF zu ca. $99,0\,\%$ genau modellieren kann. Abschließend wurde ein Modell zur Ermittlung des Energiespeicherbedarfs entwickelt. Durch 1.940.400 Simulationsdurchläufe von FTF unter Verwendung des Energiebedarfsmodells aus der zweiten Forschungsfrage und der Variation der Materialfluss- und Layoutdaten und der Ladeinfrastruktursystemverteilung wurde das Modell validiert. Der Energiespeicherbedarf von FTF für den kapazitiven Betrieb kann im Mittel zu $92,5\,\%$ genau und für den Taktbetrieb im Mittel mit $96,1\,\%$ genau ermittelt werden. Zusammenfassend erlaubt die vorgelegte Arbeit der Wissenschaft und den Anwendern, den Leistungs-, Energie- und Energiespeicherbedarf von fahrerlosen Transportsystemen hinreichend genau zu ermitteln. Damit ist eine Grundlage geschaffen, Optimierungsverfahren bezüglich des Energiebedarfs zu untersuchen. Praktiker können mit Hilfe der beschriebenen Methoden effizientere Energiespeichersysteme entwickeln und dimensionieren.

Abstract

Flexible automated guided vehicles (AGVs) have increasingly automated industrial intralogistics processes. AGVs are equipped with energy storage systems (ESS) that require a periodic charging process to ensure their flexibility in terms of free navigation with a minimum of stationary peripherals. AGV fleets are increasingly heterogeneous, which requires independent scientific investigations. A literature review showed that material flow and layout significantly impact the energy requirement of an AGV while impacting energy storage requirement (ESR). Furthermore, neither a design method for ESSs of AGVs nor a holistic model was identified with which the power requirement, energy requirement, or ESR of AGVs could be determined during operation. Therefore, this thesis examined what information material flow and layout data should include for energy considerations of AGVs (research question (RQ) 1) and how the power requirement of AGVs can be modeled considering system specifications and material flow and layout data (RQ 2). Furthermore, it was investigated how the ESR for AGVs can be determined by considering vehicle specifications, material flow and layout data, charging infrastructure system distribution, and charging strategy (RQ 3). An impact analysis showed that the description of material flow and layout data with matrices provide sufficient information for investigating the energy requirement of AGVs. A taxonomy was also developed to answer the first research question, classifying different material flow and layout data, which was applied exemplarily with a created data set of 72 material flow and layout data. The literature review showed state-based approaches for modeling the power and energy requirement. Based on this knowledge, a state-based model was developed with ten different states, and validated with real experiments of over 368 operating hours on two different industrial AGVs. The model accurately modeled the power requirement

of AGVs at approximately $99.0\,\%$. Finally, a model was developed to determine the ESR. The model was validated by $1,940,400$ simulation runs of AGVs using the energy requirement model from the second research question and by varying the material flow and layout data and the charging infrastructure system distribution. The ESR of AGVs for capacitive operation was determined with an average accuracy of $92.5\,\%$ and an average accuracy of $96.1\,\%$ for opportunity charging. In summary, this thesis can allow scientists to determine the power, energy, and ESR of AGVs with sufficient accuracy, thereby creating a basis for investigating optimization procedures concerning energy requirement. Moreover, practitioners can use the methods to develop and design more efficient ESS.

Danksagung

Die vorliegende Arbeit ist während meiner Zeit als wissenschaftlicher Mitarbeiter am Institut für Fördertechnik und Logistiksysteme des Karlsruher Instituts für Technologie entstanden. Es war eine sehr spannende und lehrreiche Zeit, für dich ich mich nachfolgend bei allen Menschen bedanken möchte, die mich maßgeblich auf diesem Weg begleitet und unterstützt haben.

Prof. Dr.-Ing. Kai Furmans danke ich für die Übernahme des Hauptreferats, für das entgegengebrachte Vertrauen und für die Möglichkeit, mich in der Forschung frei entfalten zu dürfen. Prof. Dr.-Ing. Ludger Overmeyer danke ich für die Übernahme des Korreferats.

Dr.-Ing. Maximilian Hochstein danke ich für sein Vertrauen und seine Förderung zu Beginn meiner Zeit am IFL. Dr.-Ing. Jan Oellerich danke ich für die vielen Diskussionen über die Mathematik, sowie für die Unterstützung, Mathematik als Sprachinstrument zu verstehen. Tommi Kivelä danke ich für die enge Zusammenarbeit am IFL sowie für die Unterstützung bei der Identifizierung eines eigenen Forschungsschwerpunktes. Constantin Enke und Benedikt Schulz danke ich für gemeinsame Diskussionen über standardisierbare Darstellungsformen von Materialfluss- und Layoutdaten für FTS. Pietro Schumacher danke ich für das Beleben des Büros: stets mit guter Laune und spannenden Diskussionen.

Ich danke allen Kolleg:innen für die Zusammenarbeit und schöne Zeit am IFL. Das Kickern (*Hannoversch:* Krökeln) am Nachmittag, sowie unsere Social Thursday´s werde ich vermissen.

Den Studierenden David Ackermann, Ibrahim Bouriga, Yarkin Doruk Dogan, Tobias Ferreira, Jonas Fitz, Diana Giebels, Adeline Haisch, Benedikt Heidenreich, Jacqueline Kaefer, Lacin Kertmen, Tom Kobold, Timo Kurschilgen, Saurabh Nahata, Johannes Pfeifer, Lisa-Marie Raichle, Mark Rauh, Lena Schmidt, Rufinian Schröter, Stefan Seiz und Manuel Thomas danke ich, die im Rahmen von Seminararbeiten, Bachelorarbeiten oder Masterarbeiten, HiWi-Jobs oder Praktika einen wichtigen Beitrag für meine Forschung erbracht haben.

Meiner Familie und meinen Freunden danke ich für das Verständnis zur Wahl meines Weges an das KIT und für den Zusammenhalt, trotz großer Distanz zur Heimat. Mein herzlichster Dank geht an meine Frau Denise, die mir während meiner Zeit am IFL stets zur Seite stand. Vielen Dank für deine Ausdauer, dein Vertrauen und für die vielen motivierenden Gespräche in den letzten Jahren.

Contents

Abbreviations and Symbols

Abbreviations

AAM	Alternative Approximation Method
AGV	Automated Guided Vehicle
AGVS	Automated Guided Vehicle System
AMR	Autonomous Mobile Robot
CIS	Charging Infrastructure System
CS	Charging Strategy
C	Capacitive
DCDC	Direct Current Converter
DP	Dwell Point
EDLC	Electric Double Layer Capacitor
ERM	Energy Requirement Model
ESR	Energy Storage Requirement
ESRM	Energy Storage Requirement Model
ESS	Energy Storage System
I	Interim

KIT	Karlsruher Institute for Technology
LHD	Load Handling Device
MLD	Material Flow and Layout Data
OS	Operating Strategy
O	Opportunity
RFID	Radio Frequency Identification
RQ	Research Question
SoC	State of Charge
WFC	Weasel Fleet Controller

Latin symbols and variables

$\mathbf{A}$	Set of all AGV types
a	AGV Type as an element of $\mathbf{A}$
a_{acc}	Acceleration in $[\mathrm{m/s^2}]$
A_{D}	Distance matrix
A_{T}	Transport matrix
A_{TE}	Empty run transport matrix
A_{TT}	Total transport matrix
$\mathbf{C}$	Set of all CIS distribution classes
c	CIS distribution class as an element of $\mathbf{C}$
c_{r}	Charge rate in $[1/\mathrm{h}]$
d	Distance in $[\mathrm{m}]$

a_{dec}	Deceleration in $[\mathrm{m/s^2}]$
E	Energy in [Wh]
$E_{\mathrm{R}}^{\mathrm{AGV}}$	Energy requirement per vehicle in [Wh]
E_{ESS}	Energy storage requirement in [Wh]
$E_{\mathrm{ESS}}^{\mathrm{Scl}}$	Energy storage requirement considering S_{cl} in [Wh]
$\mathbf{E}$	3×1 Energy vector
Fr	Friction force
J	Transport job list
$\mathbf{L}$	Set of all MLD
l	MLD as an element of L
m_{load}	weight of the transport load in [kg]
N, n	Number, count
p	Probability
p_{chg}	CIS probability [-]
P	Electrical power in [W]
$\mathbf{P}$	3×1 Power vector of AGV components power requirement
P_{tot}	Total electrical power in [W]
q	Dimension of $\mathbf{Z}$
Q	Source station
SoC	State of charge in [%]
S	Sink station
s_{s}	Step size in $[\mathrm{ms}]$

s	Discrete state for iterative method [-]
S_{cl}	Safety confidence level [-]
S_{F}^{-}	Safety factor and lower threshold of the S_{cl} [-]
t	Time, duration in [s]
t_{chg}	Average interim charging time in [ms]
t_{cycle}	Cycle time in [ms]
t_{op}	Operational time in [ms]
t_{ref}	Reference time in [h]
t_{sim}	Simulation time in [ms]
T	Total transport distance in [m]
U	Utilization in [%]
v	Velocity in [m/s]
$\mathbf{Z}$	Set of analysis results
z	Result of result set $\mathbf{Z}$
z_{CI}	Z-value of the one-tailed standard normal distribution [-]

Greek symbols and variables

α	Significance level [-]
Δ_{cut}	Ratio of undercut orders to all completed transport orders [-]
δ	Ratio of max distance to an average distance [-]
η_{U}	Utilizability [-]
η_{A}	Availability [-]

κ	Simplified composited expression in ESR design
λ	Order frequency between two stations [-]
λ_{exp}	Exponential distribution parameter [-]
μ_{DCDC}	DCDC efficiency in [%]
ρ	Ratio of transport orders to empty runs [-]
ρ_{OC}	Transport order completion rate [-]
σ	Standard deviation in [%]
σ_{U}	Standard deviation of the vehicle utilization in [%]
$\bar{\sigma}_{\mathrm{U}}$	Mean standard deviation of the vehicle utilization in [%]
$\boldsymbol{\sigma}_{\mathrm{U}}$	Set of standard deviations of the vehicle utilization in [%]
φ	Movement direction of an vehicle

General indexes

active	Active state
avg	Average
c	Controls
chg	charge
$\mathrm{run}^{\mathrm{chain}}$	Chained transport jobs without CIS
comp	AGV component
cut	Undercut of $SoC = 0$
d	Drives
dock	Docking

done	Completed transport orders
done^{-}	Completed transport orders with a negative SoC
eacc	No load acceleration
ec	Empty cycle
ed	No load drive
edec	No load deceleration
facc	Full load acceleration
fc	Full cycle
fd	Full load drive
fdec	Full load deceleration
lh	Load handling
$\overset{+}{\mathrm{lh}}$	Load handling picking state
$\overset{-}{\mathrm{lh}}$	Load handling dropping state
min	Minimum
max	Maximum
op	Operating
$\mathrm{preDrive}$	Prepare driving state
preLH	Prepare load handling state
state	State of the ERM
stby	Standby state
T	Transport orders without empty runs
TE	Empty run orders

tot	Total
trans	Transports
undock	Undocking state
undone	Incompleted transport orders

1 Introduction

As production facilities become increasingly automated, manual logistic processes are also increasingly being replaced by automated systems and optimized in terms of throughput and waiting times. According to Müller (2023), mobile robots have been increasingly used for intralogistics material transportation for years, for example, to supply parts to production lines, to transport semi-finished goods during assembly, or to replace fixed conveyor systems for more flexible material handling. While 31,153 units per year were in operation in 2017, the number of units in 2022 was 188,349. Figure 1.1 shows the linear growth of mobile robots for transportation between 2017 and 2022, with linear growth increasing in 2020. The literature often distinguishes between automated guided vehicles (AGVs)

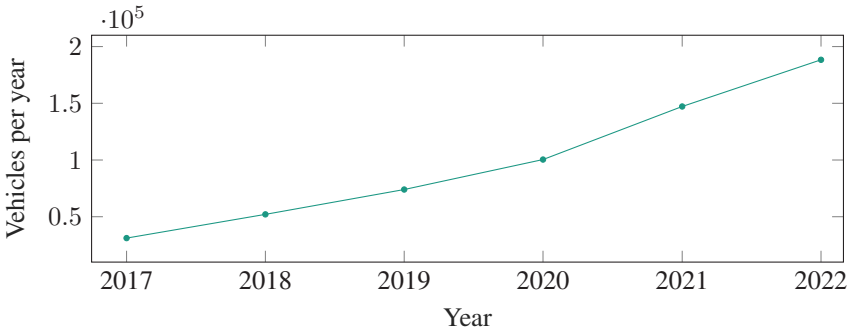

Figure 1.1: Global installed mobile robots for intralogistics transports per year, based on Müller (2020, 2021, 2022, 2023)

and autonomous mobile robots (AMRs). The main distinguishing criterion is the type of navigation and its technical design. AGVs only follow physical

guidelines on the ground, while AMRs can select their trajectories more flexibly. A common aspect of all mobile robots is that each consists of components requiring energy. These include, for example, drives, controls, electrical power supply for sensors and safety equipment, and a load handling device (LHD). The energy supply is usually realized by mobile energy storage systems (ESSs), which are either exchanged by a physical battery swap with fully charged batteries or the vehicle´s charging process at a station with a charging infrastructure system (CIS). Later on in this thesis, AGVs are referenced for individual vehicles while automated guided vehicle systems (AGVSs) reference holistic systems for mobile robots. While some studies on energy requirement aspects of AGVs appear in the literature, no approaches to modeling and designing ESS for mobile robots have been identified. Typical studies on AGVs´ energy requirement aspects are optimization methods regarding the energy requirement during operation. They often study minimization functions of parameters, which reflect important influencing factors of the energy requirements of AGVs.

As the number of mobile robots increases, the requirement for resources for mobile ESS also rises. Because of the global requirement for resources for energy storage production, which has also risen due to increasing electromobility (Xu et al. 2020) resource-saving methods must ensure that the ESS capacity for mobile robots is only sized as large as necessary for the specific application. With the development of a numerical model for calculating the energy storage requirement (ESR) of AGVs, this thesis aims to contribute to future savings in ESS capacities and the associated savings in resources.

1.1 Problem Description

Analyzing the power and energy requirement of AGVs is necessary to model the ESR of the AGVs. As Meißner and Massalski (2020) and Hamdy (2019) demonstrated, that energy requirement is affected by multiple parameters, such as data on material flow and layout, and vehicle-specific parameters. Since the detailed literature review in the following chapter could not identify a holistic

method for modeling the energy requirement of AGVs under consideration of material flow and layout, a suitable model is required. Based on the current state of research, the following three research questions (RQs) were identified:

RQ1: How can intralogistics material flow and layout data be systematically described for the model-based investigation of energy requirement considerations of AGVs?

RQ2: How can the energy requirement for AGVs be modeled, considering the material flow, layout, charging strategy, capacity utilization, and vehicle specifications?

RQ3: How can the energy storage requirement for AGVs be modeled, considering different charging strategies and operating times?

By addressing these three RQs, this thesis makes a significant scientific contribution to modeling power requirement, energy requirement, and ESR for AGVs in intralogistics under multiple constraints.

1.2 Outline

The subsequent chapters unfold systematically, progressing from a detailed literature review of the relevant topics of modeling material flow and layout, operation and charging strategies for AGVs, fleet sizing algorithms, and power and energy requirement modeling for AGVs to answering the three RQs in sequence. Figure 1.2 shows the three primary research environments modeled in the three RQs. Within this schematic representation, each RQ investigates individual system components with progressively increased depth and specificity and describes a model of the specific environment. Chapter 3 describes the analysis of material

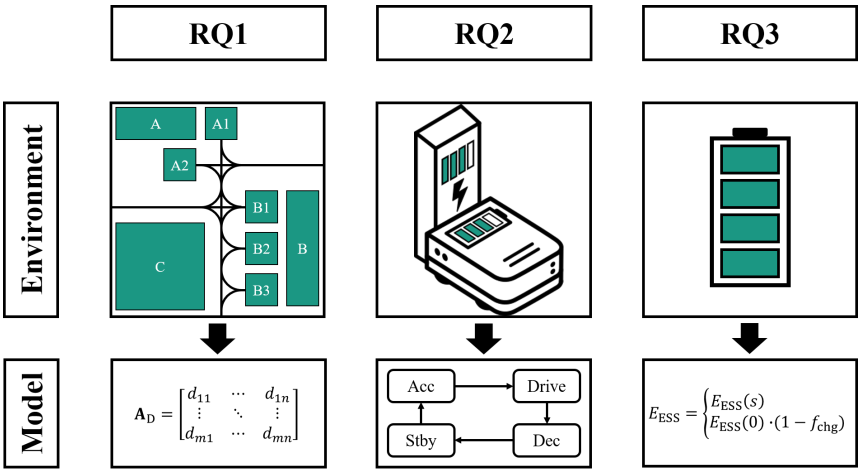

Figure 1.2: Overview of the specific topics of this thesis

flow and layout modeling for energy requirement aspects of AGVs, which answers the first RQ.

Chapter 4 presents a state-based energy requirement model (ERM) for modeling the power and energy requirement of AGVs and includes a section on the quantitative validation of this model based on real experiments. The model considers the material flow and layout data modeling from the third chapter. Subsequently Chapter 4 answers the second RQ. Chapter 5 presents a model for the modeling of ESR and verifies and validates it by executing simulations using the ERM from the second RQ to answering the third RQ. Finally, Chapter 6 summarizes the key findings and provides an outlook for future research and applications to practitioners.

2 Literature Review

Methods for modeling AGVs are required for simulation studies of the energy requirement. This section presents the most relevant preliminary work needed to model an AGV. These include operation- and charging strategies, methods for modeling material flow and layout data, methods for fleet sizing and dwell point placement, and methods for modeling the power and energy requirement of AGVs.

2.1 Operation- and Charging Strategies

Section 2.1, except 2.1.4, is based on Sperling and Kivelä (2022), Sperling et al. (2023) and Sperling and Furmans (2024). The following text are taken from those publications with editorial revisions.

An operation strategy (OS) regulates the behavior of the AGVs in the overall system, while a charging strategy (CS) describes the charging process of each vehicle at the control system level according to the International Electrotechnical Commission (2013) and Quadrini et al. (2020). Operating strategies include the task allocation problem, described in more detail in Sections 2.1.1 and 2.1.2. OSs with energy constraints differ from CSs and describe strategies on the process control level according to the International Electrotechnical Commission (2013) and Quadrini et al. (2020), where the charging states of vehicles and the utilization rates of the charging systems have an impact on the behavior regulation of AGVs.

Related work on this topic is described in Section 2.1.3, followed by a description of the most common CSs in Section 2.1.4.

2.1.1 Scheduling Strategies

The task allocation problem was divided by Fragapane et al. (2021) into the two research areas of scheduling and dispatching. Indeed, $34\,\%$ of the classified literature covers these two research areas, which are important research topics in AGV planning and control. Gen et al. (2017) investigated whether applying multi-objective generic algorithms to multi-objective scheduling problems enhances the quality of the solution, minimizes the computation time, and maximizes the effectiveness. The study was based on a transport layout, given distances, and order frequencies. Furthermore, de Ryck et al. (2021) studied decentralized task allocation considering energy constraints with a multidisciplinary study based on a transport layout. Based on the same material flow and layout data, a decentralized task allocation considering route constraints was investigated by de Ryck et al. (2022).

2.1.2 Dispatching Strategies

Dispatching describes the systematic distribution of transport orders to the vehicles of a transport system. In a centralized allocation, a fleet manager has information about the utilization of the vehicles and distributes the orders strategically. In decentralized allocation, the orders are negotiated between the vehicles and distributed (de Ryck et al. 2022).

Fragapane et al. (2021) and Vivaldini et al. (2015) summarized various methods from literature for dispatching. The methods sought to optimize task allocation according to at least one criterion. Typical optimization criteria are the minimization of the number of required AGVs, the minimization of the sum of distances to be driven, the minimization of buffer sizes at the stations (both input and output), the minimization of the waiting time of a transport order, the minimization of possible

blockages due to backlogs, and the maximization of the production ratio. In addition to single objective optimization, Zamiri Marvizadeh and Choobineh (2014) presented a dispatching method in which both input and output queues of stations were balanced. The following list shows common heuristic dispatching methods and their corresponding optimization criteria, based on Zamiri Marvizadeh and Choobineh (2014):

- STT/D - Minimizing percentage empty run time/distance
- MFCFS - Minimizing order fulfillment duration
- MOQS - Minimizing percentage parts waiting time in output queue
- ULSAT - Minimizing percentage parts waiting time in input queue
- IOQBA - Input and output queues balancing

2.1.3 Operating Strategies with Energy Constraints

Jodejko-Pietruczuk and Werbinska-Wojciechowska (2021) presented a multi-AGV simulation model for this purpose, where the state of charge (SoC) of the ESS was considered and the number of charging systems in the layout was varied. Colling et al. (2019) presented a method where the SoC of vehicles was distributed in a cycle-oriented manner to maximize the utilization of charging stations and balance the overall system availability. Further work on operating strategies was performed by Singh et al. (2022) and Abderrahim et al. (2020), where each presented and studied a scheduling model with battery constraints.

2.1.4 Charging Strategies

The three most common CSs capacitive operation (capacitive (C)), capacitive operation with intermediate charging (interim (I)), and the opportunity charging (opportunity (O)) (VDI Society Production and Logistics 2022, 2000) are shown in Figure 2.1.

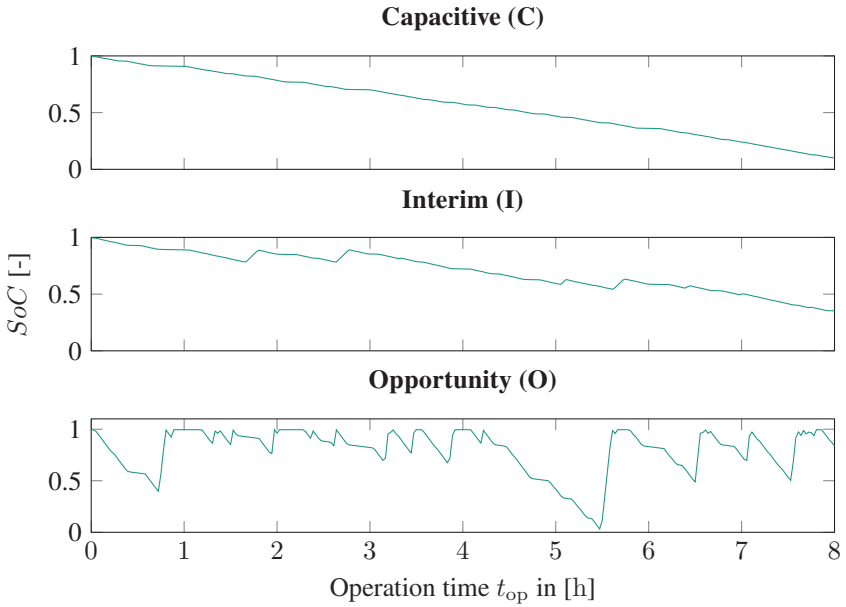

Figure 2.1: Exemplary course of a SoC of an AGV over operation time for charging strategies C, I and O

Capacitive. For CS C, a lower capacity threshold is defined. If the capacity falls below the lower capacity threshold, the current transport order is completed, and the closest charging station is sought. The ESS is charged at the CIS until an upper capacity threshold is reached, completing a full charging process.

Interim. CS I is similar to CS C, but the option of intermediate charging is added. Here, a CIS is sought if no transport orders are currently pending for the vehicle. Intermediate charging is performed at the CIS until the vehicle is assigned a new transport order. Alternatively, a CIS can also be integrated into a pick-and-drop station. For further transport orders, charging is allowed during the load transfer process, or until the vehicle is not assigned a transport order (i.e. idle). If the capacity falls below a set threshold during operation, a full charging process is performed.

Opportunity. CS O differs significantly from CSs C and I due to the higher frequency of full charging processes. At every opportunity, such as idle time or during load transfers at stations with integrated CIS, the charging process continues until the ESS reaches an upper capacity threshold.

2.2 Material Flow and Layout Planning for AGV Systems

Sections 2.2 to 2.3 are based on Sperling et al. (2023). The following text, the tables, and the figures are taken from that publication with editorial revisions.

2.2.1 Layout Topologies and Flow Path Orientation

Initial studies of flow path orientation have already been conducted by Maxwell and Muckstadt (1982) and Bozer and Srinivasan (1991). Bozer and Srinivasan (1992) and Sinriech et al. (1996) introduced bidirectional flow path orientation and investigated mixed directional flow path orientations, which enabled a higher overall system throughput for specific layouts. Furthermore, Bozer and Srinivasan (1991, 1992), and Sinriech and Tanchoco (1995) investigated a tandem layout topology. These investigations were authoritative for various subsequent flow path orientations and layout topologies. A taxonomy appears in Section 3.1. Recent works, such as Zou et al. (2021) and Roy et al. (2020), are based on the abovementioned criteria. Zou et al. (2021) presented further differentiation criteria for layouts and path topologies. For layout topologies, they distinguished between two-tier and single-tier layouts to investigate the performance of an AGV-based sorting system, whereas Roy et al. (2020) investigate single and multiloop topologies for designing container terminal operations.

2.2.2 Layout and Material Flow Planning

When planning a facility´s layout and material flow, data about the current, planned, or predicted material flow intensity between different stations are important. Asef-Vaziri and Laporte (2005) overviewed loop-based facility planning and material handling decisions for material handling equipment like AGVs. They referred to aspects of facility design like sequencing stations and locating production cells, the design, including the material handling system (layout topology), and operational issues such as home locations of idle vehicles and the avoidance of blocking and congestion. An approach to optimally locating workstations in a tandem AGV system by Salehipour and Sepehri (2014) was formalized as a mixed integer programming formulation. Aiello et al. (2002) presented an integrated genetic approach to simultaneously designing the layout and the material handling system in a facility.

2.3 Fleet Sizing

Planning AGV systems (AGVS) includes determining the number of vehicles based on influencing factors, such as transport frequency, distances between stations, and vehicle specifications. Singh et al. (2011) developed a discrete simulation model to determine the minimum number of AGVs for manufacturing distribution. Hamdy (2019) used a simulation model to investigate the optimal fleet size, considering charging strategies in a specific transport layout.
Furthermore, studies have found varied vehicle loading capacities, such as Yan et al. (2022) and Rahimikelarijani et al. (2020). Yan et al. (2022) studied the maintenance strategies for multi-load AGVs. The number of vehicles, as well as the vehicle capacity, were varied. This study was also based on transport distances, which were given as a graph with bidirectional flow path orientation. Regarding multiple load AGVs, Rahimikelarijani et al. (2020) presented a mathematical model for configuring multiple load AGVs for tandem layout topologies based on a given transport layout. Großeschallau (1984) and Fottner et al. (2022) described

a basic mathematical model for estimating the fleet size. The model considered the transport demand per period, the utilization rate η_{U}, and the system availability η_{A} linearly.

2.4 Dwell Point Placement Strategies

In addition to the fleet size, the system design also includes planning suitable positions where vehicles can stop or park in an idle state. The literature refers to these points as dwell points (DP). According to Egbelu (1993), AGVs switch to an idle state if a transport order is completed. To determine suitable DPs, Egbelu (1993) has established three basic rules:

(a) Point of release positioning rule

(b) Central zone positioning rule

(c) Circulatory loop positioning rule

The rule (a) is where the DO is the point at which a vehicle reaches the idle state. The rule (b) uses central buffer areas for all idle vehicles but does not include their positioning and the rule (c) describes using loops for all idle vehicles, as AGVs continue running on empty until they receive new orders.

Bruno et al. (2000) presented a heuristic to dynamically determine DPs considering minimizing the mean distance to the DP (1). Simulative experiments demonstrated that (1) performed better than rule (a). In addition to (1), the minimization problems $(2-4)$ were established and investigated by Ventura and Rieksts (2009) and Ventura et al. (2015).

They showed that DP placed on stations or intersections with at least three edges could reduce system response times, whereas DP at points on edge beyond stations could not improve mean response times. Dehnavi-Arani et al. (2019) presented a mathematical model (5) to minimize maximum system response time and battery swap duration based on (3). The five minimization problems are listed below:

(1) Minimizing mean distance to the DP

(2) Minimizing mean system response time

(3) Minimizing maximum system response time

(4) Advanced minimizing maximum system response time

(5) Minimize maximum system response time and battery swap duration

Using numerical experiments for a job shop layout, they showed, that an optimal position for the battery swap station could be found. However, a global optimum could not be found, which was justified by the nonlinearity of their model. In summary, based on the above sources, pick-and-drop stations are the most suitable DPs for minimizing the overall system´s maximum or mean response time. DPs are also suitable for installing charging systems since additional runs to central zones are eliminated (cf. (b)).

2.5 Power and Energy Requirement Modeling of AGVs

Section 2.5 is based on Sperling and Furmans (2024). The following text, the tables, and the figures are taken from that publication with editorial revisions.

Several studies have investigated mobile robot components' energy or power requirement, as described in this section. For instance, at the factory and logistics planning level, Freis and Günthner (2016) presented an analytical model for determining the overall energy efficiency of logistics centers. In this context, key figures for industrial trucks were considered for the intralogistics submodel for energy requirement determination and key figures include the number of vehicles, the average electrical power consumption per hour, the operating hours per year,

and the battery charging efficiency. Furthermore, Müller et al. (2013) presented an approach for energy efficiency-oriented planning of logistics systems by theoretical aspects using an AGV as an example.
At the level of logistic planning, Ebben (2001) investigated the impact of battery constraints on AGVs on logistics performance. The results of his work show that automated contact-based charging processes lead to better logistics performance than battery swapping. At the control system level (cf. International Electrotechnical Commission (2013)), Mei et al. (2006) presented a power requirement model for an AGV. By varying velocity under energy and travel time constraints, the total travel time and energy requirement were minimized compared with heuristics. At the same level, Qiu et al. (2015) presented an energy consumption minimization method for route planning of heterogeneous AGV fleets. Their experiments showed that energy consumption could be reduced by at least 6.08% compared to methods for minimizing transportation distances.
Kim and Kim (2007) presented a minimum energy translational trajectory planning algorithm for a differential-driven mobile robot. They adapted it to a three-wheel-driven mobile robot in a subsequent study by Kim and Kim (2008). Simulation experiments revealed at least 9% energy savings for differential-driven robots and 2.4% energy savings for three-wheel-driven mobile robots. Another model for minimizing energy requirement for differential-driven AGVs was shown by Liu and Sun (2014). Smooth trajectories were obtained by optimization, where the velocity was varied to minimize energy requirement. Related work was completed by Kabir and Suzuki (2019) where different routing heuristics were studied considering energy requirement.

Stampa et al. (2015) presented a mathematical model for estimating the energy consumption of an omnidirectional AGV to investigate different trajectories between the same points for their energy consumption. Comparison with data from real experiments showed that the energy consumption data from the model were coherent with the measurements. Moreover, Hou et al. (2019) presented a model to determine the power requirement of Drives and Control during the standby,

acceleration, and stable states. Real experiments to determine the energy requirement were further investigated by Niestrój et al. (2020), who presented an ERM for an AGV using a hybrid ESS consisting of Li-Ion and hydrogen. For the simulative experiments, the average energy consumption of an AGV under selected operating conditions was measured at the beginning and subsequently investigated by varying the speed and load. However, this model and the model by Stampa et al. (2015) did not consider transport orders or transport distances.
The most related works on modeling power and energy requirement of AGVs are Hamdy (2019) and Meißner and Massalski (2020). Hamdy (2019) presented a simulation model to determine the optimal number of vehicles considering energy constraints. The state-based simulation model featured the states of blocking, traveling empty, traveling loaded, accelerating empty, accelerating loaded, decelerating empty, decelerating loaded, picking, and dropping, whereby each had constant total power. The interpreted relations of the states are shown in the following Figure 2.2 as a state diagram. Finally, the work of Meißner and

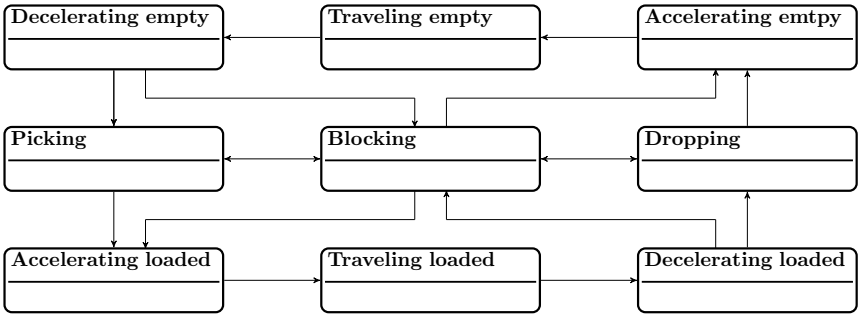

Figure 2.2: State based activity model for AGVs. Own illustration, based on Hamdy (2019), Kabir and Suzuki (2019), McHaney (1995).

Massalski (2020), in which the electrical power of the drives of an AGV with differential drives was measured and analyzed for the procedure, is mentioned. A state-based simulation model represented accelerating, driving, and decelerating states. Furthermore, the load-handling process was investigated in detail. In the experiments, the driving speed and the transported load were varied. Fife active

substates were identified through performance measurements of the LHD and data analysis, the acceleration of the LHD, lifting without load, lifting load absorption (where the lifting load increases), lifting under full load, and breaking, shown in Figure 2.3 as a state diagram.

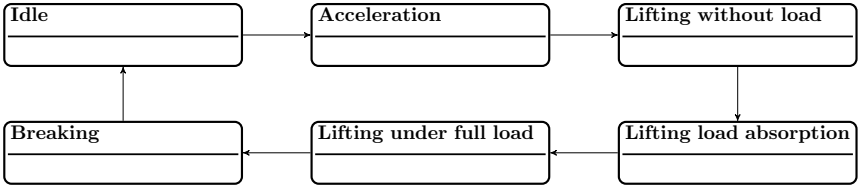

Figure 2.3: State based activity model for a LHD of an AGV. Own illustration, based on Meißner and Massalski (2020)

The findings on energy consumption were processed quantitatively and showed that the power did not vary linearly with increasing speed and transport weight. Therefore, the correlation resulting from the investigations can be further transferred into a nonlinear optimization problem to determine an optimum operating point with minimum energy consumption.

Table 2.1 classifies the previously mentioned studies on power and energy requirement modeling of AGVs according to relevant characteristics, which are explained in more detail later in this paper.

Table 2.1: Literature review on modeling power and energy requirement of AGVs. Charging strategies: C: capacitive, I: interim, O: opportunity. P_{tot}: Total vehicle power.

Literature	Simulation	Real	Drives power	Ctrl power	LHD power	Total energy	State based	CS	OS w. energy constraints	Layout	Material flow	Utilization	CIS distr.
Mei et al. (2006)	•	•	$f(m,v,a)$	$f(f_{\mathrm{cam}})$	-	$f(t)$	-	-	-	-	-	-	-
Kim and Kim (2008), Liu and Sun (2014)	•	•	$f(v)$	-	-	$f(t)$	-	-	-	-	-	-	-
Qiu et al. (2015)	•	•	$f(m)$	-	-	$f(d)$	-	-	-	•	-	-	-
Stampa et al. (2015)	•	•	$f(m,\varphi)$	-	-	$f(t)$	-	-	-	•	-	-	-
Niestrój et al. (2020)	•	•	$f(m,v)$	-	-	$f(t)$	-	-	-	-	-	-	-
Meißner and Massalski (2020)	•	•	$f(m,v)$	const.	$f(m)$	$f(t)$	-	-	-	-	-	-	-
Hou et al. (2019)	•	•	$f(v)$	$f(t)$	-	$f(t)$	•	-	-	-	-	-	-
Freis and Günthner (2016)	•	-	$P_{\mathrm{tot}} = \mathrm{const.}$			$f(t)$	-	-	-	-	-	-	
Ebben (2001)	•	-	-	-	-	$f(t)$	•	-	•	•	•	•	•
Kabir and Suzuki (2019)	•	-	$P_{\mathrm{tot}} = \mathrm{const.}$			$f(t)$	-	-	-	-	•	-	-
Hamdy (2019)	•	-	$P_{\mathrm{tot}} = \mathrm{const.}$			$f(d)$	•	C, O	•	•	•	•	•
McHaney (1995)	•	-	$P_{\mathrm{tot}} = \mathrm{const.}$			$f(t)$	•	O	-	-	-	-	-
Singh et al. (2022)	•	-	$P_{\mathrm{tot}} = \mathrm{const.}$			-	-	C	-	•	•	-	-
Abderrahim et al. (2020)	•	-	$P_{\mathrm{tot}} = \mathrm{const.}$			$f(t)$	-	C	-	-	•	-	-
Colling et al. (2019)	•	-	$P_{\mathrm{tot}} = \mathrm{const.}$			$f(d)$	-	-	•	•	•	-	-
Zhan et al. (2019)	•	-	$P_{\mathrm{tot}} = \mathrm{const.}$			$f(t)$	•	-	-	•	•	-	-
Jodejko-Pietruczuk et al. (2021)	•	-	-	-	-	-	-	-	•	-	-	•	-

Scientific studies with real experiments have noticeably neglected the characteristics of operating states, CS, layout and material flow, utilization, and CIS distribution, whereas simulation-based studies without real experiments have focused on the variation of material flow and layout. Furthermore, the modeling of load handling power and energy requirement was only investigated by Meißner and Massalski (2020). Variables marked with tot indicate the total energy or power of the vehicle without separating individual components. Drives and Controls were only considered separately by Mei et al. (2006), whereas constant values for the power and energy requirement of the Controls were assumed in other studies.

2.6 Energy Storage System Modeling

Section 2.6 is based on Sperling and Furmans (2024). The following text, the tables, and the figures are taken from that publication with editorial revisions.

Many scientific studies have modeled ESSs to learn about their behavior toward influencing factors such as calendrical and cyclic aging, temperature, and charging power (cf. Yang and Wang (2018), Gao et al. (2022), Stroe et al. (2018), Leuchter and Bauer (2015), Vidal et al. (2019), Wood et al. (2011), Saldaña et al. (2019), Hu et al. (2020), Devillers et al. (2014), Yang (2020)). Usually, only an impact on the maximum capacity of ESS was investigated. Since Chapter 4 is about modeling the power and energy requirement of AGVs under certain constraints, only a linear relation was assumed in determining the current capacity and SoC respectively. In AGV systems, lead-acid ESSs are still widely used. Even the latest guideline VDI 2510 Part 4 VDI Society Production and Logistics (2022), still includes parameters for the design of lead-acid ESS for AGVs. The most typical ESSs are lithium cobalt oxide (LCO), although other types of lithium-based ESSs are frequently used in AGVs due to their low specific energy density. The characteristics (cf. Appendix A.2) show that cell voltages, C-rates, and maximum voltage strokes

vary strongly for the ESS. Another type of energy storage is electric double layer capacitor (EDLC). This term describes capacitors with extended capacity compared to electrolytic capacitors. Unlike electrochemical ESSs, the electrical energy is stored by an electric field and has a capacitance of 1 F to over 6000 F at typically 2.7 V to 3.0 V per cell (Horn et al. 2019). The literature research did not reveal scientific studies in the sizing of energy storage systems for mobile robots. As sources from Section 2.5 showed, only the energy requirement over distance or time was determined, the value of which resulted in the desired energy storage requirement for any given limit.

2.7 Chapter Conclusion

This literature review summarized every aspect of sufficiently emulating an AGV system for simulative studies while simultaneously stating the research gap in modeling the ESR of AGVs. First, basic strategies for operating and charging AGVs were presented, highlighting typical methods for transport order distribution. Furthermore, studies on material flow and layout modeling, planning, and design were provided, from which another research gap was identified, how material flow and layout data for energy requirement considerations of AGVs can be described and classified holistically. The subsequently described methods for fleet sizing and DP placement strategies were incorporated into the design of the simulation model in a further chapter of this thesis. The final part of the literature review summarized the most important studies on power and energy requirement modeling for AGVs and assigned them to different categories in tabular form. This section revealed a third research gap, the lack of a holistic, validated model for modeling the power and energy requirements of AGVs considering drives, controls, and LHDs.

3 Material Flow and Layout Modeling

Sections 3.1 to 3.7 are based on Sperling et al. (2023). The following text, the tables, and the figures are taken from that publication with editorial revisions.

This chapter begins with a taxonomy of material flow and layout data (MLD), which describes a data set consisting of a transport matrix and a distance matrix. Further, the methods used for data acquisition and subsequent data processing are described.

3.1 Material Flow and Layout Data Taxonomy

In this section, a taxonomy of MLD according to flow path orientation, layout topology, and task structure is presented. This allows for a comparison of the quality of the methods to be investigated based on corresponding classes.

3.1.1 Flow Path Orientation

The flow path orientation defines the allowed direction of movement of the respective flow path specified in the layout. Based on Schrecker (2000), the direction of the flow paths can be distinguished as follows:

- unidirectional flow path
- bidirectional flow path
- mixed directional flow path

A layout essentially consists of nodes and edges, where nodes can also be stations or junctions. A flow path starts with a node and ends with another node. In a unidirectional flow path layout, all flow paths are limited to one direction. In a bidirectional flow path layout, however, all flow paths can be used in both directions. Combinations of both flow path types in one layout are referred to as mixed flow path layouts.

3.1.2 Layout Topology

The layout topology describes the 2D or graph arrangement of the stations and the structure of the routes in the layout. Singleloop, multiloop, tandem, and segmented topologies are distinguished. Singleloop has no branches and can have any number of stations. The stations are arranged in a ring structure. If a layout has at least one junction or at least three stations with bidirectional flow paths, it is classified as a multiloop topology.

More complex layouts with a larger number of stations and flow paths can also be described by several linked singleloop or multiloop systems. These layouts are classified as tandem topologies. Such a layout contains at least two singleloops or multiloops linked by at least one transfer station (cf. Sinriech and Tanchoco (1994, 1995), Schrecker (2000)). The basic idea of split topologies is that they can achieve higher robustness, higher throughput, and higher flexibility in terms of extensibility (cf. Bozer and Srinivasan (1991, 1992), Schrecker (2000)).

Table 3.1: Classification of layout topologies and flow path orientations. S_n describes stations. Double circled stations are transfer stations. Different line types represent subsystems. Own illustration based on Maxwell and Muckstadt (1982), Bozer and Srinivasan (1991), Schrecker (2000), Sinriech and Tanchoco (1995), Sinriech et al. (1996), Rajotia et al. (1998)

	Singleloop	**Multiloop**	**Tandem**
Unidirectional	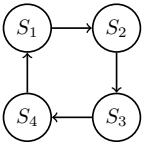 Unidirectional Singleloop Topology	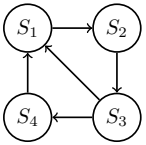 Unidirectional Multiloop Topology	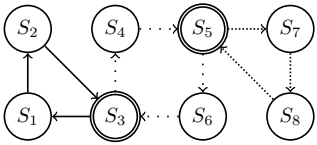 Unidirectional Tandem Topology
Bidirectional	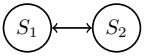 Bidirectional Singleloop Topology	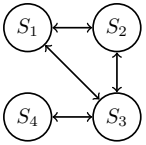 Bidirectional Multiloop Topology	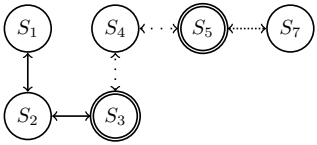 Bidirectional Tandem Topology
Mixed Directional	N/A	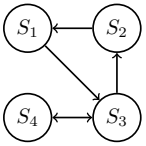 Mixed Directional Multiloop Topology	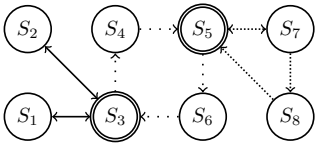 Mixed Directional Tandem Topology

3.1.3 Task Structure

A task structure describes the general transport request relationship between sources and sinks. The left digit 1 or m describes the number of sources and the right digit next to the colon with 1 or n is the number of sinks in the system. Based on Schrecker (2000), a task structure can be split into the four following listed categories:

- $(1:1)$
- $(1:n)$
- $(m:1)$
- $(m:n)$

In a $1:1$ task structure, there are exactly one source and one sink in the system. This is the case, for example, for a shuttle operation between one source and one sink. The $1:n$ task structure describes a task structure with one source and n sinks. This occurs, for example, in the supply of materials to production lines by route trains (cf. Literature02 based on Singh et al. (2011)). In contrast, an $m:1$ task structure describes a system with one sink and m sources. An example may be a waste disposal system where waste is generated at m sources and transported to a central disposal point, the one sink. The last case is the $m:n$ task structure. It describes systems with at least two sources and at least two sinks and is most common in AGVS (cf. Tables A.1 and A.2). Table 3.2 shows the possible combinations between the layout topologies and the task structures.

Table 3.2: Possible task structures based on layout topologies. Station denoted by a Q describes a source, S a sink.

	Singleloop	**Multiloop**
1:1	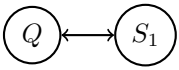 1:1 Singleloop Topology	N/A
1:n or m:1	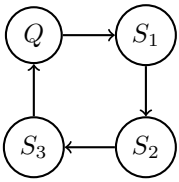 1:n Singleloop Topology	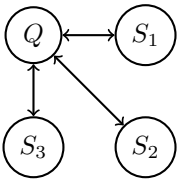 1:n Multiloop Topology
m:n	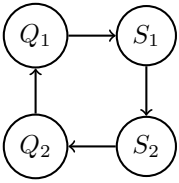 m:n Singleloop Topology	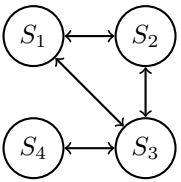 m:n Multiloop Topology

The combination of a multiloop topology with a $1:1$ task structure is not possible, since a multiloop topology is defined by more than two sink or source stations. Otherwise, it is a singleloop topology without any outgoing paths to additional sources or sinks.

3.2 Representation of Material Flow and Layout Data in Models

In order to identify a suitable representation of the data, the possible ways of modeling MLD in literature were considered and presented below, sorted by decreasing information density. For transport layouts, there is the scaled plan as a modeling type. This is the modeling variant with the highest information density. It contains information about the actual transport routes, the coordinates of the stations, as well as possible DP, flow path orientation, and further information about the system periphery, like the position and orientation of obstacles. The next abstraction level is a node-edge graph (Arnold and Furmans 2019). Information about the actual transport routes and the coordinates of the stations are represented, as in the scaled plan, only information on the periphery is lost. Through the connectivity in directed graphs, unidirectional as well as bidirectional flow path oriented transport routes can be represented. The next abstraction level is a simplified node-edge graph. It is a visual representation of the transport distance or frequency between the stations. The loss of information on the actual routes of the vehicles can be considered in form of edge weights (Arnold and Furmans 2019). The stations can be arranged in the same way as in the real layout, thus keeping the information on the actual spacial relation between each other (cf. Yao et al. (2021)). This information content can also be represented as a matrix. The matrix contains only the distance relationship (distance matrix) or the transport frequency relationship (transport matrix) between all stations in the layout (Arnold and Furmans 2019).

During the collection of MLD, it was noticed that the data was not in a uniform format. Due to the lack of information in most cases, the matrix was chosen

as the form of representation. The matrix format is suitable for automated data processing, as it inherently possesses machine-readability and no conversion is needed which would be the case for scaled plan modeling.

3.3 Data Acquisition Methods for Transport Matrix

If the transport orders are not specified as a transport matrix or on an hourly basis, the following methods were used:

- Case: Job sequences
  In some layouts, only job sequences were specified. Job sequences include only transport jobs and exclude empty runs. These occurred, for example, in systems with route trains for supplying production lines. A given job sequence followed a $1 : n$ relationship, with 1 source and n sinks. From a job sequence $(Q \rightarrow S_1 \rightarrow S_2 \rightarrow ... \rightarrow S_n)$, single trips were derived, all originating from the single source Q for the job sequence. For a given job sequence $(Q \rightarrow S_1 \rightarrow S_2 \rightarrow ... \rightarrow S_n \rightarrow Q)$ that ends at the same Q as started, the last job $(S_n \rightarrow Q)$ is not considered for the transport matrix. These examples of job sequences both result in the job list $J = \{(Q \rightarrow S_1), (Q \rightarrow S_2), ..., (Q \rightarrow S_n)\}$. If there were multiple job sequences for a source or an additional source, the job list was expanded accordingly.

- Case: Job list
  If a job list was the basis after data collection, a matrix was derived from the transport order relationships, which correspond to the transport matrix.

- Case: Not normalized period
  If transport data are given based on a time interval $t \neq 1h$, the transport data have been normalized to $t = 1h$.

3.4 Data Acquisition Methods for Distance Matrix

In order to use data of a material flow for the data set described here, specification of the transport matrix as well as a description of the station distribution, e.g. with a distance matrix, a time matrix, or a scaled layout plan, are necessary at least. Alternatively to the scaled layout plan, the specification of station coordinates or a graph is sufficient. If the description of the station distribution is not in a distance matrix format, a distance matrix was determined from the given data using the following methods:

- Case: Incomplete distance matrix
  Stations, between which no transport orders are executed, were missing. If missing distances could be determined from a graph or a scaled plan, this was done. In all other cases, no distance relation is set and therefore cannot be used. For machine readability, $d_{mn} = -1$ is used.

- Case: Time matrix
  If a time matrix was given instead of the distance matrix, an average transport velocity of $v = 1\mathrm{m/s}$ was assumed, based on the safe collaboration velocity of AGVs (Ullrich and Albrecht 2023). The multiplication of the time matrix by the scalar quantity of the average velocity v results in the distance matrix (Fottner et al. 2022).

- Case: Coordinates
  If coordinates of the stations are given and no more information about routes is available, we used the Manhattan distance method, based on Arnold and Furmans (2019). The Manhattan distance method determines the distance d_{mn} considering only rectangular route trajectories. Zhang et al. (2021) uses this method for distance determination of AGVs in a warehouse environment. The Manhattan distance between the stations $x, y \in \mathbb{R}^2$ can be described mathematically as $d_{mn} = |x_1 - y_1| + |x_2 - y_2|$, where 1 and 2 are the respective coordinates of the stations.

- Case: Scaled layout plan
  If only a scaled layout plan was given, a coordinate system was placed on the layout and the coordinates of the stations were determined. If information about the routes is known or can be seen from the layout, the distances are determined based on the scaled lengths. Flow path orientation is also taken into account. If no flow path information is available, the Manhattan method is used as an approximation of the distances between two stations (cf. case: coordinates) (Arnold and Furmans 2019, Zhang et al. 2021).

- Case: Graph
  A graph contains all stations and their distance relations. In most cases, flow path and nodes are also specified and taken into account when determining the distance. If the distance matrix is based on a graph, the shortest possible path considering the given flow path and its orientation is determined using Dijkstra's algorithm according to Arnold and Furmans (2019).

3.5 Data Treatment Methods

3.5.1 Empty Run Matrix Generation

The empty run matrix results from the need for transports or from the supply of outgoing transport jobs at the stations. For transport systems that use load carriers or vehicles, empty runs are required to fulfill the demand for vehicles or load carriers. The empty runs for the data set described in this paper are determined by minimizing the distances of all empty runs according to Arnold and Furmans (2019). Mathematically, this can be described in simplified terms by the following minimization equation of the total transport distance T:

$$T = \sum_{m=1}^{N} \sum_{n=1}^{N} \lambda_{mn} \cdot d_{mn} \tag{3.1}$$

$$\begin{aligned} \min_{\boldsymbol{\lambda} \in \mathbb{R}_+^N \setminus \{0\}} \quad & T(\boldsymbol{\lambda}) \\ \text{s.t.} \quad & \sum_{n=1}^{N} (\lambda_{in} - \lambda_{ni}) = 0, \quad i \in \{1, ..., N\} \end{aligned} \tag{3.2}$$

λ describes the frequency of empty runs between stations m and n, where d is the distance between stations m and n and N is the number of stations in the transport layout.

3.5.2 Job List Generation

A transport job describes a set of equal transport orders and its frequency. The relationship between job and order is further described in Section 3.6.6. The job list is a clearly structured and more easily processable form of provisioning transport jobs. The job list is automatically generated using the total transport matrix, which already includes the empty run matrix. During generation, all cells of the total transport matrix are created as one transport job and the frequency is adopted as an attribute. Then, all transport jobs with a frequency of $f = 0$ are filtered out.

3.6 Data Description

In this section, the data set is described in detail. The material flow data set includes 72 specific MLD, which are stored in several comma separated values (.csv) files. The following Table 3.3 summarizes all documents of each MLD, which are described in detail afterwards.

The contents within the listed files start after a header line, and for matrices after a header column. The matrices are always square, i.e. the number of rows is equal to the number of columns (cf. Section 3.6.1).

Table 3.3: File naming and their referenced chapters

Filename	**Referenced chapter**	
	data aquisition and treatment	data description
$[LayoutID]\_Transportmatrix.csv$	3.3	3.6.1
$[LayoutID]\_Distancematrix.csv$	3.4	3.6.2
$[LayoutID]\_Stationlist.csv$	N/A	3.6.3
$[LayoutID]\_Emptyrunmatrix.csv$	3.5.1	3.6.4
$[LayoutID]\_Totaltransportmatrix.csv$	N/A	3.6.5
$[LayoutID]\_Joblist.csv$	3.5.2	3.6.6

3.6.1 Transport Matrix

The transport matrix A_{T} describes the frequency of transports between all stations normalized to a time period. The first column shows the respective sources and the first row the respective sinks of a transport order. In the literature, the frequency is typically normalized to one hour and can refer either to specific transport trips or to material transports. For MLD, where the AGVs can handle multiple conveyor units simultaneously, the frequency of transport orders has been scaled to the minimum number of transport trips. For the main diagonal $\lambda_{mn} = 0, \forall\, n = m$ is valid.

$$A_{\mathrm{T}} = \begin{vmatrix} From/To & S_1 & S_2 & \dots & S_{\mathrm{n}} \\ S_1 & 0 & \lambda_{12} & \dots & \lambda_{1\mathrm{n}} \\ S_2 & \lambda_{21} & 0 & \dots & \lambda_{2\mathrm{n}} \\ \dots & \dots & \dots & \dots & \dots \\ S_{\mathrm{m}} & \lambda_{\mathrm{m}1} & \lambda_{\mathrm{m}2} & \dots & \lambda_{\mathrm{mn}} \end{vmatrix}$$

3.6.2 Distance Matrix

The distance matrix A_{D} contains the transport distances within a layout. The first column shows the respective sources and the first row the respective sinks of a transport job. The distance matrix for the description of transport distances d is typically given in meters in an intralogistics environment. As for the transport matrix, we assume that $d_{mn} = 0, \forall\, n = m$ applies to the main diagonal.

$$A_{\mathrm{D}} = \begin{vmatrix} From/To & S_1 & S_2 & \dots & S_{\mathrm{n}} \\ S_1 & 0 & d_{12} & \dots & d_{1\mathrm{n}} \\ S_2 & d_{21} & 0 & \dots & d_{2\mathrm{n}} \\ \dots & \dots & \dots & \dots & \dots \\ S_{\mathrm{m}} & d_{\mathrm{m}1} & d_{\mathrm{m}2} & \dots & d_{\mathrm{mn}} \end{vmatrix}$$

3.6.3 Station List

The station list is optional and not specified in each MLD, but includes at least a column listing all "Station IDs", as well as all "Origin station IDs" to link to the naming in the original literature. Optionally, coordinates are available in meters in some files. Furthermore, information about the station type is available. This includes the types of sink and source, which were determined by the demand and excess of the respective stations from A_{T}. Each station can also be a combination of several types. An example of a station list is shown in Table 3.4.

3.6.4 Empty Run Matrix

The empty run matrix A_{TE} is similar to a transport matrix (cf. Section 3.6.1), but only contains the empty runs based on a given transport matrix. The empty run matrices are determined according to a method, which is described in Section 3.5.1.

Table 3.4: Sample station list with specification of optional coordinates and functions (Q: source, S: sink)

Station ID	**Coordinates**		**Type**	**Origin Station ID**
	x in [m]	y in [m]	Q, S	
A	x_1	y_1	Q, S	S_1
B	x_2	y_2	Q, S	S_2
C	x_n	y_n	S	S_n

3.6.5 Total Transport Matrix

The total transport matrix A_{TT} is also similar to a transport matrix (cf. Section 3.6.1). It is the sum of the transport matrix A_{T} and the empty run matrix A_{TE} and can be mathematically represented as follows:

$$A_{\mathrm{TT}} = A_{\mathrm{T}} + A_{\mathrm{TE}} \tag{3.3}$$

By determining the empty run matrix based on the transport matrix, the sum of all incoming transport orders per station matches the sum of all outgoing transport orders of the same station. This corresponds to the constraint from (3.2).

3.6.6 Job List

Finally, a job list is specified in a file named [LayoutID]_Joblist.csv. A transport job T_j describes a set of transport orders with similar sink and source and is characterized by the properties of the transport orders and the frequency of occurrence. The UML diagram in Fig. 3.1 shows the relationship between job, station, and order, with a job being defined as a transport between exactly two stations in this data set. The job list is normalized to one hour. This allows to generate transport orders for various examinations. In addition, frequency distributions can be derived from the job list, for example, the frequency of specific

transport distances or the frequency of outgoing or incoming transport orders of the respective stations.

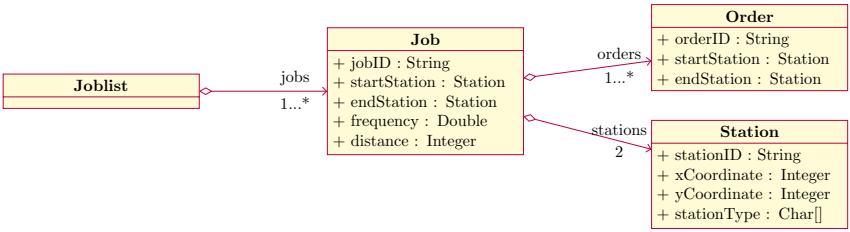

Figure 3.1: UML diagram to illustrate the relationships between joblist, job, order, and station

3.7 Data Classification

The MLD of the data set is classified in Tables A.1 and A.2 based on the taxonomy presented in Section 3.1. Fields marked with dots (•) apply according to the column description. The specified number of stations represents the number of all stations in the raw data. In two MLD, the addition "used" indicates the number of stations actually served. In all other MLD, all stations are served. This information was kept to allow further layout investigations regarding the spatial arrangement. The data acquisition and treatment methods (Sections 3.3, 3.4, and 3.5) for each MLD are presented in the appendices. In Table A.1, the 42 literature based MLD are presented. Classified by flow path orientation, there are 8 unidirectional, 30 bidirectional, and 4 mixed directional data. Only one of the layouts is in the singleloop topology class, the remaining 41 are in the multiloop topology class. Of these, 12 are also part of a total of 3 tandem groups marked as $\bullet_A$, $\bullet_B$, and $\bullet_C$ in the table. All individual layouts of a tandem group are also combined in an additional, holistic layout to provide another MLD for the dataset. Among the literature layouts, two task structures are represented, 35 times $m : n$ and 7 times $1 : n$. The number of stations in the layouts from literature varies from 3 to 20 stations, with a median of 8 and a mean of 9.025. 31 MLD also

contain further information about the coordinates that allow the physical location of the stations to be determined.

Table A.2 shows the classification of 30 industry based MLD. 19 are unidirectional layouts, 10 bidirectional, and one is a mixed directional layout. 17 layout topologies can be classified as singleloop and 13 as multiloop topologies. The $1:1$ task structure exists in 16 of 30 industrial MLD, i.e. in more than half of them. The $1:n$ task structure is represented once, the $m:n$ task structure 13 times, where the number of stations served varies between 4 and 33. Excluding the MLD with a $1:1$ task structure and two stations, the mean value is 9.8 stations and the median is 7 stations. In summary, it can be seen that $m:n$ task structures are considered in the majority ($83\,\%$) of the MLD from literature whereas in the sample of 30 MLD from industry only $47\,\%$ are considered. Similarly, only $2.4\,\%$ singleloop topologies are present in the literature data with whereas in the industry data $57\,\%$ of the layouts are classified as singleloop topologies.

Industry26 to Industry30 originate from the same system. Industry26 covers the entire system, whereas Industry27 to Industry30 describe subsystems in which different vehicle types are used. Industry28 and Industry29 collectively form a tandem group D in which four stations serve as transfer stations.

3.8 Chapter Conclusion

This chapter answered the RQ1:

> **RQ1: How can intralogistics material flow and layout data be systematically described for the model-based investigation of energy requirement considerations of AGVs?**

The findings from literature review about material flow and layout planning (cf. Section 2.2.1) were processed including how they led to a taxonomy for classifying MLD to answer RQ1. Types of MLD modeling were described and explanations

were given for focusing on the representation form of the matrices. These allowed a high degree of automation and contained the necessary information for investigating the ESR modeling of AGVs. Different MLD were required for these investigations, whose methods for acquisition and treatment were described. All files in the data set were subsequently described. Finally, a data analysis was presented in which the data was classified according to the taxonomy described above.

4 Power and Energy Requirement Modeling

Sections 4.1 to 4.5 are based on Sperling and Furmans (2024). The following text, the tables, and the figures are taken from that publication with editorial revisions.

4.1 Energy Modeling

In order to model the energy requirement of AGVs, components of an AGV that have an energy requirement must be defined first. In the next step, the power requirement of the respective system components was defined as a function of its influencing factors. Finally, the total energy requirement can be determined by summing up the power requirements of the respective system components over time.

4.1.1 System Components

The individual components vary depending on the AGV type. For this study, three main components Drives, Controls, and LHD were identified and defined (cf. Figure 4.1). Drives include the electrical power of the drives and motor controls, as a function of velocity, acceleration, and the weight of the load being transported. All remaining parameters, such as slip, expressed as friction force,

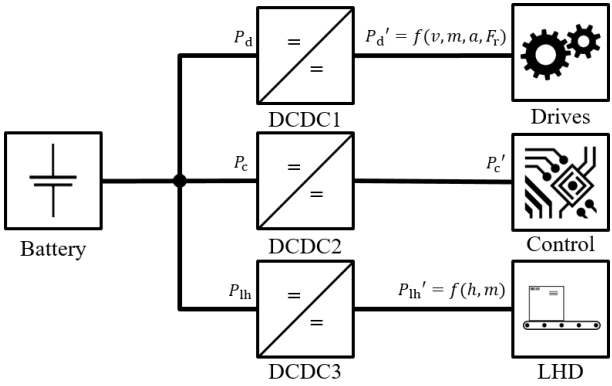

Figure 4.1: Block diagram of defined AGV power requirement components

are considered in the linear power requirement approximation. Motor controllers or regulators are also part of this power requirement component. Controls include all components that are responsible for control, communication, navigation, and localization, as well as system safety. This includes, for example, lighting equipment, safety controls, and safety sensors. Here, unlike shown in Figure 4.1, controls can consist of several individual control units (cf. Sperling and Kivelä (2022) and Hanschek et al. (2021)). Finally, LHD includes all components that are involved in the load handling process. These include lifting or transfer drives, hydraulic pumps, as well as associated control, communication, and sensor units. As shown in Figure 4.1, for each power requirement component, direct current converters (DCDC) are connected in series to regulate the voltage level between an ESS and the system components. The efficiency of the DCDCs μ_{DCDC} is typically described as a function of the output current Arbetter et al. (1995). Therefore, the power requirement of the system components P_{comp} considering DCDC is related to the actual power requirement of the components $P_{\mathrm{comp}'}$ as follows:

$$P_{\mathrm{comp}} = P_{\mathrm{comp}'} \cdot \mu_{\mathrm{DCDC}},\ with\ \mu_{\mathrm{DCDC}} \in \mathbb{R}\,(0, 1] \tag{4.1}$$

4.1.2 Process Analysis

To be able to describe the behavior of different AGVs in a holistic way, process states have to be identified. In addition to the two state diagrams presented for AGV process description (cf. Figure 2.2, and Figure 2.3), Komma et al. (2012) and Flake (2003) have presented further state diagrams to the model system behavior of AGVs. From these previous studies, the process states *Acceleration without load*, *Acceleration with load*, *Drive without load*, *Drive with load*, *Deceleration with load*, *Deceleration without load*, *Pickup*, *Deliver* and *Standby* can be distinguished. *Standby* summarizes the processes waiting, blocking, and idle. In the course of a qualitative process analysis, in which 25 different AGVs were examined, it was found that in addition to previously identified states, four additional states are required to develop a holistic description model. These are *Prepare docking*, *dock*, *undock*, and *prepare driving*. *Prepare docking* includes waiting times for process calculation and initialization of the LHD for docking. Similarly, *Prepare driving* includes process calculation waiting times and initialization of the LHD for driving. The initialization for *driving* includes substates that bring the vehicle into a state ready for driving. This includes, for example, lowering the LHD to a defined transport height.

4.1.3 Impact Analysis

After defining the power requirement components and process states for AGVs, the factors that impact the power requirements of these system components were identified. The literature review presented in Section 2.5 shows that speed, acceleration, weight of the load, and movement direction have a significant impact on the electrical power requirement of the Drives. Another impact on the power requirement of the Controls is ambient temperature. Cebrian and Natvig (2013) stated that the power requirement of processors is highly temperature dependent. Finally, the weight of the load has a significant impact on the power requirement of the LHD (cf. Table 2.1, Meißner and Massalski (2020)).Table 2.1 shows, that the energy requirement E is often modeled as a function of time t or as a function of

transport distance d. The transport time t or the transport distances d are further affected by other characteristics as mentioned in Table 2.1. These include material flow and layout, OS, dispatching method used, and CIS distribution. Based on the findings of this impact analysis, a model to approximate the energy requirement was developed, described in more detail in Section 4.1.5 and 4.1.6.

4.1.4 Linear Power Approximation

To model the power requirement of the Drives, the functional relations between mass, velocity, acceleration, deceleration, and the movement direction are simplified by linear approximation. This approach was also used in Freis and Günthner (2016), Kabir and Suzuki (2019), Hamdy (2019), McHaney (1995), Singh et al. (2022), Abderrahim et al. (2020), Colling et al. (2019), and Zhai et al. (2006). The power requirements of the individual system components are assigned to different states, which are listed in Table 4.1. They are mapped to the states of the ERM (cf. Section 4.1.5). In addition to the parameters listed above, further parameters are required for the ERM. These are acceleration a_{acc}, deceleration a_{dec}, velocity v, C-rate for charge c_{r}, typical process state times $t_{\mathrm{state},i}$ as well as MLD (cf. Chapter 3).

4.1.5 Energy Requirement Model (ERM)

Based on the identification of the system components with a power requirement (cf. Section 4.1.1), a process analysis (cf. Section 4.1.2), a power requirement impact analysis (cf. Section 4.1.3), a resulted linear power requirement approximation (cf. Section 4.1.4), and a holistic state-based model was elaborated as shown in Figure 4.2. Therefore, the ERM can approximate the power requirement of different AGVs.

Table 4.1: ERM parameter for different operation states

Parameter	Component	Description
$P_{\mathrm{d}}^{\mathrm{facc}}$	Drives	Full load acceleration
$P_{\mathrm{d}}^{\mathrm{fd}}$	Drives	Full load drive
$P_{\mathrm{d}}^{\mathrm{fdec}}$	Drives	Full load deceleration
$P_{\mathrm{d}}^{\mathrm{eacc}}$	Drives	No load acceleration
$P_{\mathrm{d}}^{\mathrm{ed}}$	Drives	No load drive
$P_{\mathrm{d}}^{\mathrm{edec}}$	Drives	No load deceleration
$P_{\mathrm{d}}^{\mathrm{stby}}$	Drives	Standby
$P_{\mathrm{d}}^{\mathrm{dock}}$	Drives	Docking
$P_{\mathrm{d}}^{\mathrm{undock}}$	Drives	Undocking
$P_{\mathrm{c}}^{\mathrm{stby}}$	Controls	Control while standby
$P_{\mathrm{c}}^{\mathrm{active}}$	Controls	Control while active
P_{lh}^{+}	LHD	Pick up load
P_{lh}^{-}	LHD	Drop off load
$P_{\mathrm{lh}}^{\mathrm{stby}}$	LHD	Standby
$P_{\mathrm{lh}}^{\mathrm{preLH}}$	LHD	Move LHD to pick/drop height
$P_{\mathrm{lh}}^{\mathrm{preDrive}}$	LHD	Move LHD to transport height

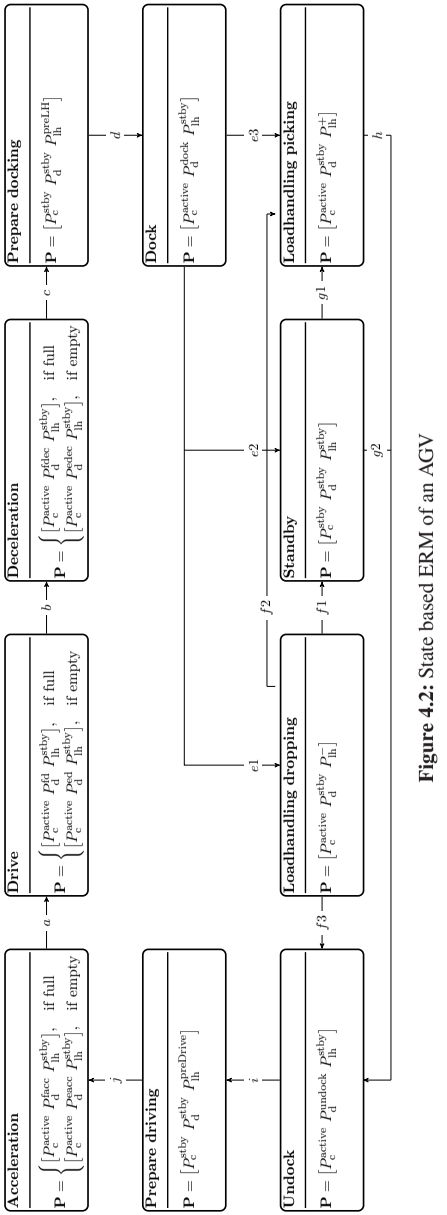

Figure 4.2: State based ERM of an AGV

Figure 4.2 shows 10 different states describing the previously mentioned process states of an AGV, each containing a vector $\mathbf{P_{state}}$, including the individual power requirements:

$$\mathbf{P_{state}} = \begin{bmatrix} P_{\mathrm{ctrl}} & P_{\mathrm{drives}} & P_{\mathrm{lh}} \end{bmatrix} \tag{4.2}$$

The arrows connecting the states describe the possible linkage of states to an overall process. The initial state is standby. After standby either a run can be started via states *Undock* (g2), *Prepare driving* (i) and *Acceleration* (j) or a load can be picked up at the current position (*LH pick up* via g1). If the vehicle is in *Acceleration* state, then state *Constant drive* is achieved after reaching the target velocity v (a). With the initiation of a braking process at the end of a run, *Deceleration* (b) becomes active. After stopping, the next states *Prepare docking* and *Dock* become active in sequence. After reaching standstill again, three states are possible, *LH pick up* via (e3), *LH drop off* via (e1), or *Standby* via (e2). *Standby* can be reached if waiting times are required due to interruptions in the operating flow. If the AGV is in *LH drop off* state, *Standby* (f1), *LH pick up* (f2) or *Undock* (f3) state is reachable accordingly. From *Standby* state, either *Undock* (g2) can be initiated directly, or a load can be picked up (*LH pick up* via g1).

4.1.6 Energy requirement Approximation

As a result of the impact analysis (cf. Section 4.1.3), the distance is not sufficient for the approximation of the total energy requirement of AGVs. To approximate the total energy requirement of an AGV in operation more accurately, data of the actual material flow and layout are required. However, the linear power requirement approximation of the AGV must be available and the power characteristics must be known. In order to determine the partial energy requirements of AGVs in the respective states according to Figure 4.2, the average durations $t_{\mathrm{state},i}$ of the corresponding process states i are required. Starting at a nominal time t_0, the

power vector $\mathbf{P}$ will be integrated until $t_0 + t_{\mathrm{state},i}$, mathematically formulated as follows:

$$\mathbf{E}_{\mathrm{state},i} = \int_{t_0}^{t_0+t_{\mathrm{state},i}} \mathbf{P}_{\mathbf{state}}(t)\,\mathrm{d}t, \quad i \in \mathbf{I} \tag{4.3}$$

$\mathbf{I}$ describes a set of all states that are within an evaluation period t. Considering v, a_{acc}, a_{dec}, and the current transport distance d_j, the process duration $t_{\mathrm{Drive},i}$ for state *Constant drive* can be determined as follows:

$$t_{\mathrm{Drive},j} = \frac{d_j}{v} - \frac{v}{2a_{\mathrm{acc}}} - \left|\frac{v}{2a_{\mathrm{dec}}}\right| \tag{4.4}$$

The total scalar energy requirement $E(t)$ is the sum of all individual states as a function of A_{T}, A_{D}, the evaluation period t, and the dispatching method used (cf. Section 2.1.2). Mathematically, this is formulated as follows:

$$E = \sum_{i \in \mathbf{I}} \sum_{k=1}^{3} \mathbf{E}_{\mathrm{state},i,k} \tag{4.5}$$

where k describes the respective entries of the vector $\mathbf{E}_{\mathrm{state}}$.

4.2 Implementation

The previously presented model was implemented as a discrete-time simulation model in Java. It comprises a central dispatcher and an upstream standalone application for generating transport orders based on MLD. The process sequence for the simulation of the power requirement of an AGV is listed below.

1. Identify power characteristics and periods of individual states according to Section 4.1.5
2. Identify MLD (cf. Chapter 3)
3. Import parameters from step 1 and 2

4. Generate order list
5. Execute simulation

4.2.1 Dispatching Implementation

A first come first served rule was chosen for the dispatching implementation, as this ensures the same processing order in the simulation and the experiment. Besides emulating the incoming transport orders, the dispatcher is also responsible for assigning transport orders to the vehicles by communicating with them. The model was developed for multi AGV fleets, whereby the experimental validation was carried out with a single AGV.

4.2.2 UML based Software Module Diagram

Based on a UML class diagram Figure 4.3 shows the most important modules with their functions and parameters as well as the interfaces within the ERM simulation model.

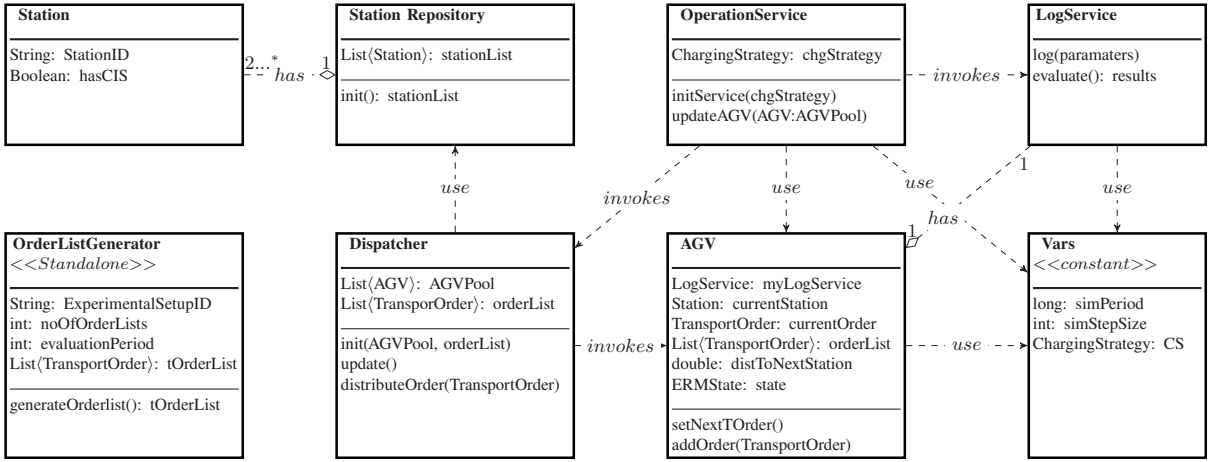

Figure 4.3: UML based software module diagram for ERM simulation

The class $Vars$ contains constant simulation parameters that are needed for the simulation. These include the evaluation period $simPeriod$, the simulation step size $simStepSize$, the applied CS, and the state power parameters (cf. Section 4.1.4). The AGV class consists of the parameters described in Section 4.1.4 as well as the variables listed in Figure 4.3. They are initialized instancing from the same named parameters from the $Vars$ class. Furthermore, AGV contains a separate function for each state presented in Section 4.1.5, where the parameters of the subclasses LHD, $Drives$, $Controls$ and ESS are updated each time the corresponding state functions are called by $OperationService.updateAGV()$. $StationRepository$ contains a list of all stations of the current MLD. The stations consist of the parameters ID, and $hasCharging$. If a $Station$ has a charging station, $hasCharging$ is true, otherwise false. The main process is programmed to run in cycles. Compared to an event based simulation, cycle based offers the opportunity for parallel time recording of the power and energy data of the individual AGVs. This simplifies the calculation of the power requirement which is time dependent as mentioned in Section 4.1.6. Furthermore, the centrally programmed dispatching is able to allocate it considering the vehicle capacity utilization. The simulation cycle runs with a step size of $simStepSize$ from class $Vars$ for the duration of $simPeriod$ (equivalent to the evaluation period t in Section 4.1.6). Before the main cycle starts, $init()$ of the $Dispatcher$ class and $initService()$ of the $OperationService$ class are called. Next, a central pool of similar AGVs is initialized. Afterwards the main process begins, in which at each simulation time step first the $update()$ method of the $Dispatcher$ and then $OperationService.update()$ is called for each AGV of the $AGVPool$.

4.2.2.1 Dispatcher

The $update()$ method of the dispatcher checks whether the timestamp of a transport order on the $orderList$ matches or is lower than the current simulation time. If one of these cases occurs, the order or orders are transferred to the vehicles of

the central $AGVPool$. Only the current transport costs, defined by the remaining transport distances of all orders in the $orderList$ of an AGV, are taken into account for order assignment. The vehicle with the lowest capacity utilization is assigned the order unless the destination station of the last transport order from the $orderList$ matches the start station of the order to be assigned. If this matches for several vehicles, the order is assigned to the lowest utilization among these vehicles. If the utilization among these vehicles matches, the order is finally assigned according to the ID of the vehicle. The order allocation is performed by calling the $addOrder()$ function of the chosen AGV from the central pool.

4.2.2.2 OperationService

The $updateAGV()$ method of $OperationService$ updates all vehicles of the vehicle pool, including the current transport order, the remaining distance to the target station, the current state and its corresponding power requirement, the current speed, and the current SoC. Depending on the current state of the vehicle, the power requirement of the system components (cf. Section 4.1.1), the current speed, and the distance to the next station $distToNextStation$ are recalculated. If $distToNextStation \leq 0$ and the state dock is completed, the current station will be overwritten with the end station of the current transport order. Afterwards, $setNextTOrder()$ is called. The current transport order $currentOrder$ is overwritten with the next order of the local $orderList$. If the list does not contain any orders, $currentOrder$ will be reset. As long as no new $TransportOrder$ is assigned to the vehicle, it remains in the standby state. At the end of the $updateAGV()$ method, the $log()$ method of the AGV associated instance of $LogService$ is called.

4.2.2.3 LogService

After the completion of a main cycle, $evaluate()$ is called for all $LogServices$ from all AGVs in the central pool. Parameters like load, total distance, number of

orders and others are determined. The results of the simulations are then stored in .csv files.

4.2.2.4 OrderListGeneration

To ensure experiments under statistically reproducible conditions, transport order lists are generated following uniformly distributed order arrival times. As depicted in Figure 4.3 the *OrderListGenerator* is a standalone application that makes use of the same classes as in the simulation. The first loop of the function creates the transport orders based on the job list generated from the transport and distance matrices of the corresponding MLD as described in Sperling et al. (2023). The guaranteed transport orders are created equal to the whole part of each frequency $f_{i,t}$, which can be calculated as $f_{i,t} = f_i + \{f_{i,t-1}\}$. where $f_{i,t=1} = 0$ is valid. The fractional part $\{f_i\}$ represents the residual frequency $\{f_{i,t}\} \in \mathbb{R}, [0..1)$ in the corresponding hour t. The remaining frequency is then used as the probability that another transport order of the same type will be created within the same hour is created under the condition that $\{f_{i,t}\} \in \mathbb{R}, [0..1)$. In the second step, the new residual frequency for the next hour $t + 1$ is calculated based on the following rule:

$$f_{i,t+1} = \begin{cases} f_{i,t} + \{f_{i,t-1}\} - 1, & \text{if order was assigned} \\ f_{i,t} + \{f_{i,t-1}\}, & \text{otherwise.} \end{cases} \tag{4.6}$$

Finally, the transport order list is sorted by the timestamp of the orders. The experimental setup for the AMR Karis only allowed for order batches with a reoccurring sequence. This ensures that the source stations of the current order have a load ready to pick up and the sink stations are free to drop off the load. Hence only the inter-arrival times of the batches within each hour are varied.

4.3 Verification and Validation

This section presents the verification of the ERM through qualitative process analysis, followed by a description of the quantitative validation.

4.3.1 Qualitative Process Analysis

To demonstrate the validity of the state-based ERM (cf. Section 4.1.5, Figure 4.2), a qualitative process analysis was performed over 25 AGVs of different types from various manufacturers. For this purpose, publicly available video material was analyzed (cf. Appendix A.5). Among all 25 AGVs, the *prepare docking* state was observed in 21 AGVs. Within these 21, 10 initialized their LHD during this state for subsequent docking. The *prepare driving* state was observed in 20 AGVs. Among these, seven AGVs initialized their LHD in this state for subsequent driving. In total, the states *dock*, *loadhandling*, and *undock* were observed in 22 AGVs. The three remaining vehicles have no active LHD. Based on the results of this qualitative analysis, it is assumed that the state-based ERM is valid for AGVs of diverse configurations. If an AGV is missing any of the established process steps, the respective duration time is set to zero in the ERM. This ensures the functionality of the model for each vehicle specific process.

4.3.2 Quantitative Validation

Further, the ERM is validated by comparison with experimental energy consumption measurement data. For this purpose, experiments were performed on two different AGV types. The experiments were equally performed by the simulation model described in Section 4.2. After evaluation of the experiments and the simulations, the average hourly energy requirements of the individual system components, as well as of the entire system, were compared. Two industrial-used AGVs were available for the experiments, as shown in Figure 4.4. The vehicles differ in their chassis geometry, LHD, navigation type as well as type of energy supply.

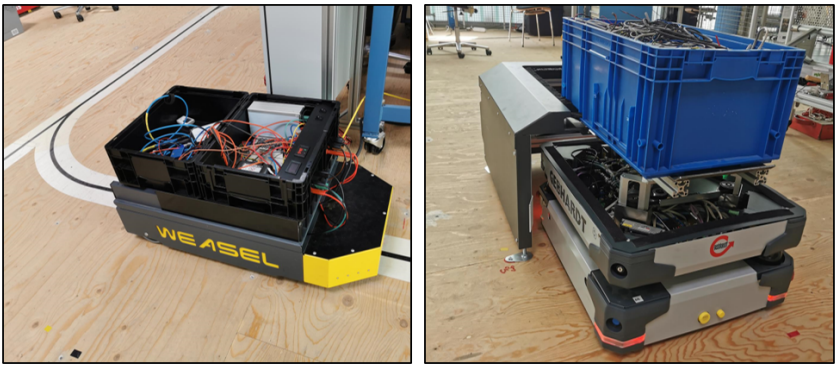

Figure 4.4: Industrial AGVs Weasel (left) and Karis (right) used in real experiments

4.3.2.1 Variation parameters

As described in Section 4.1.3, it was assumed that the speed of the vehicle, as well as the load to be transported and the transport distance or transport time, have an effect on energy consumption. Furthermore, it was expected that the utilization of the vehicles and the CS used would have a major impact on energy consumption. For this reason, in the experiments described below, speed, CS, load handling durations, vehicle utilization, load to be transported, transport layout, and the number and distribution of transport orders were varied. Within the two different vehicles, three different ESS are used.

4.3.2.2 Design of Experiments

Table 4.2 shows the parameters of the corresponding experimental setups. For AGV Weasel, in *ExperimentalSetup01A* to *EpxerimentalSetup01C*, the speed was varied for the same transport order input. Between these, *ExperimentalSetup02* and the following experimental setups the loadhandling time was varied. From *ExperimentalSetup03* to *ExperimentalSetup06*, the CS I was evaluated by varying the utilization of the vehicle as well as the CIS distribution. In *ExperimentalSetup07* to *ExperimentalSetup10*, the CS O was investigated. For this purpose,

the lead-acid ESS of AGV Weasel was replaced by an EDLC ESS. Here, the utilization of the vehicle as well as the CIS distribution was also varied. The transport orders for the experiments *ExperimentalSetup01A* to *ExperimentalSetup10* were randomly distributed as in Section 4.2.2.4. Between *ExperimentalSetup11* and *ExperimentalSetup13*, AMR Karis was used, varying both the vehicle load and the CIS distribution. Similarly, the flow path orientation differed as specified in Sperling et al. (2023). The transport tasks were generated according to a fixed sequence (cf. Appendix A.6). Depending on the workload to be achieved as seen in Table 4.2, these sequences were considered up to three times per hour for the creation of the transport order lists.

Table 4.2: Design of real experiments. S7 is the station with an CIS. C: Capacitive, I: Interim, O: Opportunity. Utilization marked with * are based on simulation results.

	ExperimentalSetup	Freq. of S7	Utilization planned	Utilization actual	t_{lh}	v	m_{load}	C-rate	CS	t_{op}	No. of Exp.
Weasel Lead-Acid	ExperimentalSetup01A	0	0.5	0.54	5s	1.0m/s	-	0.25	C	8h	4
	ExperimentalSetup01B	0	0.95	0.95	5s	0.5m/s	-	0.25	C	8h	3
	ExperimentalSetup01C	0	0.75	0.77	5s	0.7m/s	-	0.25	C	8h	3
	ExperimentalSetup02	0	0.7	0.72	15s	1.0m/s	-	0.25	C	8h	3
	ExperimentalSetup03	0.05	0.5	0.48	10s	1.0m/s	-	0.25	I	8h	3
	ExperimentalSetup04	0.05	0.9	0.89	10s	1.0m/s	-	0.25	I	8h	3
	ExperimentalSetup05	0.15	0.5	0.48	10s	1.0m/s	-	0.25	I	8h	3
	ExperimentalSetup06	0.15	0.9	0.95	10s	1.0m/s	-	0.25	I	8h	3
Weasel EDLC	ExperimentalSetup07	0.15	0.5	0.57	10s	1.0m/s	-	10	O	24h	1
	ExperimentalSetup08	0.15	0.9	0.87	10s	1.0m/s	-	10	O	24h	1
	ExperimentalSetup09	0.25	0.5	0.62	10s	1.0m/s	-	10	O	24h	1
	ExperimentalSetup10	0.25	0.9	0.87	10s	1.0m/s	-	10	O	24h	1
Karis	ExperimentalSetup11	0.143	0.9	0.96*	-	1.0m/s	10kg	1.0	O	24h	1
	ExperimentalSetup12	0.077	0.9	0.86*	-	1.0m/s	20kg	1.0	O	24h	1
	ExperimentalSetup13	0.04	1.0	1.00*	-	1.0m/s	30kg	1.0	O	24h	1

4.3.2.3 Stepsize Analysis

In order to parameterize an appropriate step size, a case study was conducted to consider the accuracies of the simulated energy requirement as the step size varied. The case study was performed on the results of *ExperimentalSetup01A*, which is made up of four real experiments, each $8\mathrm{h}$ in duration. The simulation of the corresponding experiments was performed with step sizes $s_\mathrm{s} \in \{10\mathrm{ms}, 50\mathrm{ms}, 100\mathrm{ms}, 500\mathrm{ms}, 1000\mathrm{ms}\}$. Figure 4.5 shows the variation of the relative deviation of the hourly approximated energy requirement of the Drives, as well as the relative deviation of the hourly approximated energy requirement of the Controls as a function of the step size s_s. In addition to the course of the relative

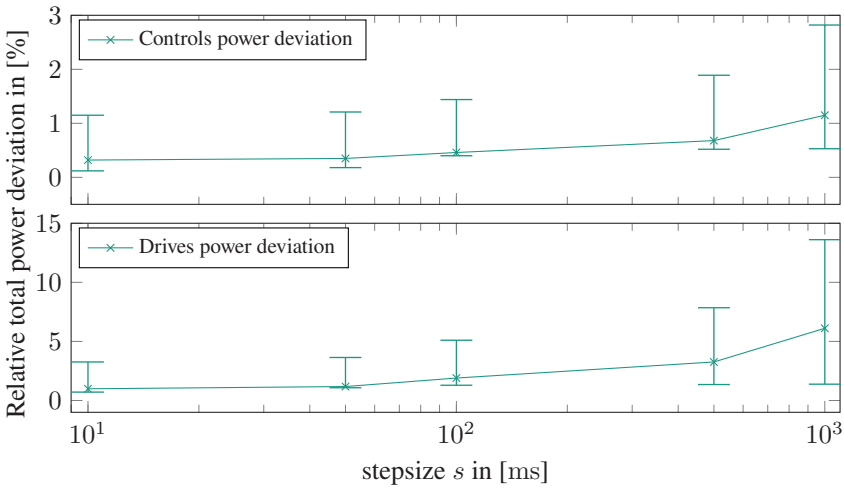

Figure 4.5: Step size analysis

deviation, the diagram also shows the lower and upper limits of the confidence interval at a significance level of $\alpha = 0.01$. With regard to efficient simulation and a limited quality improvement at a stepsize of $s_\mathrm{s} \leq 100\mathrm{ms}$, $s_\mathrm{s} = 100\mathrm{ms}$ was applied for all simulations described below.

4.3.2.4 Sample Size Estimation

In order to obtain significant results for the energy requirement, extended test periods are required. For this purpose, the observation period for determining the energy requirement was set to one hour. Within this hour, each vehicle-specific process (cf. Section 4.1.5) is run entirely for at least 10 times. Again *ExperimentalSetup01A* is used to determine the required sample rate per experiment. The sample size of $n = 24$ was chosen under the assumption of a normal distribution of the results (cf. Appendix A.10) and considering a typical operation time of an AGV of $24\mathrm{h}$. The Anderson Darling Test can be applied to the results of the study as described in Dodge (2008) and Berlinger (2021). The evaluation allows assuming normally distributed results which therefore will be applied to all subsequent experiments.

4.3.3 Experimental Setup

The experimental setup at the test area of the Institute of Material Handling and Logistics at the KIT consisted of a variable transport layout, several transfer stations, CISs, and the two mentioned industrial AGVs. For the AGV Weasel, the experimental setup further consists of the Weasel Fleet Controller (WFC) and a custom designed CIS. The transport layout for this vehicle was installed with optical lines on the ground and associated radio frequency identification (RFID) tags, as shown in Figure 4.6. The CIS was installed at station S7. Since AMR Karis is controlled decentrally, there is no central master control as the WFC. Compared to AGV Weasel, AMR Karis uses a manufacturer-specific CIS, which was placed at S7x. A load transfer is not possible here. Three load transfer stations were placed at S1x, S4x and S6x. The stations S1, S4, S6, and S7 are served, which correspond to the same stations of the AGV Weasel layout. In the case of AMR Karis, however, the docking process is added, in which the vehicle docks from the position $\mathrm{S}i$ to the corresponding station $\mathrm{S}i\mathrm{x}$. The navigation and localization is performed by environment detection with a 2D laser scanner.

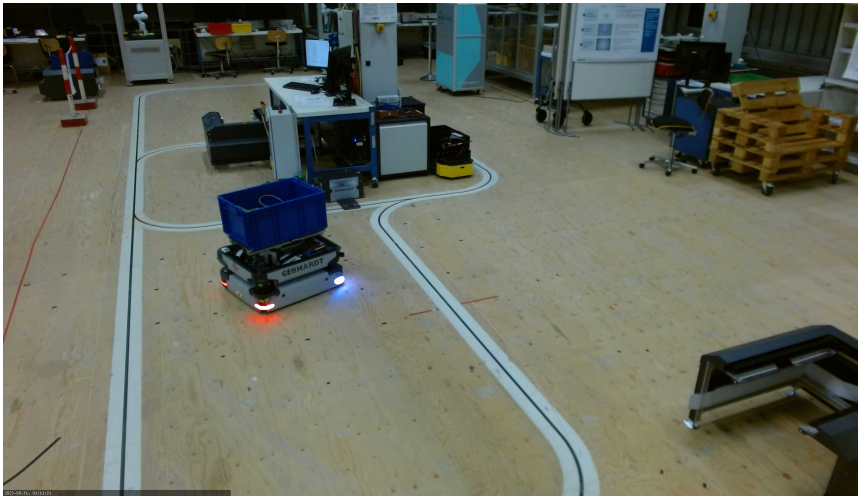

Figure 4.6: Combined experimental setup for AMR Karis (left) and AGV Weasel (center), transport layout with optical track for AGV Weasel and three load transfer stations for AMR Karis

Figure 4.7 shows the transport layout as a representation of a directed graph. The continuous paths are visually marked routes for AGV Weasel. The path to and from station S7 is marked grey, as this is only used for charging or for jobs that start or end at S7. This represents a path with a high edge weight, which may be the case, in busy traffic areas in an intralogistics environment. A virtual line was defined for AMR Karis, which is represented by a dotted line. The nodes marked with a • allow AMR Karis to leave the given virtual line in order to approach the corresponding stations. For both systems, a central application was developed in Java that emulates the assignment of the transport orders of the corresponding transport order lists. The application saves the start and end time of the experiments and sends transport orders into the master control (cf. WFC) or directly into the order buffer of the AMR Karis. The transport orders were assigned to the vehicles as described in Section 2.1.2.

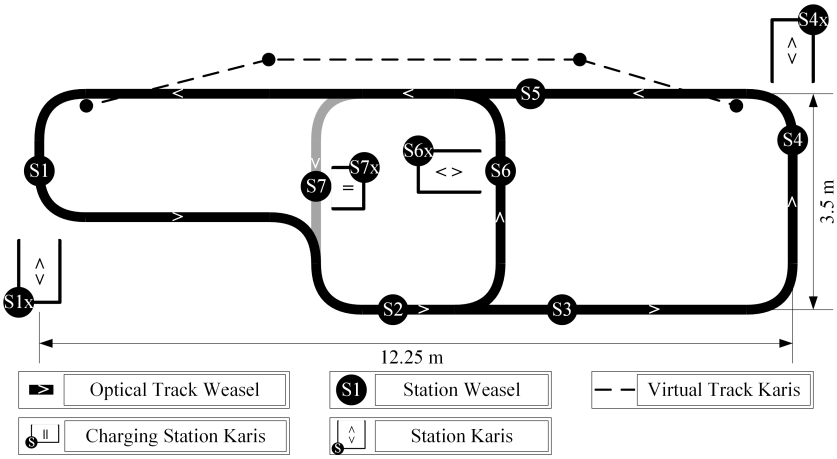

Figure 4.7: Experimental layout for AGV Weasel and AMR Karis

4.3.4 Measurement System

The energy measurement is performed by a measuring system of the company Klaric as shown in Figure 4.8. The measurement system consists of a KLARICORD 5 data logger and four LP-Probe-10mR probes for power consumption measurement. The power supply for the measurement system is provided by an external Makita $18.0\mathrm{V}, 3.0\mathrm{Ah}$ battery. The data logger samples the power consumption data at a frequency of $100\mathrm{kHz}$ and stores the data with a moving average of $1.0\mathrm{kHz}$ on an external data carrier. Appendices A.1 and A.2 show the measurement concepts for the two vehicles fitted to the respective system components. A channel describes a probe of the type LP-Probe-10mR, measuring both the current and the voltage. If several channels were connected to the same voltage potential, the voltage was only measured with one of these channels in order to minimize the amount of data to be stored. The measurement system also includes a temperature data logger from Testo, type 174T which was parameterized to a recording rate of 60 values per hour.

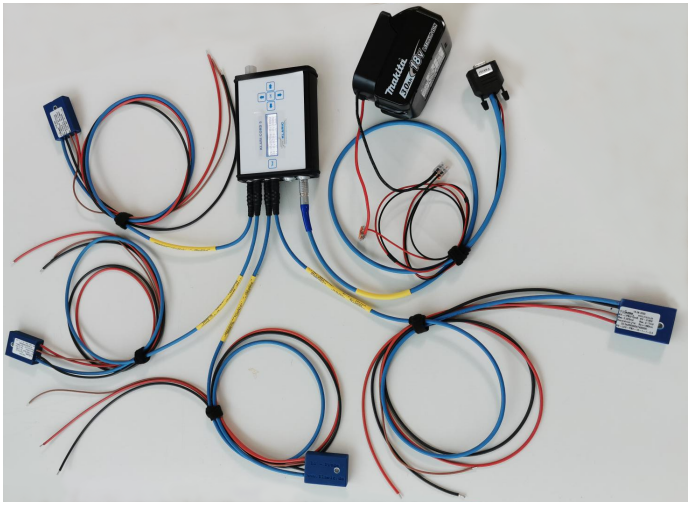

Figure 4.8: Klaric Measurement System

4.3.5 Experimental Data Evaluation

To evaluate the collected data of each measurement channel as well as the temperature data, they were read in a Matlab script. After reading the start and end timestamp from the respective experiment, the data were synchronized and trimmed to the time period to be considered.
By analyzing the measured power consumption data, it was possible to determine threshold values in the different measurement channels to identify the different process states according to Section 4.1.5. Subsequently, the power consumptions were divided into classes corresponding to the processes of the ERM. Each class was finally analyzed individually for process duration and average power consumption to linearize the process specific power requirements. These results are required as input parameters for the ERM. Furthermore, the average energy requirements per hour were determined. These are the values that are used as comparison parameters with the simulation model subsequently. The results of the experimental data evaluation can be found in Appendix A.9.

4.4 Results

To validate the ERM and to determine its quality, 15 real experiments with two test vehicles were conducted. During these experiments, energy consumption data was recorded over 296 h of operating time for AGV Weasel and 70 h of operating time for AMR Karis in total. During the experiments, the AGV Weasel drove a total distance of 202 km and the AMR Karis 13.6 km.

4.4.1 ERM and Experiments Comparison

The experiments performed were simulated (cf. Section 4.2) and the results were compared. Figure 4.9 shows an example plot of the power consumption data of AMR Karis during a randomly selected transport cycle from *ExperimentalSetup13*. Starting with a loadhandling dropping process (A), the system subsequently goes through the states undock (B), prepare driving (C), drive (D), prepare docking (E), dock (F), and picking (G). The prepare docking as well as dock states are repeated four times in this random cycle until the dock operation is completed. The three diagrams in Figure 4.9 show the power consumption of the Controls, the Drives, and the LHD from top to bottom. The dotted lines describe the modeled linear power consumption according to Section 4.1.4. The vertical black lines show the bounds of the respective states of the model (cf. Section 4.3.5). Since the power consumption of the Drives during the drive state did not provide assignable power peaks for acceleration and deceleration, the acceleration and deceleration states were not parameterized in the simulation. The acceleration and deceleration phases were therefore implicitly taken into account by the state drive.

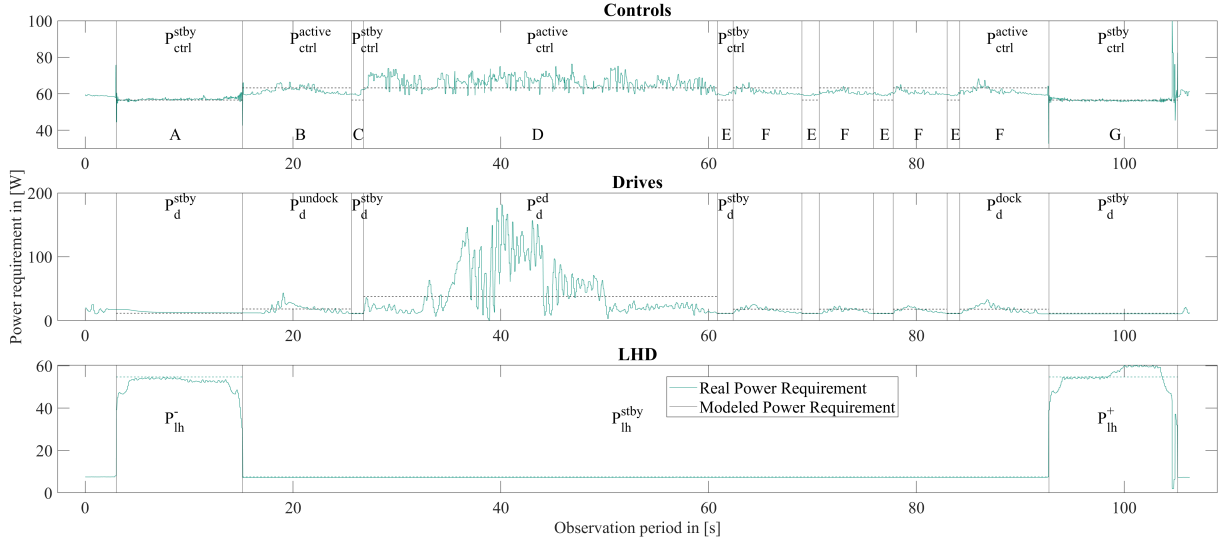

Figure 4.9: Comparison of measured power consumption and modeled power requirement

4.4.2 Evaluation

The quality of the model is evaluated by comparing the simulative results with the experimental results. The results of the comparison are the relative deviations Δ_{P} of the average power requirements of the individual system components k (cf. Section 4.1.1) and were calculated according to the following calculation rule:

$$\Delta_{\mathrm{P},k} = \frac{P_{\mathrm{Sim},k} - P_{\mathrm{Exp},k}}{P_{\mathrm{Exp},k}} \tag{4.7}$$

The comparison results are hereafter referred to as samples. After assuming the normal distribution of the samples (cf. Section 4.3.2.4), a confidence interval procedure was chosen to determine the quality of the model Schiefer and Schiefer (2021) and Plaue (2023). Based on the samples of relative deviations of energy requirement, the lower and upper bounds of the confidence intervals for the significance levels of $\alpha = 0.05$ and $\alpha = 0.01$ were set. They can be found in Appendix A.10. In the upper part of Figure 4.10 the relative energy requirement deviation of the corresponding system components of the AGV Weasel is shown. Whereas in the lower part, the deviations of the AMR Karis can be seen. The marked points describe the corresponding mean value of all tests performed with the respective vehicle. The horizontal lines describe the limits of the confidence intervals at a significance level of $\alpha = 0.01$. It can be seen that the Controls were modeled within the confidence interval of $-0.82\,\%$ to $-0.37\,\%$. The accuracy of the energy requirement approximation for the Drives varies between the two vehicles. For AGV Weasel, the confidence interval is in the range of $-2.98\,\%$ to $-1.84\,\%$ whereas for AMR Karis, the confidence interval is in the range of $-0.67\,\%$ to $0.33\,\%$. Due to the technical equipment, the energy requirement of the LHD could only be investigated for the AGV Karis. The relative deviation of the energy requirement of the LHD lies in the confidence interval of $-2.50\,\%$ to $-1.60\,\%$. Overall, the total energy requirements of the AGV Weasel was determined within a confidence interval of $-1.86\,\%$ to $-1.14\,\%$ and for the AMR Karis within a confidence interval of $-0.73\,\%$ to $-0.31\,\%$, each at a significance level of $\alpha = 0.01$. These, as well as the results of each individual experiment and for a further significance level of $\alpha = 0.05$, can be found in Appendix A.10.

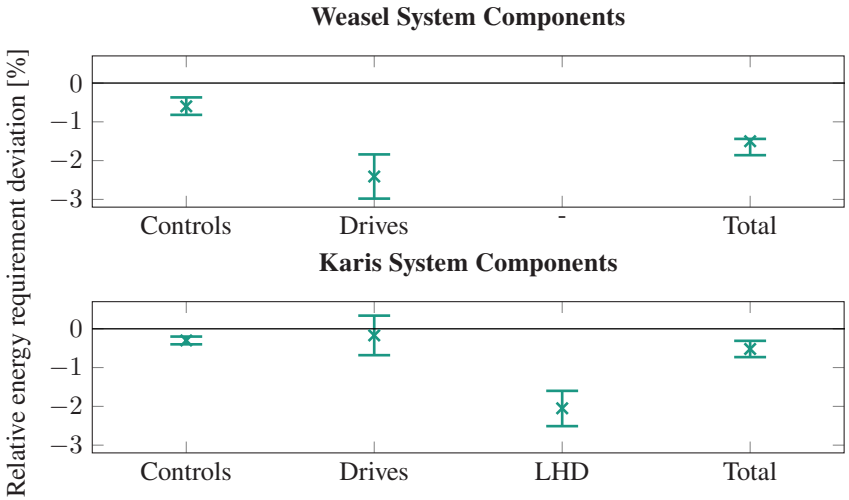

Figure 4.10: System component dependent relative energy requirement deviation, calculation based on Equation 4.7

4.4.3 Discussion

The results show that the controls could be modeled more accurately compared to the Drives and the LHD. This can be attributed to environmental affect such as friction force, as Liu and Sun (2014), Meißner and Massalski (2020) have shown. Furthermore, the modeling of the Drives for AMR Karis was more accurate than that of the AGV Weasel. One possible explanation for this is that the rated power of the Drives of the AGV Weasel is only about $1/3$ of the rated power of the Drives of the AMR Karis. Environmental impacts, such as the friction force mentioned earlier, may have a greater relative impact on the power required here. In most cases, the energy requirement was underestimated.

Furthermore, necessary assumptions for the experimental setups were made. In regard to the real experiments, the CISs were always installed directly at load transfer stations which is valid for experiments with CS I and O. A charging process always starts simultaneously with a load handling process. For the implementation of the dispatching method for real experiments and simulations, each transport

order starts with a load pickup and ends with a load delivery, a load handling process is not performed while empty runs. In addition to the assumptions, one of the limitations of the ERM is, that since a linear power approximation is performed in the ERM, efficiencies of DCDC as well as acceleration and deceleration cannot be specified as a functional quantity. Further, the ERM cannot consider possible collisions or traffic rules of AGVs, which are further assumed to be single load. Finally, the ERM cannot consider the influencing factors of various ESS and CIS.

4.4.4 Further Findings

In addition to these observations, further findings are shown in Figures 4.11 and 4.12. Figure 4.11 shows the impact of the three factors load, vehicle utilization and CS to the relative total energy deviation. Considering the influencing factor "load", it can be seen that the accuracy of the energy requirement approximation decreases with increasing load. The width of the confidence interval also widens. For one case, it can be seen that the accuracy decreases with increasing utilization and the width of the confidence intervals also widens. In the bottom graph, it can be seen that the experiments with the CS O could be estimated with an interval of $-2.62\,\%$ to $-0.26\,\%$, followed by the CS C with an interval of $-4.98\,\%$ to $1.86\,\%$. The experiments with the CS I have been estimated worst with an interval of $-6.64\,\%$ to $0.31\,\%$, where all intervals consider the minimum lower limit and maximum upper limit of the confidence intervals of the respective experiments. Another finding is the unexpected impact of the controls on the total energy requirement of an AGV. In contrast to the studies mentioned in the literature review (cf. Section 2.5), Controls also have a major impact on the total energy consumption of an AGV. Figure 4.12 shows the relative energy requirements of each system component in an AGV. The left part of the figure shows the relative energy consumption of the AGV Weasel for *ExperimentalSetup01A* to *ExperimentalSetup10*. On average, the Controls make up $54\,\%$ and the Drives $46\,\%$ of the total energy consumption. The right part shows that for the AMR Karis with *ExperimentalSetup11* to *ExperimentalSetup13*. On average, the controls make up $63\,\%$, the Drives $24\,\%$ and the LHD $13\,\%$ of the total energy consumption.

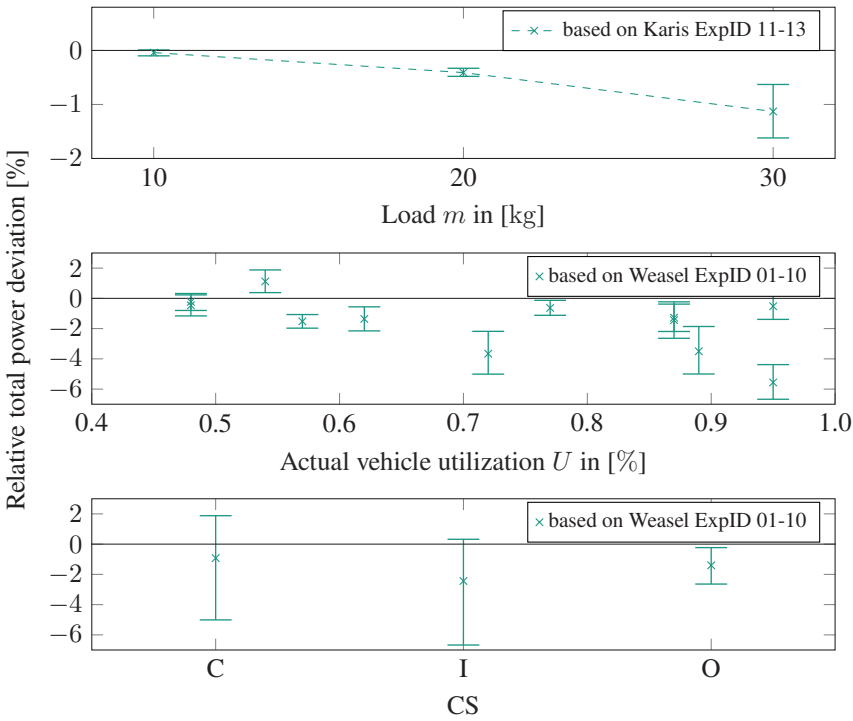

Figure 4.11: Relative power requirement accuracy deviation contrasted by various experiment parameters, calculation based on Equation 4.7

4.5 Chapter Conclusion

This chapter answered RQ2:

> **RQ2: How can the energy requirement for AGVs be modeled, considering the material flow, layout, charging strategy, capacity utilization, and vehicle specifications?**

The ERM for AGVs was presented to answer this research question. The state-based model was verified by comprehensive process analysis and validated with

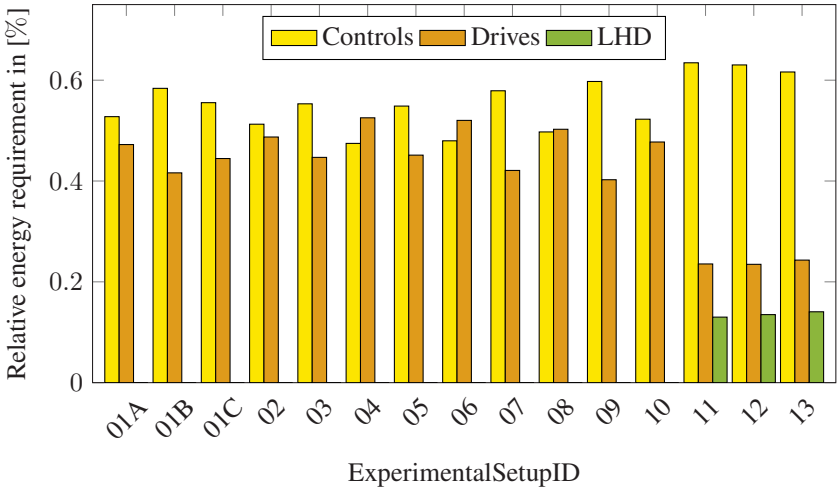

Figure 4.12: Relative energy requirements of each system component of AGV Weasel (01A to 10) and AMR Karis (11 to 13)

real experiments to allow an accurate estimation of the energy requirement of AGVs under multiple constraints. The model had mean estimation accuracies of energy requirement of approximately $99\,\%$ at a significance level of $\alpha = 0.01$ which provided opportunities to estimate the energy requirement of AGVs in advance while considering influencing factors to derive possible energy efficiency measures or to optimize the design of ESS for AGVs. Although this model provided accurate energy requirement estimations for the two vehicle types studied, further investigations were needed to establish the generality of this model. The state-based model could be extended for more complex system behaviors if required and applied to energy requirement modeling of storage shuttle systems through adjustments to the process steps of the ERM. Further investigations are needed to validate these statements with real experiments.

5 Energy Storage Requirement Modeling

5.1 Energy Storage Requirement Model (ESRM)

This section presents the energy storage requirement model (ESRM), which numerically calculates the ESR of AGVs, considering material flow and layout, vehicle types, CIS distributions, and CSs. The ESR indicates the required capacity of the ESS in Wh.

Figure 5.1 shows the input and output parameters of the ESRM. The input parameters include the material flow and layout data in the transport matrix A_{T}, the reference time t_{ref}, and a distance matrix A_{D} (cf. Section 3.6). Furthermore, vehicle-specific parameters must be given, such as the state power requirements and state durations, which are introduced in Section 4.1.5 (cf. Table 4.1), vehicle physics, and the C-rate as a key figure for the charging speed. Finally, design parameters are required, which must be defined beforehand. These include the capacity utilization of the vehicles η_{U}, the availability of the vehicles η_{A}, the operation time t_{op}, the CIS probability p_{chg}, the ratio of transport runs to total runs ρ, and the probability of chained transport orders without CIS (p) for CS O. The results of the ESRM are the fleet size N_{AGV}, the ESR E_{ESS}, and the charging power P_{chg}.

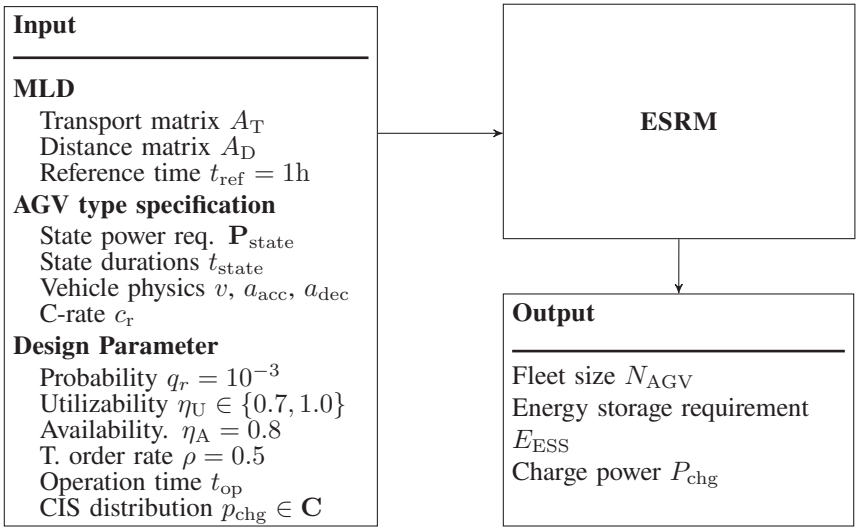

Figure 5.1: Input Model Output diagram for ESRM

5.1.1 Fleet Size Estimation

The first part of the numerical model contains a procedure for calculating the fleet size for each corresponding MLD, considering the type of vehicle used and the CS. For this purpose, the following steps are implemented:

1. Calculating the average transport distance d_{avg} of the specific MLD,
2. Calculating the average transport cycle duration of an AGV t_{cycle},
3. Calculating the number of runs per hour N_{run}, and
4. Calculating the fleet size N_{AGV}.

5.1.1.1 Average Transport Distance

The first step determines the average transport distance d_{avg} of the MLD. T is calculated as Equation 3.1, set to the sum of all transport requests N_{trans} from the transport matrix A_{T}, mathematically described as follows:

$$N_{\mathrm{trans}} = \sum_{m=1}^{N} \sum_{n=1}^{N} \lambda_{mn} \tag{5.1}$$

$$d_{\mathrm{avg}} = \frac{T}{N_{\mathrm{trans}}} \tag{5.2}$$

where λ_{mn} describes the elements of the transport matrix A_{T}. Furthermore, the ratio of the maximum distance d_{max} to the average distance d_{avg} is determined, as the lower limit for the ESR estimation, which is calculated as follows:

$$d_{\mathrm{max}} = \max\{A_{\mathrm{D}}\} \tag{5.3}$$

$$\delta_{\mathrm{d}} = \frac{d_{\mathrm{max}}}{d_{\mathrm{avg}}} \tag{5.4}$$

5.1.1.2 Average Transport Cycle Duration

By assuming linear acceleration, the durations for acceleration and deceleration can be determined based on $t_{\mathrm{acc}} = v \cdot a_{\mathrm{acc}}$ and $t_{\mathrm{dec}} = v \cdot |a_{\mathrm{dec}}|$. Based on the average transport distance d_{avg}, the duration for the state drive can be determined based on Equation 4.4. All other state durations are input parameters of the simulation, as described in Section 4.1.5. The sum of all state durations, except standby, forms the average duration of a transport cycle, considering the MLD and AGV type. Only the duration for load handling is weighted by a ratio ρ

of transport runs fc to all runs including empty runs $\mathrm{fc} + \mathrm{ec}$, mathematically expressed as follows:

$$\rho = \frac{N^{\mathrm{fc}}}{N^{\mathrm{fc}} + N^{\mathrm{ec}}} \quad \text{and} \tag{5.5}$$

$$\begin{aligned} t_{\mathrm{cycle}} = t_{\mathrm{acc}} + t_{\mathrm{drive}} + t_{\mathrm{dec}} + t_{\mathrm{preLH}} + t_{\mathrm{dock}} \\ + \rho \cdot (t_{\mathrm{lh}}^{+} + t_{\mathrm{lh}}^{-}) + t_{\mathrm{undock}} + t_{\mathrm{preDrive}} \end{aligned} \tag{5.6}$$

5.1.1.3 Transport Demand

The number of runs N_{run} is then determined according to the MLD, whereby the number of transport runs N_{trans} from Equation 5.1 is multiplied by the reciprocal value of ρ, including the maximum required empty runs within the operation requirement D_{op}. The result is subsequently multiplied by t_{cycle} from Equation 5.6, resulting in the operation requirement D_{op}.

$$N_{\mathrm{run}} = \frac{N_{\mathrm{trans}}}{\rho} \tag{5.7}$$

$$D_{\mathrm{op}} = N_{\mathrm{run}} \cdot t_{\mathrm{cycle}} \cdot \frac{1}{t_{\mathrm{ref}}} \tag{5.8}$$

5.1.1.4 Fleet Size

Finally, the fleet size N_{AGV} is required. According to Fottner et al. (2022) N_{AGV} is determined as follows:

$$N_{\mathrm{AGV}} = \left\lceil \frac{D_{\mathrm{op}}}{\eta_{\mathrm{U}} \cdot \eta_{\mathrm{A}}} \right\rceil \tag{5.9}$$

where η_{U} describes the degree of utilization of the vehicles and η_{A} describes the degree of availability of the vehicles. The fleet size is rounded to the next higher integer value. For studies using CS C and CS I, capacity utilization of $\eta_{\mathrm{U}} = 1.0$ is assumed since no faults, full charging cycles, or traffic situations are considered. A value of $\eta_{\mathrm{U}} = 0.7$ is assumed for CS O since full charge cycles are considered.

5.1.2 Energy Storage Requirement Estimation

After determining the fleet size N_{AGV}, the number of required runs N_{run}, the operation requirement D_{op}, and other parameters, and the ESR of the AGVs can now be determined, considering the CS. The following steps are implemented for this purpose:

1. Calculating the average energy requirement per cycle E_{cycle},
2. Calculating the energy requirement on standby E_{stby},
3. Calculating the number of runs per vehicle$N_{\mathrm{run}}^{\mathrm{AGV}}$, and
4. Calculating the ESR considering CS $E_{\mathrm{ESS}}^{(CS)}$.

5.1.2.1 Average Energy Requirement per Cycle

Based on the linear power approximation in Section 4.1.4, the energy requirement per cycle can be determined by summing all energy requirements $\mathbf{E}_{\mathrm{state},i}$ of the individual states according to the ERM (cf. Section 4.1.5). Only the energy requirement of the states lh^{+} and lh^{-} are multiplied by the weighting factor ρ according to Equation 5.5, mathematically described as follows:

$$\begin{aligned} E_{\mathrm{cycle}} = E_{\mathrm{acc}} + E_{\mathrm{drive}} + E_{\mathrm{dec}} + E_{\mathrm{preLH}} + E_{\mathrm{dock}} \\ + \rho \cdot (E_{\mathrm{lh}}^{-} + E_{\mathrm{lh}}^{+}) + E_{\mathrm{undock}} + E_{\mathrm{preDrive}} \end{aligned} \tag{5.10}$$

5.1.2.2 Energy Requirement on Standby

The energy requirement of all standby states must be determined to measure the energy requirement of the vehicles. Hence, the energy requirement of all standby states must also be determined. To do this, the total standby time t_{stby} is calculated as a function of the vehicle utilization U_{AGV}. The scalar product with the power vector $\mathbf{P}_{\mathrm{stby}}$ is subsequently determined. The vehicle utilization U_{AGV}

is calculated by the operation requirement D_{op} (cf. Equation 5.8) to the number of vehicles N_{AGV}, mathematically expressed as follows:

$$U_{\mathrm{AGV}} = \frac{D_{\mathrm{op}}}{N_{\mathrm{AGV}}} \tag{5.11}$$

$$t_{\mathrm{stby}} = t_{\mathrm{ref}} \cdot (1 - U_{\mathrm{AGV}}) \tag{5.12}$$

$$E_{\mathrm{stby}} = \mathbf{P}_{\mathrm{stby}} \cdot t_{\mathrm{stby}} \tag{5.13}$$

5.1.2.3 Number of Runs per Vehicle

As a final preparatory step, the number of runs per vehicle $N_{\mathrm{run}}^{\mathrm{AGV}}$ is determined before calculating the ESR. N_{run} from Equation 5.7 is normalized to one hour and is set to the fleet size N_{AGV}, mathematically expressed as follows:

$$N_{\mathrm{run}}^{\mathrm{AGV}} = \left\lceil \frac{N_{\mathrm{run}}}{N_{\mathrm{AGV}}} \right\rceil \tag{5.14}$$

5.1.2.4 ESR Considering CS

Finally, the ESR $E_{\mathrm{ESS}}^{(CS)}$ can be determined. The procedure varies for different CS as described below.

Capacitive (C)

For CS C, the energy requirement per cycle E_{cycle} is multiplied by the number of runs per vehicle and hour $N_{\mathrm{run}}^{\mathrm{AGV}}$, added to the energy requirement on standby E_{stby} and finally multiplied by the operational time t_{op}, mathematically described as follows:

$$E_{\mathrm{ESS}}^{\mathrm{C}} = (E_{\mathrm{cycle}} \cdot N_{\mathrm{run}}^{\mathrm{AGV}} + E_{\mathrm{stby}}) \cdot t_{\mathrm{op}} \cdot \frac{1}{t_{\mathrm{ref}}} \tag{5.15}$$

Interim (I)

Next, for CS I, the ESR E_{ESS} can be calculated from the E_{ESS} based on Equation 5.15 and the energy added to the system by intermediate charges within the operating time t_{op}:

$$P_{\mathrm{chg}} = E_{\mathrm{ESS}} \cdot c_{\mathrm{r}} \tag{5.16}$$

$$E_{\mathrm{chg}} = P_{\mathrm{chg}} \cdot t_{\mathrm{chg}} \cdot N_{\mathrm{run}}^{\mathrm{AGV}} \cdot \rho \cdot p_{\mathrm{chg}} \cdot t_{\mathrm{op}} \cdot \frac{1}{t_{\mathrm{ref}}^2} \tag{5.17}$$

Substituting Equation 5.16 into Equation 5.17 results in:

$$E_{\mathrm{chg}} = E_{\mathrm{ESS}} \cdot c_{\mathrm{r}} \cdot t_{\mathrm{chg}} \cdot N_{\mathrm{run}}^{\mathrm{AGV}} \cdot \rho \cdot p_{\mathrm{chg}} \cdot t_{\mathrm{op}} \cdot \frac{1}{t_{\mathrm{ref}}^2} \tag{5.18}$$

where t_{chg} is assumed to be the minimum intermediate charging time:

$$t_{\mathrm{chg}} = \frac{t_{\mathrm{lh}}^{+} + t_{\mathrm{lh}}^{-}}{2} \tag{5.19}$$

As the charging power P_{chg} and the ESS capacity E_{ESS} are interdependent, a numerical approach is required to determine the ESS capacity, given as a function of the discrete state s:

$$E_{\mathrm{ESS}}(s+1) = E_{\mathrm{ESS}}(0) - E_{\mathrm{chg}}(s) \tag{5.20}$$

With the composite variable κ of the state independent constant parameters (cf. Equation 5.18), a simplified iterative relation is established:

$$\kappa = c_{\mathrm{r}} \cdot t_{\mathrm{chg}} \cdot N_{\mathrm{run}}^{\mathrm{AGV}} \cdot \rho \cdot p_{\mathrm{chg}} \cdot t_{\mathrm{op}} \cdot \frac{1}{t_{\mathrm{ref}}^2} \tag{5.21}$$

$$E_{\mathrm{ESS}}(s+1) = E_{\mathrm{ESS}}(0) - E_{\mathrm{ESS}}(s) \cdot \kappa \tag{5.22}$$

whereby the initial condition $E_{\mathrm{ESS}}(s=0) = E_{\mathrm{ESS}}^{\mathrm{C}}$ is valid. Next, the iterative procedure is set up for the discrete states $s = \{0, 1, 2\}$.

$$\begin{aligned} E_{\mathrm{ESS}}(1) &= E_{\mathrm{ESS}}(0) - E_{\mathrm{ESS}}(0) \cdot \kappa \\ &= E_{\mathrm{ESS}}(0) \cdot (1-\kappa) \end{aligned} \qquad \text{for } s=0 \tag{5.23}$$

$$\begin{aligned} E_{\mathrm{ESS}}(2) &= E_{\mathrm{ESS}}(0) - E_{\mathrm{ESS}}(1) \cdot \kappa \\ &= E_{\mathrm{ESS}}(0) - E_{\mathrm{ESS}}(0) \cdot (1-\kappa) \cdot \kappa \\ &= E_{\mathrm{ESS}}(0) \cdot (1-\kappa+\kappa^2) \end{aligned} \qquad \text{for } s=1 \tag{5.24}$$

$$\begin{aligned} E_{\mathrm{ESS}}(3) &= E_{\mathrm{ESS}}(0) - E_{\mathrm{ESS}}(2) \cdot \kappa \\ &= E_{\mathrm{ESS}}(0) - E_{\mathrm{ESS}}(0) \cdot (1-\kappa+\kappa^2) \cdot \kappa \\ &= E_{\mathrm{ESS}}(0) \cdot (1-\kappa+\kappa^2-\kappa^3) \end{aligned} \qquad \text{for } s=2 \tag{5.25}$$

Equation 5.25 shows an alternating behavior with potential growth of factor κ. This behavior can be described as a mathematical series:

$$E_{\mathrm{ESS}}(s) = E_{\mathrm{ESS}}(0) \sum_{i=0}^{s} (-\kappa)^i \tag{5.26}$$

A mathematical induction was performed to prove Equation 5.26 for all $s > 0 \in \mathbb{N}_0$. First, the base case was verified by $s = 0$:

$$E_{\mathrm{ESS}}(0) = E_{\mathrm{ESS}}(0) \sum_{i=0}^{0} (-\kappa)^i = E_{\mathrm{ESS}}(0) \cdot (-\kappa)^0 \tag{5.27}$$

This results in:

$$E_{\mathrm{ESS}}(0) = E_{\mathrm{ESS}}(0) \cdot 1 \tag{5.28}$$

With this result, the base case for $s = 0$ was verified. Next, the inductive hypothesis was set for $s = k + 1$:

$$\begin{aligned} E_{\mathrm{ESS}}(k+1) &= E_{\mathrm{ESS}}(0) \sum_{i=0}^{k+1} (-\kappa)^i \\ &= E_{\mathrm{ESS}}(0) \cdot \left(\sum_{i=0}^{k} (-\kappa)^i + (-\kappa)^{k+1} \right) \\ &= E_{\mathrm{ESS}}(0) \cdot \sum_{i=0}^{k} (-\kappa)^i + E_{\mathrm{ESS}}(0) \cdot (-\kappa)^{k+1} \end{aligned} \tag{5.29}$$

The inductive hypothesis showed, that:

$$E_{\mathrm{ESS}}(k+1) = E_{\mathrm{ESS}}(k) + E_{\mathrm{ESS}}(0) \cdot (-\kappa)^{k+1} \tag{5.30}$$

When $k = s$ is used, the following occurs:

$$E_{\mathrm{ESS}}(s+1) = E_{\mathrm{ESS}}(s) + E_{\mathrm{ESS}}(0) \cdot (-\kappa)^{s+1} \tag{5.31}$$

Substitution of Equation 5.26 yields:

$$\begin{aligned} E_{\mathrm{ESS}}(s+1) &= E_{\mathrm{ESS}}(0) \sum_{i=0}^{s} (-\kappa)^i + E_{\mathrm{ESS}}(0) \cdot (-\kappa)^{s+1} \\ &= E_{\mathrm{ESS}}(0) \sum_{i=0}^{s+1} (-\kappa)^i \end{aligned} \tag{5.32}$$

Therefore, the inductive hypothesis holds for $s = k + 1$ and concludes by proving Equation 5.26 for all $s \in \mathbb{N}_0$.

For the computation of the series in finite time, the termination criterion is that the magnitude of the gradient must be less than ε:

$$\frac{|E_{\mathrm{ESS}}(s) - E_{\mathrm{ESS}}(s+1)|}{E_{\mathrm{ESS}}(s)} \leq \varepsilon \tag{5.33}$$

A termination criterion of $\varepsilon = 10^{-5}$ was used for the simulation. If $\kappa \geq 1.0$, the amount of energy for CS I E_{chg} would exceed the initial ESR $E_{\mathrm{ESS}}(s = 0)$ and the ESR $E_{\mathrm{ESS}}^{\mathrm{I}}$ would become 0. Therefore, the folloging rule was established to avoid negative ESR:

$$E_{\mathrm{ESS}}^{\mathrm{I}} = \begin{cases} E_{\mathrm{ESS}}(s), & \text{if} \quad \kappa \in \mathbb{R}\,[0, 1) \\ E_{\mathrm{ESS}}^{\mathrm{C}} \cdot (1 - p_{\mathrm{chg}}), & \text{otherwise.} \end{cases} \tag{5.34}$$

Opportunity (O)

For CS O, the ESR is determined by multiplying the energy requirement per cycle E_{cycle} by the number of chained average runs without intermediate charging $N_{\mathrm{run}}^{\mathrm{chain}}$. This number is subject to a probability p_{r}. The probability of reaching a CIS after a single run corresponds to the relative frequency of CIS in the layout and is called p_{chg}. According to the binomial distribution, the cumulative probabilities have the relation $P_{\mathrm{cum}} = p^n$, where p is the individual probability and n is the number of cumulative probabilities. In this case, the cumulative probability of not reaching a CIS after $N_{\mathrm{run}}^{\mathrm{chain}}$ runs is determined as follows:

$$P = (1 - p_{\mathrm{chg}})^{N_{\mathrm{run}}^{\mathrm{chain}}}, \tag{5.35}$$

where $1 - p_{\mathrm{chg}}$ is the complementary probability of p_{chg} and describes the probability of not reaching a CIS. The probability of reaching at least one CIS after $N_{\mathrm{run}}^{\mathrm{chain}}$ runs is the complementary probability of Equation 5.35 and is called p_{r}:

$$p_{\mathrm{r}} = 1 - (1 - p_{\mathrm{chg}})^{N_{\mathrm{run}}^{\mathrm{chain}}} \tag{5.36}$$

To calculate the minimum number of runs $N_{\mathrm{run}}^{\mathrm{chain}}$ required to reach at least one CIS with a reliability of $q_{\mathrm{r}} = 1 - p_{\mathrm{r}}$, the equation is converted to $N_{\mathrm{run}}^{\mathrm{chain}}$ and results in the first step:

$$1 - p_{\mathrm{r}} = (1 - p_{\mathrm{chg}})^{N_{\mathrm{run}}^{\mathrm{chain}}} \tag{5.37}$$

By applying the natural logarithm to both sides, we obtain:

$$\ln(1 - p_\mathrm{r}) = N_\mathrm{run}^\mathrm{chain} \cdot \ln(1 - p_\mathrm{chg}) \tag{5.38}$$

After conversion, the following relationship results for $N_\mathrm{run}^\mathrm{chain}$:

$$N_\mathrm{run}^\mathrm{chain} = \frac{\ln(1 - p_\mathrm{r})}{\ln(1 - p_\mathrm{chg})} \tag{5.39}$$

This equation specifies the minimum number of runs $N_\mathrm{run}^\mathrm{chain}$ needed to reach a CIS with reliability of q_r and given probability p_chg. Figure 5.2 shows the course of $N_\mathrm{run}^\mathrm{chain}$ as a function of the CIS probability p_chg for five different values of $q_\mathrm{r} = 1 - p_\mathrm{r}$. Considering the limit of $p_\mathrm{chg} = 0$, $N_\mathrm{run}^\mathrm{chain}$ runs towards infinity,

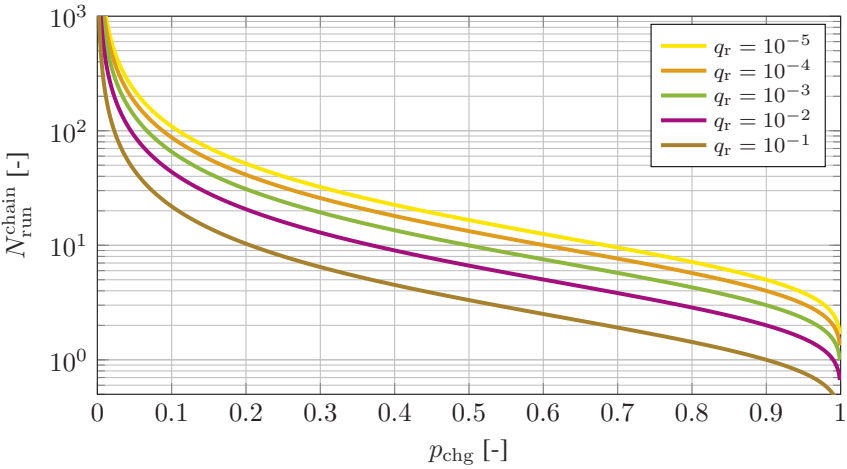

Figure 5.2: Number of subsequent transport runs without charging as a function of the CIS probability p_chg and the reliability q_r

leading to an infinite ESR, as no charging is planned. For the upper limit of $p_\mathrm{chg} = 1$, the number of subsequent chained runs without intermediate charging approaches $N_\mathrm{run}^\mathrm{chain} = 0$. However, $N_\mathrm{run}^\mathrm{chain}$ must be greater than the ratio of the

maximum distance to the average distance δ_{d}, otherwise, the ESR calculated in the next step would be insufficient for transport with maximum distance $d_{\max}$, mathematically expressed as follows:

$$N_{\mathrm{run}}^{\mathrm{chain}} = \begin{cases} \dfrac{\ln(1-p_{\mathrm{r}})}{\ln(1-p_{\mathrm{chg}})}, & \text{if} \quad N_{\mathrm{run}}^{\mathrm{chain}} \geq \delta_{\mathrm{d}} \\ \delta_{\mathrm{d}}, & \text{if} \quad N_{\mathrm{run}}^{\mathrm{chain}} < \delta_{\mathrm{d}} \end{cases} \tag{5.40}$$

$$E_{\mathrm{ESS}}^{\mathrm{O}} = E_{\mathrm{cycle}} \cdot N_{\mathrm{run}}^{\mathrm{chain}} \tag{5.41}$$

This rule also considers that the calculation rule for $N_{\mathrm{run}}^{\mathrm{chain}}$ according to the Equation 5.39 can also assume $N_{\mathrm{run}}^{\mathrm{chain}} < 1$, which is not sufficient for application-oriented operation since even with an area-wide installation of CIS ($p_{\mathrm{chg}} = 1.0$), at least one run to the next CIS must be taken into account when sizing the ESS.

5.2 Design of Experiments

A preparatory design of experiments was conducted for the validation. For each CS with a corresponding operation time t_{op}, the following variations were carried out in the corresponding order:

1. MLD: MLD list $(n_1 = 72)$
2. CIS distribution: CIS distribution list $(n_2 = 876/72)$
3. AGV type: AGV type list $(n_3 = 70)$
4. Orderlist: List of transportorder lists $(n_4 = 10)$

Considering that no CIS distribution lists varied for CS C, the sum of all planned simulation runs was $n_{\mathrm{sim}} = 1,940,400$. Based on the step size analysis in Section 4.3.2.3, a step size of $s_{\mathrm{s}} = 100\,\mathrm{ms}$ was defined for all simulations.

5.2.1 Operation Time

This study did not map holistic charging processes for CSs C and I since the ESS was assumed to be fully charged ($SoC \geq 99.5\,\%$) after an idle time of at least $8\mathrm{h}$. This assumption resulted in the maximum considered operating time of the vehicles with CSs C and I of $16\,\mathrm{h}$, equivalent to a typical two-shift operation. Furthermore, two independent investigations were conducted for the operating times $t_{op} = 8\,\mathrm{h}$ and $t_{op} = 16\mathrm{h}$ to validate the ESRM for single-shift and two-shift operations of AGVs. Only in CS O was an operating time of $t_{op} = 24\,\mathrm{h}$ selected, since more regular, shorter-term full charging processes occurred compared to CS C. Moreover validation of the ESRM for $24/7$ operation was possible. In summary, the following operation times t_{op} were selected for the different CSs:

$$t_{\mathrm{op}} = \begin{cases} 8\mathrm{h}, 16\mathrm{h}, & \text{for CS C and I} \\ 24\mathrm{h}, & \text{for CS O.} \end{cases} \tag{5.42}$$

5.2.2 Material Flow and Layout

As stated in the literature review (cf. Section 2.5), material flow and layout significantly affected the energy requirement of AGVs. For this purpose, a dataset with MLD was established to validate the ESRM, as described in Section 3.6. For this purpose, different CIS distributions and AGV types were varied for each MLD, considering the different CSs.

5.2.3 AGV Types

Based on the findings from the literature review on modeling power and energy requirement (cf. Section 2.5) of AGVs and the experimental results from Chapter 4, the parameters in Table 5.1 describe the energetic behavior of AGVs.

The first parameter is vehicle speed v, which significantly impacts the duration of a transport run. This parameter was varied from $0.3\,\mathrm{m/s}$ to $2.0\,\mathrm{m/s}$, representing

Table 5.1: Variation parameters according to DoE

Variation parameter		**Linked parameter**			
Parameter	Variation range	Parameter	Variation range		Unit
v	[0.3...2.0]	-	-		m/s
$P_{\text{drive}}^{\text{active}}$	[10...1500]	$P_{\text{drive}}^{\text{stby}}$	[0.1...0.3]	$\cdot P_{\text{drive}}^{\text{active}}$	W
		$P_{\text{drive}}^{\text{acc}}$	3	$\cdot P_{\text{drive}}^{\text{active}}$	W
		$P_{\text{drive}}^{\text{dec}}$	-1	$\cdot P_{\text{drive}}^{\text{active}}$	W
$P_{\text{ctrl}}^{\text{active}}$	[10...500]	$P_{\text{ctrl}}^{\text{stby}}$	[0.5...1.0]	$\cdot P_{\text{ctrl}}^{\text{active}}$	W
$P_{\text{lhd}}^{\text{active}}$	[10...1500]	$P_{\text{lhd}}^{\text{stby}}$	[0.1...0.3]	$\cdot P_{\text{lhd}}^{\text{active}}$	W
t_{lh}	[1...30]	t_{dock}	1.0	$\cdot t_{\text{lh}}$	s
		t_{undock}	0.5	$\cdot t_{\text{dock}}$	s
t_{preDock}	[1...10]	t_{preDrive}	1.0	$\cdot t_{\text{preDock}}$	s
c_{r}^{I}	[0.1...1.0]	c_{r}^{O}	10.0	$\cdot c_{\text{r}}^{\text{I}}$	1/h

typical AGV speeds. Furthermore, the power characteristics of the individual system components varied in the active state, which significantly affected the power requirement of the vehicle. The limits of the variation ranges were based on the typical power requirements of small-scale AGVs for the transportation of small load carriers (cf. Appendix A.9) up to forklift AGVs (cf. Pacheco et al. (2019)). The times for load transfer t_{lh}, as well as the times for the preDock t_{preDock} and preDrive t_{preDrive} processes were based on the results of the process analysis for ERM verification (cf. Section 4.1.2) and the ERM validation (cf. Appendix A.9). Finally, the charging power was assumed to affect the ESR significantly, which was calculated using Equation 5.16. The equation included C-rate c_{r} as a constant parameter in the range of $0.1 \leq c_{\text{r}} \leq 1.0$ for CS I and $1 \leq c_{\text{r}} \leq 10$ for CS O while varied. The different variation ranges of the C-rate were caused by the differences in the CS. In CS O, too small C-rates that are too small led to very long charging times while decreasing the utilization of the AGV. However, the charging behavior would approach the behavior of CS O if the C-rates in CS I were too high.

Furthermore, the linked parameters were the dependent variables of the seven variation parameters. For this purpose, the assumption was made that the energy requirement of the same component in the standby state was lower than in the active state. The ratio for the power of the drives $P_{\mathrm{drive}}^{\mathrm{stby}}$ and the power of the LHD $P_{\mathrm{LHD}}^{\mathrm{stby}}$ was assumed to be between $10\,\%$ to $30\,\%$ of the nominal power in action state, for the power of the controller $P_{\mathrm{ctrl}}^{\mathrm{stby}}$ between $50\,\%$ to $100\,\%$ of the nominal power in action state. The power requirement of the drives during the acceleration and deceleration process was also assumed to be proportional to $P_{\mathrm{drives}}^{\mathrm{active}}$. Based on the measuring results from the validation of the ERM, the time of the docking process was assumed to correspond to the duration of the load handling process since the undocking process t_{undock} comprised $50\,\%$ of the duration of the docking process t_{dock} (cf. Appendix A.9), while the states *preDock* and *preDrive* were assumed to have the same duration. The c_{r} was selected depending on the CS, the variation range of which differed by a factor of 10. Therefore, a parameter set was generated using the variation parameters based on the Latin hypercube method, according to Cavazzuti (2013) and Jones et al. (1998), creating a homogeneous multidimensional distribution of the different parameters. This approach allowed a parameter selection within the given variation ranges, enabling optimal coverage of the parameter domain. The parameter set size resulted from the number of parameters multiplied by ten variations respectively (cf. Jones et al. (1998)), which resulted in $n_3 = 7 \cdot 10 = 70$. The complete parameter set was generated using the Matlab function *lhsdesign(n,p)* (The MathWorks Inc. 2024a) and appears in Appendix A.11.

5.2.4 CIS Distribution Lists

The distribution of the CIS within the layout is assumed to be another factor influencing the ESR based on MLD. Section 2.4 presented related work on investigations of suitable positions for waiting and charging. However, no method was presented in these studies to determine the CIS distribution for simulative energy requirement considerations. For this reason, a method was developed to generate uniformly distributed CIS distributions based on the station frequency.

The variation of the CIS probability is part of the DoE (cf. Section 5.2) and requires uniformity to derive statements about the impact of the CIS distribution on the ESR. However, the model can only assign CIS to known stations within the layout and not allow new stations or positions for CIS. As a result, the CIS distribution is the sum of all station frequencies of the stations, where a CIS is installed. Within a station with CIS, it was assumed that an infinite number of CIS are available in parallel. Hence, the following steps were performed successively:

1. Determining all stations and their frequencies,
2. Determining all possible CIS distributions, and
3. Selecting one distribution for each of the CIS distribution classes.

Figure 5.3 shows an intended CIS distribution, where each of the 18 classes with a width of 0.05 and within the limits of $0.05 \leq p_{\mathrm{chg}} < 0.95$ has exactly one CIS probability. Probabilities $p_{\mathrm{chg}} < 0.05$ and $p_{\mathrm{chg}} \geq 0.95$ were omitted since, depending on the CS, they enabled too many or too few charging processes to apply the methods for ESS dimensioning from Section 5.1.2.4 (cf. Figure 5.2).

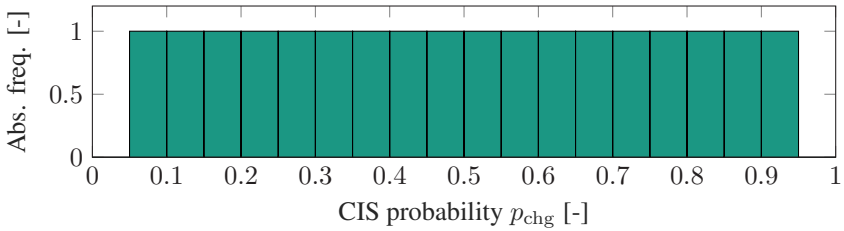

Figure 5.3: Intended CIS Distribution per Layout with 18 classes with a class width of 0.05

If no combination was determined within a CIS distribution class, it was omitted for the corresponding MLD. The number of subsequent simulations is reduced accordingly (cf. Section 5.2). Figure 5.4 shows the relative frequencies of the CIS distribution classes of the several CIS probabilities of the MLD dataset as intended. It is shown, that the frequency of the CIS distribution within the CIS distribution class $0.5 \geq p_{\mathrm{chg}} < 0.55$ was generated 67 times, which is more than

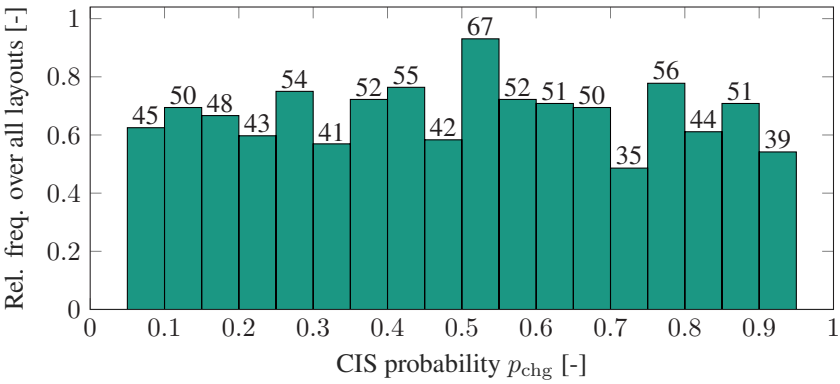

Figure 5.4: CIS distribution of all layouts within the MLD dataset with 18 classes with a class width each 0.05

15% compared to all other CIS distribution classes. The number of MLD with a $1:1$ task structure occurring in the data set could explain this result since the CIS distribution could assume exactly three CIS distributions $p_{\mathrm{chg}} \in 0, 0.5, 1.0$ due to the number of stations of 2.

5.2.5 Transport Order Lists

According to Schrecker (2000), transport orders can occur either deterministically or stochastically. In the case of deterministic transport orders, the arrival times are known. Since the validation of the ESRM required stochastic interarrival times of the transport orders to simulate stochastic impacts in real operation, a method was required to assign the transport orders to the vehicles within the simulation. The method had the following four steps:

1. Reading the job list,
2. Generating transport orders from the job list,
3. Generating random timestamps and assigning them to each transport order, and

4. Repeating these steps as often as required by the list length in $[\mathrm{h}]$.

In the first step, the job list of a corresponding MLD (cf. Section 3.5.2), containing the frequency of all transports per hour, was imported. The number of transport orders for each job was generated based on the corresponding transport demand per hour. In the third step, randomly generated timestamps were assigned to all transport orders and followed an exponential distribution with $\lambda_{\mathrm{exp}} = 1.0$, according to DeGroot and Schervish (2012). They were determined using the Java function shown in Figure 5.5, where *random* was an instance of *java.util.Random*, *lambda* was λ_{exp}, and *Math* corresponded to the class *java.lang.Math*. The

```
public double generateExpRandomValue() {
        // Generate a uniform random value between 0 and 1
        double u = random.nextDouble();
        // Transform to exponential distribution
        return -Math.log(1 - u) / lambda;
    }
```

Figure 5.5: Java function for generating a exponentially distributed random value

remaining, not integer transport frequencies from the job list were considered residual probability and added to the set of transport frequencies for the next hour. The residual probability was reduced by 1.0 when the corresponding job was assigned. This process was repeated until the desired total length of the transport order list in hours was reached. The calculation rule for the remaining probability was selected to avoid excessive deviations between the transport order volumes of the respective hours. Adding up the residual probabilities made the order more likely to be placed in the following hour if it was not allocated, thereby ensuring the order volume distribution more evenly. For each MLD (cf. Section 5.2.2), ten transport order lists were generated using this method.

5.3 Implementation

This section describes the implementation. For this purpose, Figure 5.6 shows the connections between the simulation and its input data, output data, and the ESRM, as described in Section 5.1.

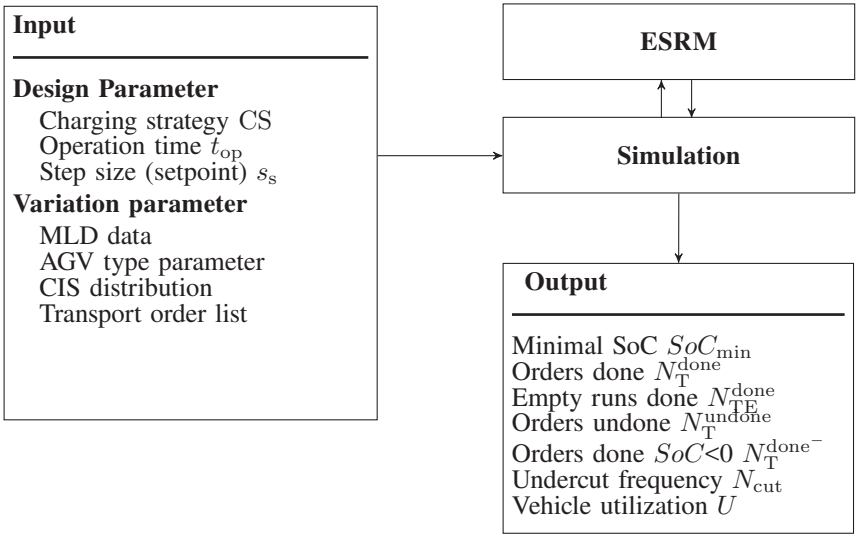

Figure 5.6: Input Model Output diagram for simulation for ESRM validation

5.3.1 Input

The input parameters consisted of the default values and the variation parameters. The default values included the CS to be analyzed, $\mathrm{CS} \in \{\mathrm{C}, \mathrm{I}, \mathrm{O}\}$, its corresponding operation times t_{op}, and the step size s_{s} for the discrete-time simulation. The variation parameters include randomly distributed transport order lists (cf. Section 3.5.2), different CIS distributions (cf. Section 5.2.4), material

flow and layout specific parameters, and AGV type specific parameters. The MLD were based on the data set described in Chapter 3. The AGV type parameters were based on the AGV process analysis and validation of the ERM (cf. Chapter 4), as described in Section 5.2.3.

5.3.2 Simulation Model

The simulation was successively parameterized and executed for all combinations of the variation parameters. The following six steps were required to initialize the simulation cycle:

1. Setting the variation parameters,
2. Initializing the station repository with the MLD and CIS distributions,
3. Setting the AGV type specific parameter,
4. Running the ESRM,
5. Initializing an AGVPool with N_{AGV} AGV instances, and
6. Initializing the dispatcher with AGVPool and the transport order list.

The subsequent method *mainSim()* for simulating the vehicles was described in Figure 5.7. The first *for* loop was the discrete-time execution of the simulation starting at $t_{\mathrm{sim}} = 0\,\mathrm{ms}$ with a step size of $s_{\mathrm{s}} = 100\,\mathrm{ms}$ until the operation time t_{op} was reached. It determined whether new orders were received in each step and distributed these possible orders to the AGVs (cf. Section 4.2.2.1). In the second step, the current status of each AGV instance, according to the ERM, was updated from the AGVPool. The OperationService class assumed the coordination of the ERM, with the AGV instances saving the states. Data were saved for each AGV instance in the third step, evaluated in the fourth step after the main loop´s completion, and saved in a .csv file.

```
public void mainSim(){
    for (int tSim = 0; tSim <= tOP; tSim = tSim + s) {
        //Check for new tOrders from orderlist
        Dispatcher.update(tSim); //and allocate orders to AGVs
        for (AGV A : AGVPool) {
            OperationService.updateAGV(A); //update ERM
            A.log(); //log A specific data
        }
    }
    for (AGV A : AGVPool) {
        A.evaluate(); //evaluate logged data and write to .csv file
    }
}
```

Figure 5.7: Java function mainSim() for time discrete simulation of AGVs

5.3.3 Output

The .csv files were named according to the MLD, AGV type, and CIS distribution. The files contained the output parameters of the ESRM (cf. Figure 5.1) and the output parameters listed in Figure 5.6 for each instance of an AGV and all simulation repetitions by transport order lists. The $SoC_{\min}$ specified the relative remaining ESS capacity within the operation time for each vehicle instance. The following parameters were key figures for the order fulfillment of each vehicle instance. These included the number of completed transport orders without empty runs $N_{\mathrm{T}}^{\mathrm{done}}$, the number of completed empty runs $N_{\mathrm{TE}}^{\mathrm{done}}$, the number of uncompleted transport orders $N_{\mathrm{T}}^{\mathrm{undone}}$, and the number of completed transport orders without empty runs where the remaining capacity at the end of the transport run was $SoC < 0.0$ was $N_{\mathrm{T}}^{\mathrm{done}^-}$. N_{cut} was a key figure describing how often the SoC fell below 0 within the operation time. The theoretical consideration of negative SoC allows the over- or underestimation to be quantified. The last key figure was vehicle utilization U_{AGV}, which described the ratio of the time spent in the standby state to the operation time. A charging process at CS O was considered a standby state once the previous load handling process was completed.

5.3.4 Data Analysis Methodology

As stated in the previous section, the MLD, CIS distribution classes, and AGV types varied, and the results from each combination were logged into separate .csv files. This section describes the methods used to generate the samples for verification and validation. First, the sets of the variation parameters MLD, CIS distribution, and AGV types were defined:

- $\mathbf{L}$ is the set of all MLD,
- $\mathbf{C}$ is the set of all CIS distribution classes, and
- $\mathbf{A}$ is the set of all AGV types.

The cardinalities of the sets were defined as follows:

$$\mathbf{L}_\mathrm{c} = |L| = 72 \tag{5.43}$$

$$\mathbf{C}_\mathrm{c} = |C| = 18 \tag{5.44}$$

$$\mathbf{A}_\mathrm{c} = |A| = 70 \tag{5.45}$$

The set of all possible combinations from $\mathbf{L}$, $\mathbf{C}$, and $\mathbf{A}$ was defined as

$$\mathbf{L} \times \mathbf{C} \times \mathbf{A} = \{(l, c, a) | l \in \mathbf{L}, c \in \mathbf{C}, a \in \mathbf{A}\} \tag{5.46}$$

The following methods for data evaluation were based on Equation 5.46, each invoking the function $analyze()$, which returned result set $\mathbf{Z}$. The dimension q of $\mathbf{Z}$ varied depending on the set considered.

$$\mathbf{Z} = \bigcup_{l \in \mathbf{L}} \bigcup_{a \in \mathbf{A}} analyse(l, \mathbf{C}, a), \qquad \mathbf{Z} \in \mathbb{R}^{\mathbf{L}_c \times \mathbf{A}_c \times q} \tag{5.47}$$

$$\mathbf{Z} = \bigcup_{a \in \mathbf{A}} analyse(\mathbf{L}, \mathbf{C}, a), \qquad \mathbf{Z} \in \mathbb{R}^{\mathbf{A}_c \times q} \tag{5.48}$$

$$\mathbf{Z} = \bigcup_{l \in \mathbf{L}} analyse(l, \mathbf{C}, \mathbf{A}), \qquad \mathbf{Z} \in \mathbb{R}^{\mathbf{L}_c \times q} \tag{5.49}$$

$$\mathbf{Z} = \bigcup_{c \in \mathbf{C}} analyse(\mathbf{L}, c, \mathbf{A}), \qquad \mathbf{Z} \in \mathbb{R}^{\mathbf{C}_c \times q} \tag{5.50}$$

$$\mathbf{Z} = \bigcup_{l \in \mathbf{L}} \bigcup_{c \in \mathbf{C}} \bigcup_{a \in \mathbf{A}} analyse(l, c, a), \qquad \mathbf{Z} \in \mathbb{R}^{\mathbf{L}_c \times \mathbf{C}_c \times \mathbf{A}_c \times q} \tag{5.51}$$

where $\cup$ describes the union parameter for set theory. Equation 5.47 described a method, where each AGV type and MLD combination $analyze()$ was called and returned result $\mathbf{Z}$ in the dimension of $\mathbf{L}_c \times \mathbf{A}_c \times q$. Equation 5.48 described a method where, each AGV type, the function $analyze()$ was called and returned result $\mathbf{Z}$ whereas, in Equation 5.49, the same applied for each MLD. The Equation 5.50 described a method in which $analyze()$ was called for each CIS distribution class. Finally, the Equation 5.51 described a method in which $analyze()$ was called for each AGV type, MLD, and CIS distribution class combination. The function $analyze()$ returned result $\mathbf{Z}$ in the dimension $q = 4 \times 17$, which contained the minimum, maximum, mean, and standard deviation σ for each output parameter, described in Section 5.3.3.

5.4 Verification

The correct functioning of the individual submethods of the ESRM and the simulation were first ensured to validate the results from the simulations described above. The verification and validation for the ERM were detailed in Chapter 4.

Other submethods were the fleet size estimation model (cf. Section 5.1.1), the function for calculating the $N_{\mathrm{run}}^{\mathrm{chain}}$ for the CS O (cf. Equation 5.40), the alternative approximation (AAM) method for determining the ESR for CS I (cf. Equation 5.34), and the dispatching algorithm for multiple vehicle fleets. Hence, an analysis was conducted for each of these four submethods to verify their functionality.

5.4.1 Fleet Size Estimation Analysis

Data analysis was carried out for the three CSs with their respective operation times, starting with an analysis of the fleet size estimation (cf. Section 5.1.1). Figure 5.8 shows ten subfigures with 70 data points each, where the analysis was based on Equation 5.48. Two figures in each line were assigned to a CS with an associated operation time t_{op}. The figures on the left show the order completion rate ρ_{OC} compared to the fleet size N_{AGV}. The ρ_{OC} indicates the relative mean number of all completed transport orders at the end of the simulation $t > t_{\mathrm{op}}$. The figures on the right show the mean vehicle utilization compared to the fleet size N_{AGV}. The figures on the right also show a linear data interpolation line, highlighting the decreasing behavior of vehicle utilization with an increasing number of vehicles. The Matlab function *polyfit(x,y,n)* (The MathWorks Inc. 2024b) was used for this purpose. Appendix A.3 contains the same figure format for a data analysis based on Equation 5.49.

Notably, N_{AGV} compared to ρ_{OC} and utilization for CSs C and I with their respective $t_{\mathrm{op}} \in \{8\,\mathrm{h}, 16\,\mathrm{h}\}$ hardly differed because the fleet size estimation procedure, according to Section 5.1.1, was identical for CSs C and I. A utilization set size of $\eta_{\mathrm{U}} = 0.8$ was selected, marked with a black line in the top four subfigures on the right-hand side. With an average ρ_{OC} of $98.66\,\%$ and $\sigma = 2.13\,\%$, the fleet size model was assumed to be sufficiently accurate for the application in CSs C and I for the investigations on energy requirement considerations. The varying vehicle utilization resulted from rounding up to the next integer number (cf. Equation 5.9)

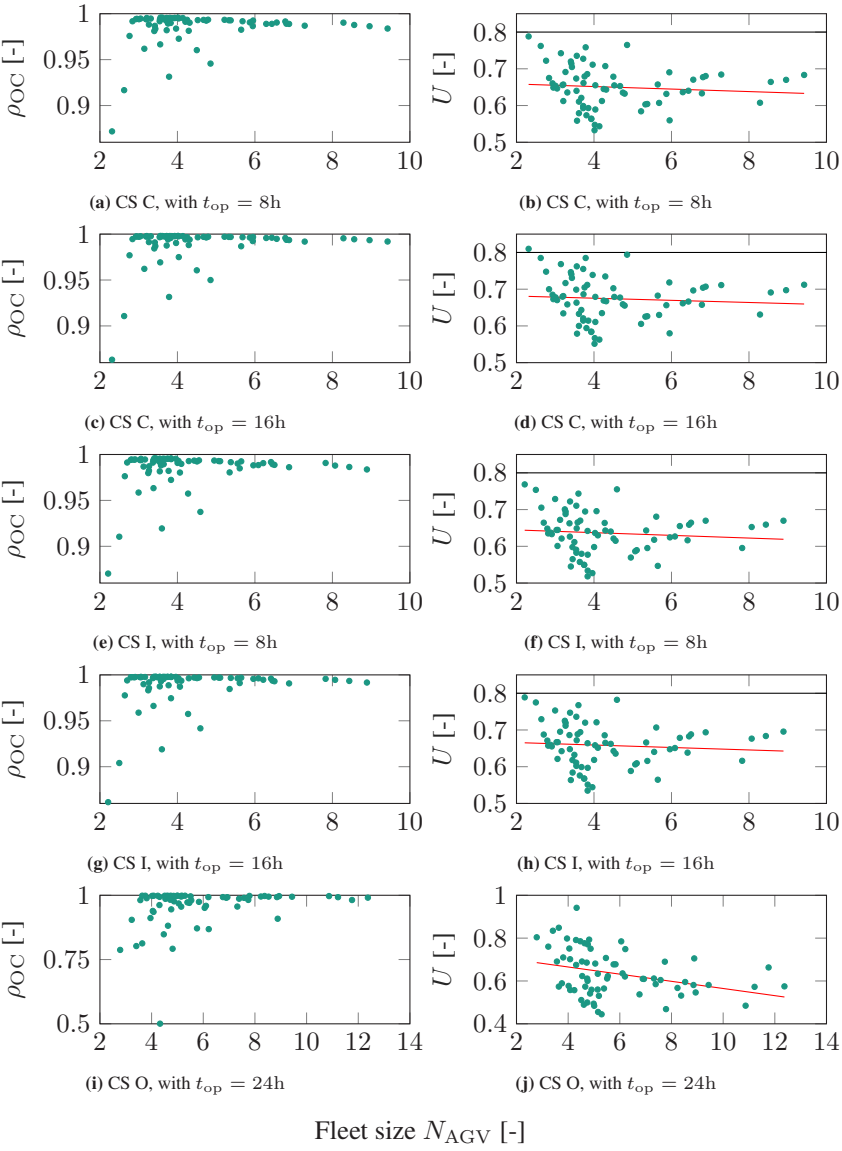

(a) CS C, with $t_{op} = 8h$
(b) CS C, with $t_{op} = 8h$
(c) CS C, with $t_{op} = 16h$
(d) CS C, with $t_{op} = 16h$
(e) CS I, with $t_{op} = 8h$
(f) CS I, with $t_{op} = 8h$
(g) CS I, with $t_{op} = 16h$
(h) CS I, with $t_{op} = 16h$
(i) CS O, with $t_{op} = 24h$
(j) CS O, with $t_{op} = 24h$

Figure 5.8: Fleet size model analysis for different CS, analysis based on Equation 5.48

and the stochastic incoming transport orders. When analyzing the fleet size estimation for CS O, the mean of N_{AGV} was higher than for the other CSs because the operating time was $t_{\mathrm{op}} = 24\,\mathrm{h}$ and, unlike C and I, the full charge cycles must occur within t_{op}. For these reasons, in addition to $\eta_{\mathrm{U}} = 0.8$, $\eta_{\mathrm{A}} = 0.7$ was also assumed as a fixed approximation value for CS O. With an average ρ_{OC} of $95.8\,\%$ and $\sigma = 7.73\,\%$, the method showed greater deviations concerning the fulfillment rate of transport orders compared to CSs C and I. The right-hand subplot of CS O also showed that the mean vehicle utilization of $U = 0.8$ exceeds four out of 70 AGV types. Since optimization concerning the number of vehicles or utilization of AGVs is not the focus of this thesis, and the mean ρ_{OC} for all CS exceeded $95\,\%$, the fleet size calculation model was assumed to be a suitable method for ESRM validation.

5.4.2 Chained Run Determination Method Analysis

An exponential function was set up for the ESR calculation method (cf. Equation 5.40) that resulted in a minimum number of chained runs $N_{\mathrm{run}}^{\mathrm{chain}}$, considering CIS probability p_{chg} and probability p. Thus, the number of mean cuts of an $SoC < 0$ N_{cut} was set to the mean of the completed transport orders $N_{\mathrm{T}}^{\mathrm{done}}$ to verify this method:

$$\Delta_{\mathrm{cut}} = \frac{N_{\mathrm{cut}}}{N_{\mathrm{T}}^{\mathrm{done}}} \tag{5.52}$$

with the data analysis is based on Equation 5.47. With a set of $p = 10^{-3}$, the mean Δ_{cut} should be $0.1\,\%$, drawn as a horizontal line in Figure 5.9. The mean probability of $p = 10^{-3}$ was exceeded with the fourth CIS distribution class $0.2 \leq p_{\mathrm{chg}} < 0.25$. From $p_{\mathrm{chg}} \geq 0.65$, $\Delta_{\mathrm{cut}} = 0.5\,\%$ was exceeded. Considering the data for $p_{\mathrm{chg}} < 0.65$ and $p = 10^{-3}$, $\Delta_{\mathrm{cut}} = 0.5\,\%$ was not exceeded, which was assumed to be a tolerable measure for validating the ESRM. A $\Delta_{\mathrm{cut}} = 0.5\,\%$ meant that on average $0.5\,\%$ of all transport orders could not be carried out due to a lack of ESS capacity. This limitation could be fixed by an OS rule that prevents capacity underruns due to capacity prediction and sends

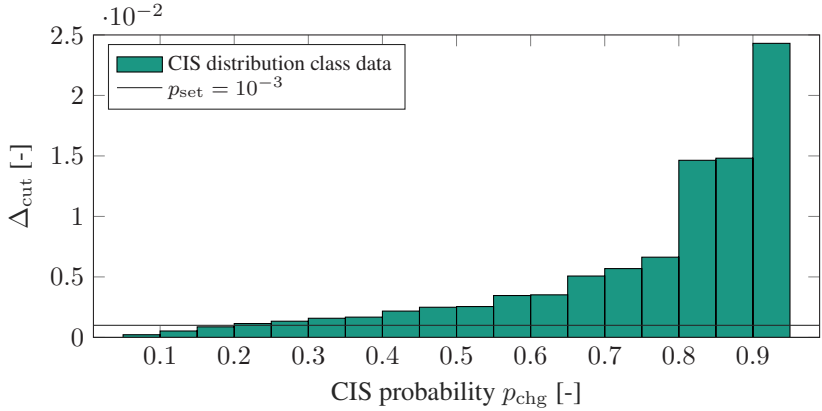

Figure 5.9: Chained run determination method analysis plot over all CIS distribution classes

the AGV to a station with a CIS in time. Figure 5.2 shows that reducing the p-value for $p_{\text{chg}} \geq 0.65$ had less effect on the number of chained runs than for $p_{\text{chg}} < 0.65$. The consequence of a smaller p was that the ESR was significantly oversized for layouts with CIS distributions of $p_{\text{chg}} < 0.65$. Hence, the remaining capacity also increases significantly. Only for $p_{\text{chg}} \geq 0.65$ was the number of minimum remaining capacities reduced. With increasing CIS probabilities $p_{\text{chg}} \geq 0.65$, $\Delta_{\text{cut}} = 0.5\,\%$ increased significantly, thereby questioning the suitability of the calculation method for $p_{\text{chg}} \geq 0.65$. In summary, the calculation method (cf. Equation 5.40) for $p_{\text{chg}} < 0.65$ with a maximum mean $\Delta_{\text{cut}} = 0.5\,\%$ was assumed to be sufficiently well suited for determining the $N_{\text{run}}^{\text{chain}}$. It required a separate consideration of the simulation results for $p_{\text{chg}} < 0.65$.

5.4.3 Alternative Approximation Method Analysis

The calculation method for the ESR in CS I included an alternative approximation method (AAM) if the condition $0 \leq \kappa < 1$ was not met (cf. Equation 5.34). This analysis checked how often the alternative approach was used in the simulations. While the AAM was used with $t_{\text{op}} = 8\,\text{h}$, for 2 of $61,320$ ESRM executions (*Industry11*, *AGV23*, $p_{\text{chg}} \in \{0.885, 0.91\}$), the number increased significantly

to 633 by a $t_{\mathrm{op}} = 16\,\mathrm{h}$. Appendix A.4 shows the relative frequency of AAM usage for all ESRM executions of each AGV type and layout combination where at least one AAM execution was identified, based on Equation 5.47. The legend shows the relative frequency of the AAM execution, an increasing relative frequency represents an increasing temperature color. Notably, the combination of *AGV23* and *Industry11* had particularly high relative frequencies. *AGV23* was the AGV that showed the most significant difference in the power requirements of the three system components Drives, Controls, and LHD (cf. Appendix A.11) between the respective states active and standby, which may have been a reason for the above-average frequency of AAM execution. However, no clear characteristic was determined for *Industry11* for how the above-average number of AAM executions were derived. Finally, Figure 5.10 showed that the AAM was only executed if

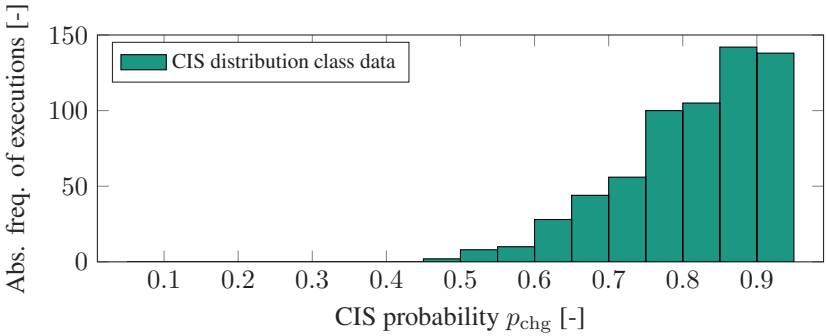

Figure 5.10: Absolute frequency of using AAM for CS I with $t_{\mathrm{op}} = 16\,\mathrm{h}$ out of a total of $61,320$ executions, analysis based on Equation 5.50

$p_{\mathrm{chg}} \geq 0.45$, and its frequency increased exponentially with an increasing p_{chg}. Since the AAM was only executed at $1.0\,\%$, the method was assumed to be suitable for only a few ESR calculations, so the main iterative procedure was primarily evaluated during validation.

5.4.4 Dispatching Analysis

Finally, the dispatching algorithm for fleet sizes $N_{\mathrm{AGV}} > 1$ was verified, as described in Section 4.2.2.1 and validated for fleet sizes of $N_{\mathrm{AGV}} = 1$. For this purpose, data analysis based on Equation 5.51 was performed, in which the standard deviation of the utilization σ_{U} from the analysis result z from the set $\mathbf{Z}$ was the relevant key figure. Subset $\boldsymbol{\sigma}_{\mathrm{U}}$ was then formed, in which the σ_{U} were sorted by number N_{AGV} and their mean values of $\bar{\sigma}_{\mathrm{U}}$ were subsequently determined. The values $\bar{\sigma}_{\mathrm{U},i}$ of the subset $\boldsymbol{\sigma}_{\mathrm{U}}$ were found for the three CSs with their respective t_{op} in Figure 5.11. A constant line at $\bar{\sigma}_{\mathrm{U}} = 1.26\,\%$ showed the

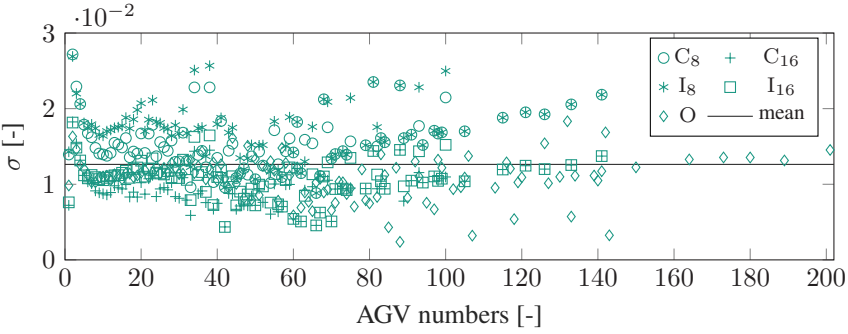

Figure 5.11: Plot of mean standard deviations of the vehicle utilization over fleet size

mean value of all elements of $\boldsymbol{\sigma}_{\mathrm{U}}$. The $\bar{\sigma}_{\mathrm{U},i}$ was greater at $t_{\mathrm{op}} = 8\,\mathrm{h}$ than at $t_{\mathrm{op}} \geq 16\,\mathrm{h}$, and the maximum $\bar{\sigma}_{\mathrm{U},i}$ was $\bar{\sigma}_{\mathrm{U}} = 2.72\,\%$. Due to transport order workloads that could not be distributed equally to all vehicles, $\bar{\sigma}_{\mathrm{U}} > 0$ results. Therefore, the mean $\bar{\sigma}_{\mathrm{U}} = 1.26\,\%$ over all CS and operation times was assumed to have sufficient quality of the dispatching algorithm from Section 4.2.2.1 for fleet sizes $N_{\mathrm{AGV}} > 1$ and was suitable for ESRM validation.

5.5 Results and Validation

After the relevant functions of the design procedure and the simulation model were verified, the results of the ESRM analysis were validated. This section is divided into the three CSs, which are compared and contrasted in a fourth subsection.

5.5.1 ESRM Analysis for CS Capacitive

Figure 5.12 shows the frequency distribution of the relative remaining capacity for $t_{\mathrm{op}} = 8\,\mathrm{h}$ (a) for $t_{\mathrm{op}} = 16\,\mathrm{h}$ (b) in a histogram. The normal distribution functions determined from the samples were plotted in the figures. When comparing the courses of the histogram data with the normal distribution functions, a normal distribution was assumed for both operation times, which allowed the determination of confidence intervals. The results of this analysis, based on Equation 5.47, appear in Table 5.2.

Table 5.2: ESRM Results for CS C

CS	Sample size	Rel. remaining capacity						Freq. neg. capacity
		mean	σ	$\alpha = 1\%$		$\alpha = 5\%$		
				Δ_{low}	Δ_{high}	Δ_{low}	Δ_{high}	
C_8	$5,040$	8.50%	11.74%	8.07%	8.93%	8.18%	8.82%	19.11%
C_{16}	$5,040$	6.43%	11.35%	6.02%	6.84%	6.12%	6.74%	24.27%

The mean relative remaining capacities of $8.50\,\%$ and $6.43\,\%$ indicated that the ESRM had determined a sufficient average ESR for both operation times. However, the frequencies of the negative remaining capacities (Freq. neg. capacity) also showed that the ESR was sized insufficiently for $19.11\,\%$ and $24.27\,\%$ of all ESRM executions. A further investigation of the utilization in Figure 5.13 showed that the relative remaining capacity decreased with increasing vehicle utilization. The analysis method according to Equation 5.48 was used for (a) and (b) and

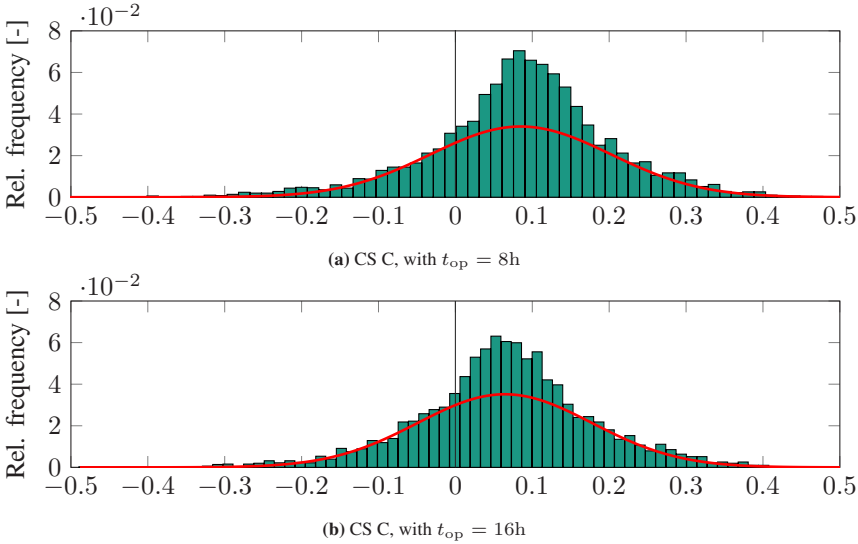

(a) CS C, with $t_{\mathrm{op}} = 8\mathrm{h}$

(b) CS C, with $t_{\mathrm{op}} = 16\mathrm{h}$

Figure 5.12: Relative remaining capacity for CS C, analysis based on Equation 5.47

the analysis method according to Equation 5.49 was used for (c) and (d). When classifying the vehicle-specific results in (a) and (b), a clear trend was observed with a mean relative remaining capacity of $0\,\%$ at a vehicle utilization of approx. $72.5\,\%$. However, a stronger scattering of the measurement points was seen when classifying the MLD-specific results in (c) and (d). A linear data interpolation could not performed here. These results indicated that according th the ESRM, the frequency of undersized ESRs could minimized by reducing vehicle utilization.

In a final analysis of CS C, the relative remaining capacity values were assigned to the corresponding layout classes. The data analysis was based on Equation 5.47, where $\mathbf{L}$ described the set of all layouts of a corresponding MLD class (cf. Section 3.7). The results of this analysis appear as two boxplot diagrams in Figure 5.14.

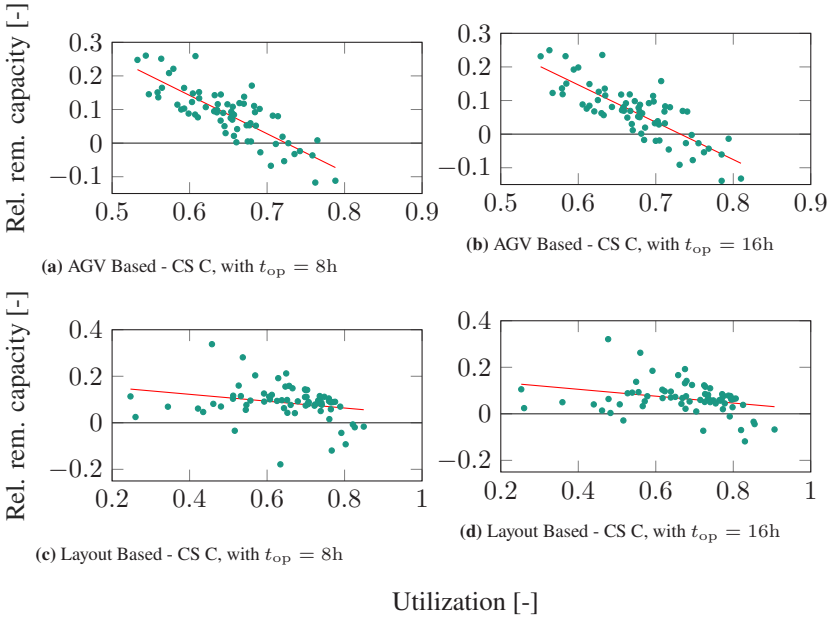

(a) AGV Based - CS C, with $t_{\mathrm{op}} = 8\mathrm{h}$

(b) AGV Based - CS C, with $t_{\mathrm{op}} = 16\mathrm{h}$

(c) Layout Based - CS C, with $t_{\mathrm{op}} = 8\mathrm{h}$

(d) Layout Based - CS C, with $t_{\mathrm{op}} = 16\mathrm{h}$

Figure 5.13: Rel. remaining capacity over utilization for CS C with $t_{\mathrm{op}} \in \{8\mathrm{h}, 16\mathrm{h}\}$, analysis based on Equation 5.47

Indeed, the MLD classes *Industry mixed dir.* and *Literature singleloop* had a negative mean remaining capacity at both operating times. However, since these classes only contained one MLD each, a larger MLD data set was required to make more significant, MLD class-specific conclusions.

5.5.2 ESRM Analysis for CS Opportunity

To validate the ESRM for CS O, an analysis of the minimum relative remaining capacity over CIS distribution classes (p_{chg}) was performed initially, based on Eq. 5.50. The data was presented as a histogram in Figure 5.15. The minimum relative remaining capacity assumed negative values from a CIS distribution class with $p_{\mathrm{chg}} > 0.65$. This limit was marked with a vertical line. Across all CIS

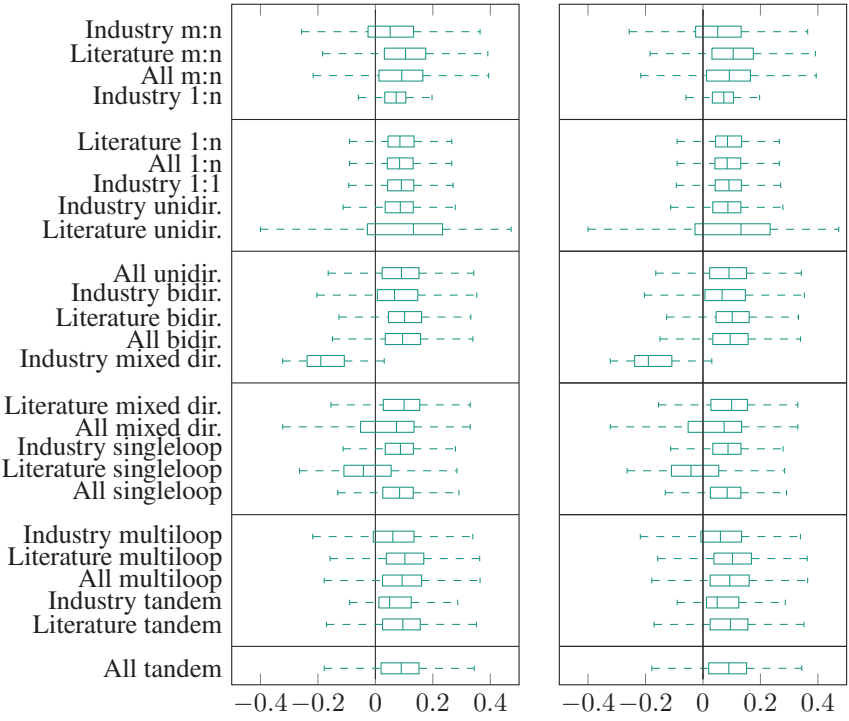

(a) CS C, with $t_{\mathrm{op}} = 8\mathrm{h}$

(b) CS C, with $t_{\mathrm{op}} = 16\mathrm{h}$

Figure 5.14: CS C Layout class specific analysis, analysis based on Equation 5.47

distribution classes, the minimum relative remaining capacity decreased when p_{chg} increased. Based on these findings, additional analyses were conducted for CIS distributions with $p_{\mathrm{chg}} < 0.65$ and all CIS distributions. Considering the distribution of the relative frequency of the mean relative remaining capacity in Figure 5.16, a bell-shaped distribution was evident, based on an analysis according to Eq. 5.47. Hence, these data were normally distributed, allowing the calculation of confidence intervals. The second maxima at approximately $80\,\%$ relative

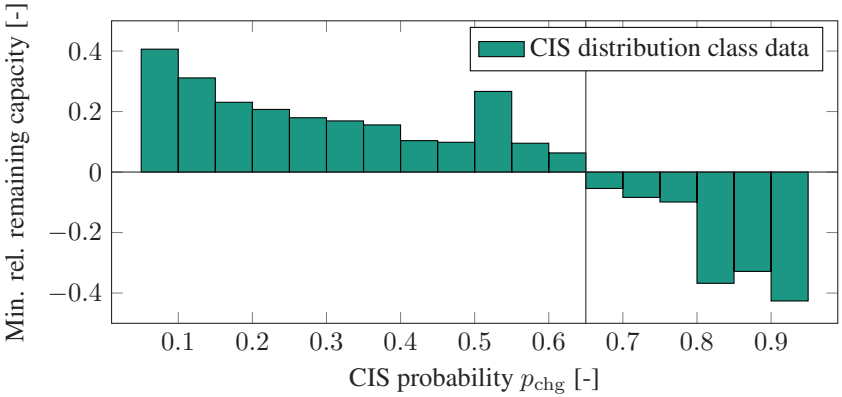

Figure 5.15: Histogram of the minimum rel. remaining capacity of the 18 CIS distribution classes for CS O, analysis based on Equation 5.50

remaining capacity was due to the results of an investigated MLD, as described later in this section (cf. Figure 5.17).

Table 5.3: ESRM Results for CS O

CIS distr. classes	Sample size	Remaining capacity						Freq. neg. capacity
		mean	σ	$\alpha = 1\%$		$\alpha = 5\%$		
p_{chg}				Δ_{low}	Δ_{high}	Δ_{low}	Δ_{high}	
All	$58,240$	3.90%	47.23%	3.40%	4.41%	3.52%	4.29%	34.85%
< 0.65	$39,970$	16.49%	33.91%	16.05%	16.92%	16.15%	16.82%	24.04%

Table 5.3 shows the results of the distributions. When considering all CIS distribution classes, the mean minimum SoC of $3.90\,\%$ with a relative frequency of underestimations of $34.95\,\%$ were achieved. When considering CIS distribution classes with $p_{\mathrm{chg}} < 0.65$, the relative frequency of underestimates was reduced to $24.04\,\%$. However, the mean remaining capacity increased to $16.49\,\%$ (see in Figure 5.16 for the rightward shift of the distribution function in (b) compared to (a)). Finally, the relative remaining capacity of the different MLD classes was

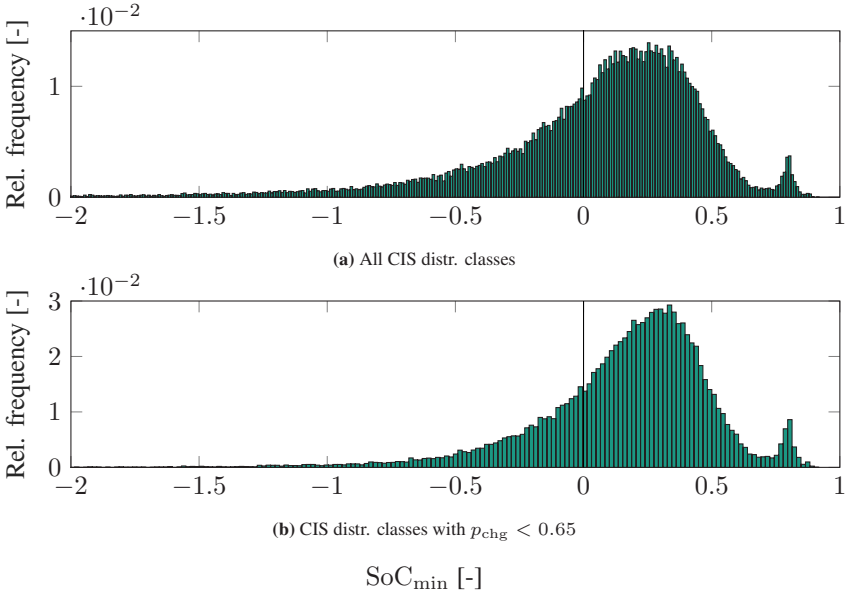

(a) All CIS distr. classes

(b) CIS distr. classes with $p_{\mathrm{chg}} < 0.65$

Figure 5.16: $\mathrm{SoC}_{\mathrm{min}}$ for CS O, analysis based on Equation 5.47

analyzed based on Equation 5.47, whereby the quantity $\mathbf{C}$ differed for the two CIS distribution class-based investigations. The results appear in Figure 5.17.

The boxplots on the left (a) show those based on all CIS distribution classes, whereas the boxplots on the right (b) show those for CIS distribution classes with $p_{\mathrm{chg}} < 0.65$. Notably, the classes *Industry 1:1* and *Industry singleloop* showed a low scatter with a high mean relative remaining capacity of about $80\,\%$ in both studies, as the second maximum in Figure 5.16. The MLD classes contained many layouts with exactly two stations. Thus, $p_{\mathrm{chg}} = 0.5$ resulted in the number of chained runs of $N_{\mathrm{run}}^{\mathrm{chain}} = 10$, whereby the real number was given by the singleloop layout with $N_{\mathrm{run}}^{\mathrm{chain}} = 2$. This calculation overestimated $N_{\mathrm{run}}^{\mathrm{chain}}$ of $(10 - 2)/2 = 400\,\%$, which resulted in a mean relative remaining capacity of $80\,\%$. The MLD class *Literature singleloop* had the only negative relative remaining capacities within the interquartile range in this analysis, with the median in (a) and (b) assuming positive relative remaining capacity. For all

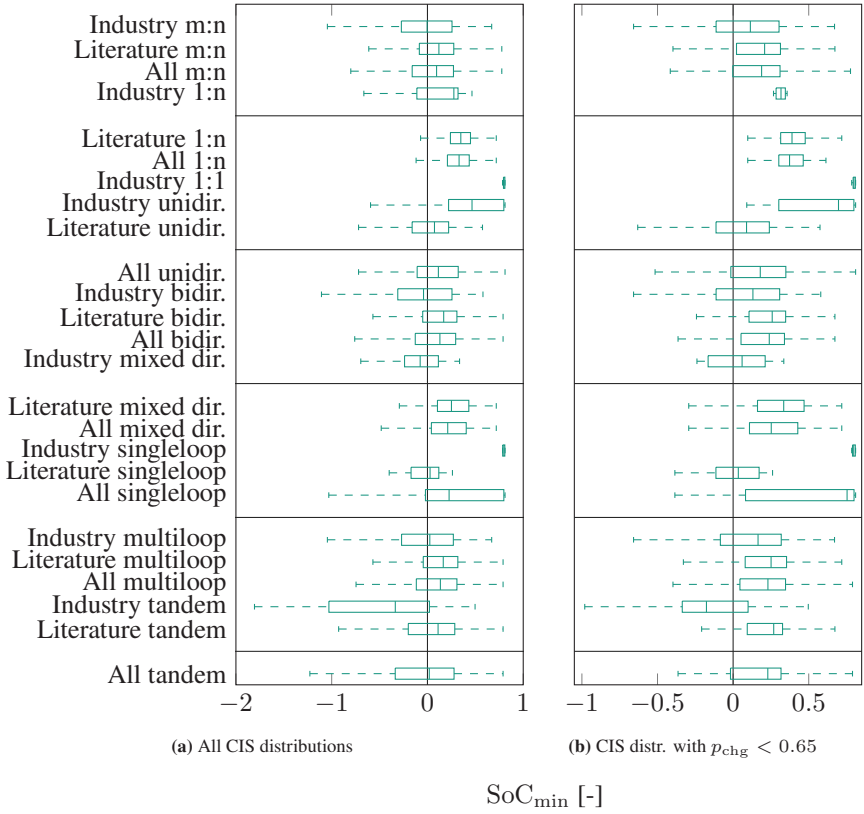

(a) All CIS distributions

(b) CIS distr. with $p_{\text{chg}} < 0.65$

Figure 5.17: CS O Layout class specific analysis for each CIS distribution, analysis based on Equation 5.47

other MLD classes, no significant behaviors were identified. In summary, the ESRM for CS O with a mean relative remaining capacity of $3.90\,\%$ was deemed suitable for approximating the ESR of AGVs. However, a CIS probability of $p_{\text{chg}} > 0.65$ was more probable to lead to a negative mean remaining capacity.

5.5.3 ESRM Analysis for CS Interim

Based on the verification of the AAM, an increasing p_{chg} was correlated with an increasing frequency of use of the AAM. For this reason, a second consideration of the data with CIS distribution classes with $p_{\mathrm{chg}} < 0.65$ was added to the analysis. This limit is based on the findings during the verification of the AAM (cf. Section 5.4.3), and the subset of all CIS distribution classes to analyze the CS O (cf. Section 5.5.2). Figure 5.18 shows the relative frequency of the relative remaining capacity after the simulation ended.
In Figure 5.18, (a) and (b) depict the course for CS I with $t_{\mathrm{op}} = 8\,\mathrm{h}$ (I_8), where (a) includes all data according to Equation 5.47, but for (b) $\mathbf{C}$, only the set of all CIS distribution classes with probabilities $p_{\mathrm{chg}} < 0.65$ was considered. The same applied to (c) and (d) for $t_{\mathrm{op}} = 16\,\mathrm{h}$ (I_{16}), whereby (c) included all CIS distribution classes while (d) only included the CIS distribution classes equivalent to (b). According to the histograms with all CIS distribution classes, a peak of the relative frequency was formed at a relative remaining capacity of $88.8\,\%$ for I_8 and $93.4\,\%$ for I_{16}. For the data with CIS probabilities $p_{\mathrm{chg}} < 0.65$ (cf. (b) and (d)), the amplitude of the peaks reduced compared to (a) and (b) due to the lower number of executions of the AAM, since the approximation was significantly less accurate while the ESR was significantly overestimated (cf. Section 5.4.3).
Table 5.4 shows the mean, σ, and confidence intervals of the remaining capacity

Table 5.4: ESRM Results for CS I

CS	CIS distr. classes	Sample size	Remaining capacity mean	σ	$\alpha = 1\%$		$\alpha = 5\%$		Freq. neg. capacity
	p_{chg}				Δ_{low}	Δ_{high}	Δ_{low}	Δ_{high}	
I_8	All	$58,240$	52.41%	30.60%	52.09%	52.74%	52.17%	52.66%	4.63%
	< 0.65	$39,970$	45.99%	30.11%	45.60%	46.38%	45.69%	46.28%	5.77%
I_{16}	All	$58,240$	61.31%	42.87%	60.85%	61.77%	60.96%	61.66%	6.03%
	< 0.65	$39,970$	56.67%	33.75%	56.23%	57.10%	56.34%	57.00%	6.80%

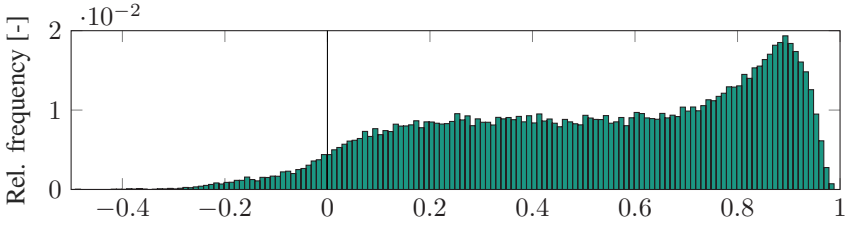

(a) All CIS distr. classes for CS I, with $t_{\mathrm{op}} = 8\mathrm{h}$

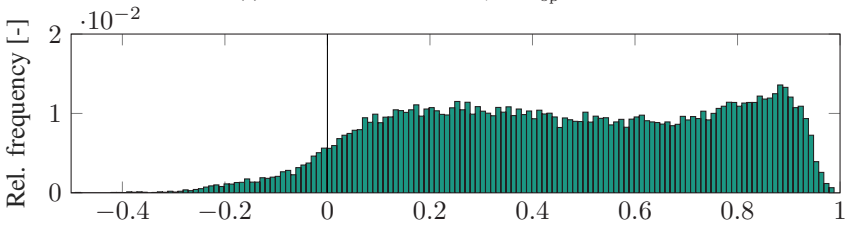

(b) CIS distr. classes with $p_{\mathrm{chg}} < 0.65$ CS I, with $t_{\mathrm{op}} = 8\mathrm{h}$

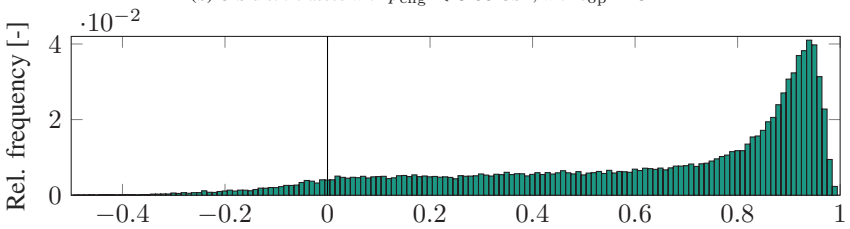

(c) All CIS distr. classes for CS I, with $t_{\mathrm{op}} = 16\mathrm{h}$

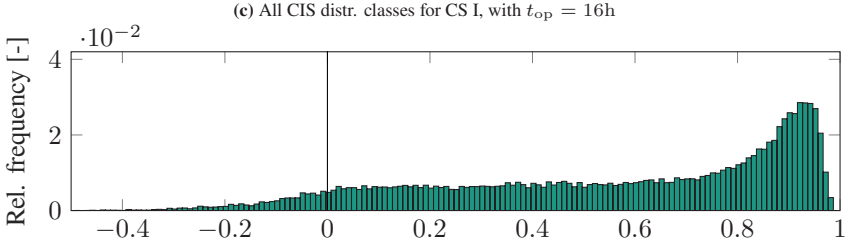

(d) CIS distr. classes with $p_{\mathrm{chg}} < 0.65$ for CS I, with $t_{\mathrm{op}} = 16\mathrm{h}$

Relative remaining capacity [-]

Figure 5.18: Relative remaining capacity for CS I, analysis based on Equation 5.47

and the relative frequencies of negative remaining capacities for all four previously mentioned cases. The mean frequencies of negative remaining capacities of $4.63\,\%$ for I_8 and $6.03\,\%$ for I_{16} showed that a sufficient ESR was determined in approximately $95\,\%$ of the ESRM executions. However, with average remaining capacities of $52.41\,\%$ for I_8 and $61.31\,\%$ for I_{16}, the results also showed that the ESR was significantly overestimated on average. When comparing the mean and σ of the rel. remaining capacity and the frequency of negative remaining capacities, for I_8 with a lower probability of underestimating the ESR, a more accurate estimate of the ESR was possible than for I_{16}. The more accurate estimate produced a smaller average overestimation of the ESR and was quantified by a smaller mean and σ remaining capacity. When comparing the data between all CIS distribution classes and those with $p_{\mathrm{chg}} < 0.65$ for one operation time each, I_8 and I_{16} showed a reduction in the mean overestimation of $6.42\,\%$ for I_8 and $4.64\,\%$ for I_{16}, whereby the frequency of a negative remaining capacity increased by $1.14\,\%$ for I_8 and $0.77\,\%$ for I_{16}.

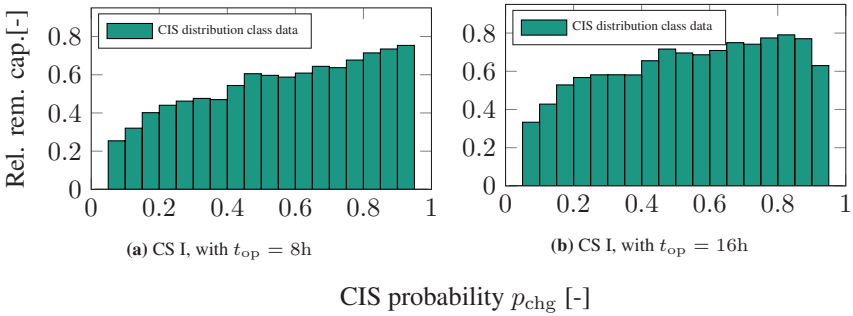

(a) CS I, with $t_{\mathrm{op}} = 8\mathrm{h}$

(b) CS I, with $t_{\mathrm{op}} = 16\mathrm{h}$

Figure 5.19: Relative remaining capacity over CIS distributions p_{chg} for CS I with $t_{\mathrm{op}} \in \{8\mathrm{h}, 16\mathrm{h}\}$, analysis based on Equation 5.47

Moreover, in Figure 5.19, the relative remaining capacity for each I_8 and I_{16} was compared to the CIS distribution classes as histograms. For I_8 (cf. (a)), the relative remaining capacity increased with an increasing p_{chg}. The data I_{16} (cf. (b)) showed a similar behavior, whereby a peak was reached at the CIS distribution class $0.8 \leq p_{\mathrm{chg}} < 0.85$ with a rel. remaining capacity of $79.1\,\%$ that

dropped slightly at $p_{\mathrm{chg}} \geq 0.85$. This behavior was due to two parameters of the ESRM for CS I, the assumed intermediate charging time t_{chg} and the weighting factor ρ of transport and empty runs. According to Equation 5.19, the minimum intermediate charging time t_{chg} was assumed for the intermediate charging time, corresponding to the duration of an average load handling. In the case of chained transport orders where a station was both a sink and a source, the intermediate charging time doubled, for example. The weighting factor ρ was assumed to be $\rho = 0.5$ for these investigations. However, if fewer empty runs than transport runs were required within a simulation run, the actual weighting changed, resulting in a higher frequency of intermediate charges (cf. Equation 5.17). However, this higher frequency was not considered in the previous design of the ESR by the ESRM and caused an overestimation of the ESR.

A final analysis of the MLD class data for CS I showed that for I_8 and I_{16}, all medians of the relative remaining capacities were positive. Furthermore, the results showed that the upper whisker of all MLD classes except for *Industry mixed dir.* achieved a relative remaining capacity of $> 95\,\%$. This result could be explained by the frequency of execution of the AAM, which was used at least once for 38 of 72 MLD (cf. Appendix A.4). Thus, the AAM led to a significant overestimation of the ESR (cf. Section 5.4.3).
To summarize, the ESRM significantly overestimated the ESR for CS I with an average of approximately $50\,\%$ due to stochastic influencing factors, such as the stochastic occurrence of transport orders with varied sequences of the chained orders. A data analysis of all simulations with $p_{\mathrm{chg}} < 0.65$ also showed high mean overestimates of the ESR at approximately $51\,\%$. Therefore, the ESRM for CS I applied to the size of an ESS for AGVs, determined a sufficiently large ESS capacity in $95.37\,\%$ of all examined cases. However, the ESRM was not suitable for the exact modeling of the ESR for CS I, as the mean overestimate of $54.1\,\%$ was too large.

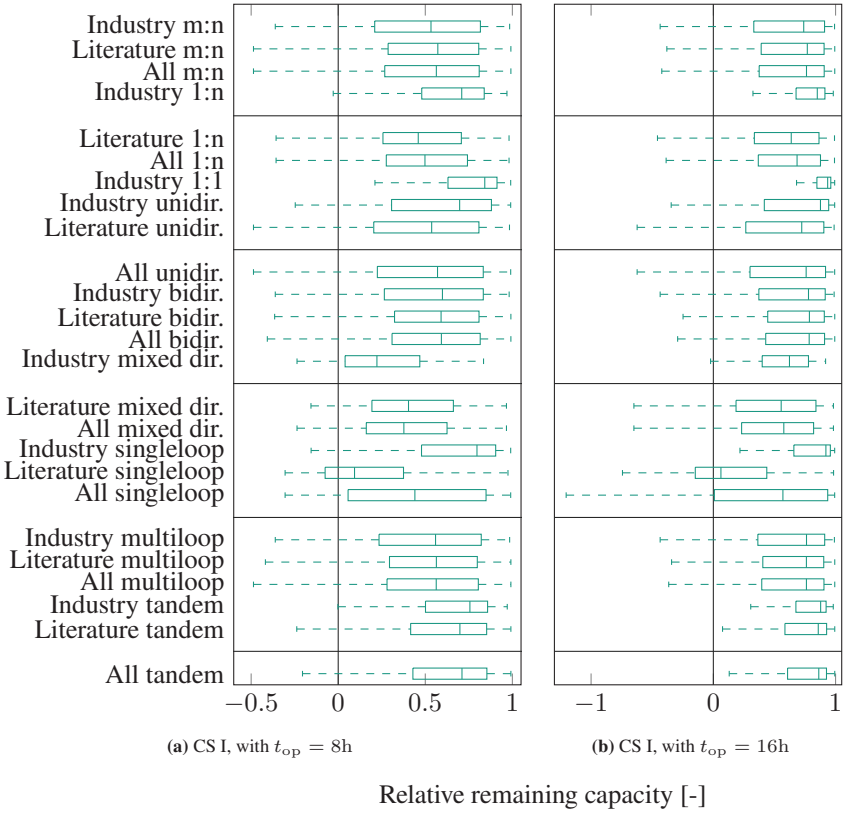

(a) CS I, with $t_{\mathrm{op}} = 8\mathrm{h}$ **(b)** CS I, with $t_{\mathrm{op}} = 16\mathrm{h}$

Figure 5.20: CS I Layout class specific analysis for each CIS distribution, analysis based on Equation 5.49

5.5.4 Safety Confidence of the ESR

As the results in Figure 5.12, Figure 5.16, and Figure 5.18 show, the ESR is often underestimated. Another design criterion, the safety confidence level (S_{cl}), is required to avoid this and to size a reliable ESS. The S_{cl} describes a one-sided confidence interval with a lower limit. The lower limit of the S_{cl} corresponds to the safety factor S_{F}^{-}, which is added to the modeled ESR. The S_{F}^{-} can be

calculated using the following Equation 5.53, according to Schiefer and Schiefer (2021):

$$S_{\mathrm{F}}^{-} = \mu - z_{\mathrm{CI}}(S_{\mathrm{cl}}) \cdot \frac{\sigma}{\sqrt{n}} \tag{5.53}$$

where μ is the mean value of the ESR, z_{CI} is the z-value of a normal distribution depending on S_{cl}, σ is the standard deviation of the ESR, and n is the number of identical simulation runs. As there is only one run of all simulations, n is 1. Since $\sqrt{1} = 1$, this is shortened in the equation, resulting in the following relationship:

$$S_{\mathrm{F}}^{-} = \mu - z_{\mathrm{CI}}(S_{\mathrm{cl}}) \cdot \sigma \tag{5.54}$$

As assumed, the z-value for normal distributions are taken from the z-distribution table (cf Appendix A.12).

The new ESR $E_{\mathrm{ESS}}^{\mathrm{Scl}}$ consider the S_{cl} and is determined as follows:

$$E_{\mathrm{ESS}}^{\mathrm{Scl}} = E_{\mathrm{ESS}} \cdot (1 - S_{\mathrm{F}}^{-}) \tag{5.55}$$

A qualitative analysis was performed to verify this calculation rule for the three charging strategies C, I, and O. For all CS in the ESRM, E_{cycle} (cf. Equation 5.10), E_{stby} (cf. Equation 5.13), and $N_{\mathrm{run}}^{\mathrm{AGV}}$ (Equation 5.13) are independent of E_{ESS}. Since no charging processes are considered in the modeling of CS C, an average, linearly decreasing course of the capacity over time was observed. An increase of the E_{ESS} by considering the S_{F}^{-} only leads to an increase of the basic capacity but does not affect the energy requirement of the AGVs. The absolute capacity decrease over the operating time t_{op} does not vary.
With CS I, the charging power P_{chg} and the E_{ESS} are interdependent (cf. Equation 5.17). According to this, an increase in the capacity of the ESS by

the S_{F}^{-} leads to an increase in P_{chg}. While the average time available for intermediate charging t_{chg} remains constant, the amount of energy E_{chg} increases, which has a positive effect on the SoC of the ESS during the operating time t_{op}. The behavior of an increase in E_{ESS} with CS O is similar to that of CS I, since the P_{chg} is also increased proportionally (cf. Equation 5.16). Charging time is reduced with CS O because only full charge cycles are considered. This results in lower vehicle utilization U. The effect of each system parameter as E_{ESS} increases is shown in the following Table 5.5.

If E_{ESS} decreases, the charging capacities would be reduced and the opposite

Table 5.5: Impact analysis of the SF^{-}. $E_{\mathrm{R}}^{\mathrm{AGV}}$: Energy requirement per vehicle, ↑: increase, ↓: decrease, −: remain steady

CS	E_{ESS}	U	P_{chg}	t_{chg}	$E_{\mathrm{R}}^{\mathrm{AGV}}$
Capacitive	↑	−	N/A	N/A	−
Interim	↑	−	↑	−	−
Opportunity	↑	↓	↑	↓	−

effect would occur concerning the reduction of E_{ESS} underestimates. For this reason, E_{ESS} must be extended with the following case differentiation to consider only safety confidence levels that also correspond to an underestimated value of E_{ESS}:

$$E_{\mathrm{ESS}}^{\mathrm{Scl}} = \begin{cases} E_{\mathrm{ESS}} \cdot (1 - S_{\mathrm{F}}^{-}), & \text{if } S_{\mathrm{F}}^{-} < 0 \\ E_{\mathrm{ESS}}, & \text{otherwise.} \end{cases} \tag{5.56}$$

Table 5.6 shows the amount of the safety factors $|S_{\mathrm{F}}^{-}|$ for the respective results of the CS for $S_{\mathrm{cl}} = \{95.0\%, 99.0\%, 99.9\%\}$.
In the case of CS I with an $S_{\mathrm{cl}} = 95\%$, the case differentiation according to Equation 5.56 was needed in two of the four cases.
Due to the decreasing ESR, it can be assumed that the utilization U also decreases for CS O. This leads to a further positive influence on the safety level by sizing

Table 5.6: Complementary amount of the safety factors $|S_{\mathrm{F}}^{-}|$ for different S_{cl} and t_{op}. Lim: $p_{\mathrm{chg}} < 0.65$

CIS		CS C -		CS I ALL		CS I Lim		CS O ALL	CS O Lim
S_{cl}	z_{CI}	8h	16h	8h	16h	8h	16h	24h	24h
95.0%	1.65	10.8%	12.2%	0.00%	9.2%	3.5%	0.0%	73.8%	39.3%
99.0%	2.33	18.9%	20.0%	17.6%	38.6%	24.2%	22.0%	106.2%	62.5%
99.9%	3.09	27.8%	28.6%	40.5%	71.2%	47.1%	47.6%	142.0%	88.3%

a sufficient-sized ESS. However, the amount of the average overestimation will increase.

5.5.5 Comparison of the Results for Different CS

After the ESRM for the respective CS was examined individually, the absolute ESR of the respective CS was compared. For this purpose, Figure 5.21 shows five boxplots to illustrate the dispersion of the ESR of CSs C_8, C_{16}, I_8, I_{16}, and O. With CSs C and I, a smaller operation time resulted in a smaller ESR.

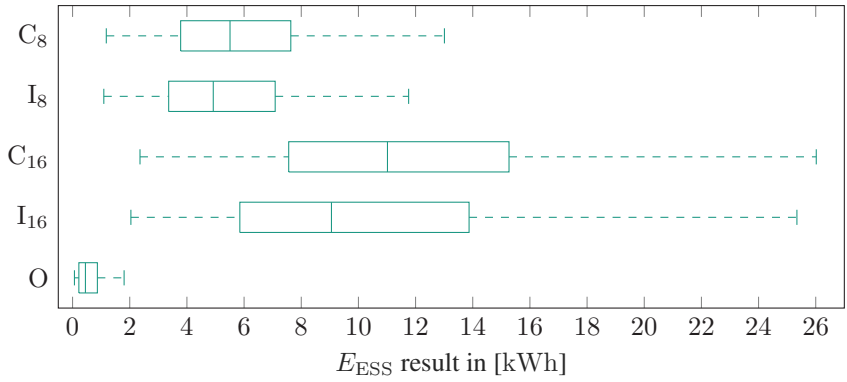

Figure 5.21: Comparison of total ESR of the different CS, analysis based on Equation 5.47

When comparing C_8 with I_8 and C_{16} with I_{16}, CS I always had a lower median ESR. The scatter below the median ESR was also narrower. The results of CS O showed that significant savings in ESR could achieved compared to CS C and I. A further comparison of the five smallest AGVs investigated in terms of the smallest electrical power ratings of Controls and Drives can be found in Appendix A.5. Figure 5.22 shows the curves of the mean ESR (cf. Table 5.7) as a function of the

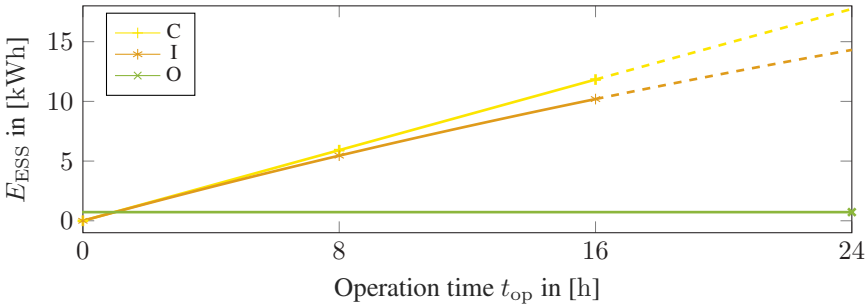

Figure 5.22: Sensitivity analysis of the ESR as a function of t_{op} for all CS. Dotted lines represent assumed course.

operation time t_{op} for CSs C, I, and O. For this purpose, interpolation functions were determined based on the determined mean ESR and assuming that the ESR at $t_{\mathrm{op}} = 0$ was 0 for the CS C and I. The curve of the ESR of CS C showed that it increased linearly with the operation time, corresponding to the linear relationship from Equation 5.15. While the ESR for CS C doubled between $t_{\mathrm{op}} = 8\,\mathrm{h}$ and $t_{\mathrm{op}} = 16\,\mathrm{h}$, the ESR for CS I only increased by $86.5\,\%$. However, due to the small number of measurement points ($t_{\mathrm{op}} \in \{8\,\mathrm{h}, 16\,\mathrm{h}\}$), no clear statement could be made about the interpolated exponential course of the ESR for CS I. Finally, the mean ESR for CS O was plotted according to Equation 5.41. The ESR for this CS was independent of the operational time. The quantitative results appear in Table 5.7.

Finally, an analysis of the ESR as a function of the CIS probability p_{chg} was conducted for CSs I and O. Figure 5.23 shows the results of this analysis for CSs O, $\mathbf{I}_8$, and $\mathbf{I}_{16}$, where each bar starts at an $E_{\mathrm{ESS}} = 0\,\mathrm{Wh}$. While for $\mathbf{I}_8$

Table 5.7: Quantitative ESR result comparison between different CS, analysis based on Eq. 5.47

CS	t_{op}	Sample size	E_{ESS} in [Wh] mean	σ	$\alpha = 1\%$		$\alpha = 5\%$	
					Δ_{low}	Δ_{high}	Δ_{low}	Δ_{high}
C	8h	5,040	5,915	2,800	5,813	6,016	5,837	5,992
C	16h	5,040	11,829	5,601	11,626	12,033	11,675	11,984
I	8h	5,040	5,454	2,691	5,356	5,552	5,380	5,528
I	16h	5,040	10,194	5,248	10,004	10,385	10,049	10,339
O	24h	5,040	724	824	695	754	702	747

and $\mathbf{I}_{16}$, the ESR decreased linearly with an increasing p_{chg}, the ESR for CS O decreased exponentially with an increasing p_{chg}. Red data interpolation lines show the corresponding curves. According to Equation 5.20 of the ESRM for CS I, a linear behavior was expected since, with an increasing p_{chg}, the amount of energy gained by intermediate charging was subtracted from the ESR. According to Equation 5.41 of the ESRM for CS O, the expected exponential behavior is shown in Figure 5.23.

In summary, comparing the different CSs with the different operating times indicated that an average ESR saving of at least $86.7\,\%$ could be achieved with CS O for longer operating times than for CSs C and I. It also showed that an average ESR saving of $7.8\,\%$ could be achieved through regular intermediate charges with CS I compared to CS C. Finally, the analysis of the total ESR as a function of the CIS probability indicated it had a significant impact on the size of the ESR and reduced the ESR continuously as the probability increased.

5.6 Chapter Conclusion

This chapter answered RQ3:

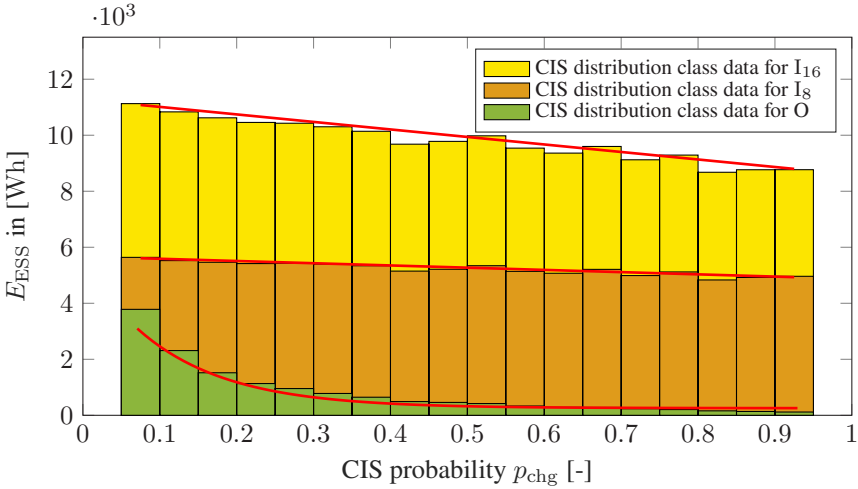

Figure 5.23: Total ESR comparison between CS I and O, analysis based on Equation 5.47

RQ3: How can the energy storage requirement for AGVs be modeled, considering different charging strategies and operating times?

An ESRM was presented to answer this question by determining the ESR for AGVs numerically, considering various influencing factors such as material flow and layout. The first step determined the fleet size using a numerical approximation method. The ESR was then calculated considering the CSs C, I, and O. For the subsequent validation of the ESRM, a design of experiments was conducted at the beginning, in which all parameters were varied and their variation limits were dimensioned. Furthermore, the implementation of the simulation model was described, and individual functions, such as dispatching and fleet size estimation, were verified. In the last part, the simulation results were analyzed individually for each CS and compared. The ESRM was suitable for CS C and CS O, sizing an ESS capacity for the operation of AGVs and performing an accurate estimation of the mean ESR. Furthermore, the ESRM for the CS I was found to only be applicable for a sufficient sizing of the ESS capacity, but the estimation of the

mean ESR was too inaccurate. This finding required a revision of the model for CS I in which stochastic influencing factors were more strongly included in the ESR calculation process.

6 Conclusion and Outlook

6.1 Summary

This thesis aimed to develop a model for determining the ESR of mobile robots, considering material flow and layout, vehicle specifications, CSs, and CIS distributions. After the relevant literature review in Chapter 2, the first RQ was addressed and answered in Chapter 3:

> **RQ1: How can intralogistics material flow and layout data be systematically described for the model-based investigation of energy requirement considerations of AGVs?**

The analysis of the requirements for the description of material flow and layout for energy requirement considerations identified that the description by two matrices, transport and distance matrix contained sufficient information. This finding was also confirmed by the results of the ERM validation in Chapter 4, in which the MLD were processed in the form of these matrices. Furthermore, a taxonomy was developed to classify MLD uniformly, allowing MLD class-specific result evaluations for various research disciplines. Furthermore, a data set with 72 MLD data from the literature and industry was created, providing the data basis for the following validations of the ESRM. Chapter 4 presented a state-based ERM to model the power and energy requirement and the cycle times of AGVs in different process states. The validation of the ERM by comparison with real tests of two different industrial vehicles showed an average deviation of the modeled power requirement of approximately $-1.0\,\%$. The validation showed that for

AGVs with an average total power consumption while state driving of $\leq 100\,\mathrm{W}$, accurate modeling in the confidence interval of $-1.3\,\%$ to $-0.73\,\%$ was possible at a significance level of $\alpha = 0.01$, thereby answering the second RQ:

> **RQ2: How can the energy requirement for AGVs be modeled, considering the material flow, layout, charging strategy, capacity utilization, and vehicle specifications?**

Finally, Chapter 5 presented the ESRM to calculate the ESR for ESS for AGVs, considering material flow and layout, vehicle specifications, CSs, operation times, and CIS probabilities. In the beginning, the partial methods of the model and the simulation tool were verified, including the fleet size modeling, the chained run determination method for CS O, the AAM for CS I, and the dispatching method for multiple vehicles. After successfully verifying these partial methods and functions, a final validation was conducted in which the CIS distribution, AGV type, MLD, and CS were varied. A total number of $n_{\mathrm{sim}} = 1,940,400$ simulation runs were executed and evaluated. The ESRM for CS C showed an accurate mean relative estimation of the required ESS capacity of approximately $92.5\,\%$. Hence, the model tended to overestimate. For CS O, the accuracy of the mean relative estimation of the ESR was $96.1\,\%$. Further data analysis, in which the CIS probabilities $p_{\mathrm{chg}} \geq 0.65$ were filtered out, showed that the mean relative estimation of the ESR fell to approximately $83.5\,\%$. Overall, the mean ESR for CS O tended to be overestimated. For CS I, the ESRM showed a mean accuracy of the ESR approximation of $43.14\,\%$. Due to the high mean overestimation, the number of negative ESRs was $5.33\,\%$, which answered the third RQ:

> **RQ3: How can the energy storage requirement for AGVs be modeled, considering different charging strategies and operating times?**

In conclusion, the state-based ERM proved to be a suitable model for approximating the power and energy requirement of AGVs under multiple constraints. The

ESRM, on the other hand, could be used for CS C and CS O as a suitable model for approximating the mean ESR, whereas the ESRM for CS I could only be used as a rough design strategy for ESS sizing.

6.2 Limitations

Even though the MLD data set created with 72 MLD (cf. Chapter 3) was comprehensive, it was insufficient for the MLD class-based investigations since some classes included only one MLD, so no representative results were obtained for all MLD classes. The process analysis of 25 different AGVs was conducted to make an initial statement about the applicability of the ERM (cf. Chapter 4) for different AGVs. For more general statements, however, further vehicle types needed to be analyzed, and more detailed delimitations of the model needed to be defined in case of possible deviations.

The ERM was validated based on real experiments with two different industrial vehicles with a maximum average total power consumption while driving of $100.2\,\mathrm{W}$ and a maximum average power of the LHD in the active load handling state of $53.83\,\mathrm{W}$. More real experiments with AGVs of higher power classes, such as forklift AGVs, are required to make a more general statement on the applicability of the model.

The ESRM, described in Chapter 5, only considered CSs C, I, and O at present. Therefore, further CSs may require adaptations for applicability. When analyzing the model for the three CSs mentioned, the operation times $t_{\mathrm{op}} \in \{8\,\mathrm{h}, 16\,\mathrm{h}, 24\,\mathrm{h}\}$ were examined and validated, from which a curve was interpolated at other operation times. For CS I, in particular, investigating other operation times could reveal further information about the dependency of the operation time within the ESR. During the validation of the ESRM through simulations, traffic situations and traffic regulations of the vehicles were neglected. The vehicle-specific utilization of load transfer and charging stations was also neglected. Further investigations could determine what impact such mutual affects have on the ESR. As the summary of scientific studies on the modeling of ESS in Section 2.6 showed, ESS

modeling strongly depends on the specific chemical properties of the ESS cells. For this reason, the behavior of electrochemical and electrical ESS was assumed to be linear, while the factors of temperature, aging, the number of cycles, and charging and discharging current were neglected.

6.3 Implications for Further Research

Section 2.4 overviewed scientific studies on the optimal location of DPs suitable for idle positions and the CIS installation. This thesis used the CIS probability p_{chg} as a scalar variable to quantify the probability of reaching a station with CIS. However, no distinction was made between stations with the CIS performing the function of a sink, a source, or both. In the case of CS I, this lack of differentiation meant that the p_{chg} was insufficient to predict an intermediate charge with an associated probability. With CS O, vehicles remained at sink and source stations with a CIS until the ESS was fully charged. In contrast, with CS I, a vehicle can never charge at a station that functions exclusively as a sink for more than the time required for the load-handling picking process. Therefore, more detailed differentiation could improve the accuracy of the ESRM for CS I.

In addition to the insufficiently detailed key figure of the CIS probability for CS I, the accuracy of the ESR approximation showed a large scatter and average relative remaining capacities of over $50\,\%$. The AAM verification (cf. Section 5.10) also showed that an AAM was frequently used. The model was built and extended as a linear model based on CS C, whereby the intermediate charges occurred stochastically. In further investigations, an exponential model considering stochastic variables, such as the probability of reaching a charging station and the distinction of the station characteristic, as described above, could achieve more accurate results.

The numerical method used to calculate the fleet size according to Section 5.1.1 could also be improved in future studies to enable a more precise estimation depending on the distribution of the vehicle interactions and charging speeds due to the factor c_{r}. Compared to the simulative methods in Section 2.3, the numerical method offered a faster and less computationally intensive solution. The aim was to maximize the number of relatively completed transport orders on average $\rho_{\mathrm{OC}} \rightarrow 1.0$, whereby the achieved results should have a lower scatter $\sigma \rightarrow 0$.

6.4 Applications to Practitioners

Finally, companies in various industries can benefit from the results of this work. Mobile robot manufacturers can design more efficient ESS by precisely modeling the ESR, thereby saving space in the vehicle while contributing to an overall more compact vehicle design. Assuming that ESSs with larger capacities are also more cost-intensive opens the possibility of reducing costs and gaining a competitive advantage. Manufacturers of ESSs can use the ESRM in this work to carry out targeted sizing for ESSs in mobile robots, provided that relevant data such as material flow, layout, and vehicle specifications are available. There is also an opportunity to gain a competitive advantage by developing customized, resource-efficient ESSs. For layout planners and system planners, the findings of this thesis provide a selection aid for the optimal distribution of CIS and ESS types, which applies in particular in consideration of the known material flow and layout, enabling a well-founded decision-making basis for the number and distribution of CISs in the layout.

A Appendix

A.1 MLD Dataset

Table A.1: Literature based layout data classification

Layout ID	Flow Path			Layout Topology			Task structure	Number of Stations
	unidir.	bidir.	mixed dir.	singleloop	multiloop	tandem	1:1,1:n,m:n	
Literature01	•				•		m:n	9
Literature02			•		•		1:n	20
Literature03		•			•		m:n	8
Literature04		•			•		m:n	8
Literature05		•			•		m:n	8
Literature06		•			•		m:n	8
Literature07		•			•		m:n	8
Literature08		•			•		m:n	16
Literature09		•			•		m:n	16
Literature10		•			•		m:n	16
Literature11		•			•		m:n	16

Continued on next page

Layout ID	Flow Path			Layout Topology			Task Structure	Number of Stations
	unidir.	bidir.	mixed dir.	singleloop	multiloop	tandem	1:1,1:n,m:n	
Literature12		•			•		m:n	16
Literature13	•				•		1:n	10
Literature14		•			•		1:n	10
Literature15		•			•	$\bullet_A$	1:n	3
Literature16		•			•	$\bullet_A$	1:n	4
Literature17		•			•	$\bullet_A$	1:n	5
Literature18		•			•	$\bullet_A$	m:n	4
Literature19	•				•		m:n	20
Literature20		•			•	$\bullet_B$	m:n	7
Literature21		•			•	$\bullet_B$	m:n	8
Literature22		•			•	$\bullet_B$	m:n	8
Literature23		•			•	$\bullet_B$	m:n	3
Literature24		•			•	$\bullet_C$	m:n	7
Literature25		•			•	$\bullet_C$	m:n	7
Literature26		•			•	$\bullet_C$	m:n	6
Literature27		•			•	$\bullet_C$	m:n	6
Literature28			•		•		m:n	9
Literature29		•			•		m:n	7
Literature30	•			•			m:n	7
Literature31	•				•		m:n	11
Literature32		•			•		m:n	11

Continued on next page

Layout ID	Flow Path			Layout Topology			Task Structure	Number of Stations
	unidir.	bidir.	mixed dir.	singleloop	multiloop	tandem	1:1,1:n,m:n	
Literature33			•		•		m:n	11
Literature34		•			•		m:n	6
Literature35	•				•		m:n	7
Literature36		•			•		m:n	11
Literature37	•				•		m:n	20
Literature38		•			•		m:n	8
Literature39		•			•		m:n	4
Literature40			•		•		1:n	7
Literature41	•				•		m:n	6
Literature42		•			•		m:n	8

Table A.2: Industry based layout data classification

Layout ID	Flow Path			Layout Topology			Task structure	Number of stations
	unidir.	bidir.	mixed dir.	singleloop	multiloop	tandem	1:1, 1:n, m:n	
Industry01	•				•		m:n	7
Industry02	•			•			m:n	4

Continued on next page

Layout ID	Flow Path			Layout Topology			Task structure	Number of stations
	unidir.	bidir.	mixed dir.	singleloop	multiloop	tandem	1:1, 1:n, m:n	
Industry03		•			•		m:n	15
Industry04	•			•			1:1	2
Industry05		•			•		m:n	10
Industry06			•		•		m:n	58 (33 used)
Industry07	•			•			1:1	2
Industry08	•				•		m:n	4
Industry09	•			•			1:1	2
Industry10		•			•		1:n	7
Industry11		•			•		m:n	9
Industry12		•			•		m:n	7
Industry13	•			•			1:1	2
Industry14	•			•			1:1	2
Industry15	•			•			1:1	2
Industry16	•			•			1:1	2
Industry17	•			•			1:1	2
Industry18	•			•			1:1	2
Industry19	•			•			1:1	2
Industry20	•			•			1:1	2
Industry21	•			•			1:1	2
Industry22	•			•			1:1	2
Industry23	•			•			1:1	2

Continued on next page

Layout ID	Flow Path			Layout Topology			Task structure	Number of stations
	unidir.	bidir.	mixed dir.	singleloop	multiloop	tandem	1:1, 1:n, m:n	
Industry24	•			•			1:1	2
Industry25	•			•			1:1	2
Industry26		•			•		m:n	23 (22 used)
Industry27		•			•		m:n	6
Industry28		•			•	$\bullet_D$	m:n	9
Industry29		•			•	$\bullet_D$	m:n	10
Industry30		•			•		m:n	5

Table A.3: Applied data acquisition and treatment methods based on literature data

Layout ID	A_D based on					A_T based on			Coord.		Reference
	Distance matrix	Time matrix	Graph	Manhattan	Scaled plan	Job sequence	Job list	Transport matrix	given	assumed	based on
Literature01			•					•		•	Kaspi and Tanchoco (1990), Kaspi et al. (2002)
Literature02	•						•				Singh et al. (2011)
Literature03			•		•		•			•	Schrecker (2000)

Continued on next page

Layout ID	A_D based on					A_T based on			Coord.		Reference
	Distance matrix	Time matrix	Graph	Manhattan	Scaled plan	Job sequence	Job list	Transport matrix	given	assumed	based on
Literature04			•		•		•			•	Schrecker (2000)
Literature05			•		•		•			•	Schrecker (2000)
Literature06			•		•		•			•	Schrecker (2000)
Literature07			•		•		•			•	Schrecker (2000)
Literature08			•		•		•			•	Schrecker (2000)
Literature09			•		•		•			•	Schrecker (2000)
Literature10			•		•		•			•	Schrecker (2000)
Literature11			•		•		•			•	Schrecker (2000)
Literature12			•		•		•			•	Schrecker (2000)
Literature13			•	•		•			•		Yu and Egbelu (2001)
Literature14			•	•		•			•		Yu and Egbelu (2001)
Literature15			•	•		•			•		Yu and Egbelu (2001)
Literature16			•	•		•			•		Yu and Egbelu (2001)
Literature17			•	•		•			•		Yu and Egbelu (2001)
Literature18			•	•		•			•		Yu and Egbelu (2001)
Literature19			•	•		•			•		Yu and Egbelu (2001)
Literature20			•	•		•			•		Yu and Egbelu (2001)
Literature21			•	•		•			•		Yu and Egbelu (2001)
Literature22			•	•		•			•		Yu and Egbelu (2001)
Literature23			•	•		•			•		Yu and Egbelu (2001)

Continued on next page

Layout ID	A_D based on					A_T based on			Coord.		Reference
	Distance matrix	Time matrix	Graph	Manhattan	Scaled plan	Job sequence	Job list	Transport matrix	given	assumed	based on
Literature24			•	•		•			•		Yu and Egbelu (2001)
Literature25			•	•		•			•		Yu and Egbelu (2001)
Literature26			•	•		•			•		Yu and Egbelu (2001)
Literature27			•	•		•			•		Yu and Egbelu (2001)
Literature28		•						•		•	Maxwell and Muckstadt (1982)
Literature29			•					•		•	Sinriech and Tanchoco (1993)
Literature30			•					•		•	Sinriech and Tanchoco (1993)
Literature31			•					•			Gourgand et al. (1995)
Literature32			•					•			Gourgand et al. (1995)
Literature33			•					•			Gourgand et al. (1995)
Literature34					•			•		•	Uttendorf and Overmeyer (2015)
Literature35	•							•			Srinivasan et al. (1994)
Literature36	•							•			Srinivasan et al. (1994)
Literature37	•							•			Srinivasan et al. (1994)
Literature38	•							•			Fottner et al. (2022)
Literature39	•							•			Fottner et al. (2022)
Literature40		•	•			•					Reddy and Rao (2006)

Continued on next page

Layout ID	A_D based on					A_T based on			Coord.		Reference
	Distance matrix	Time matrix	Graph	Manhattan	Scaled plan	Job sequence	Job list	Transport matrix	given	assumed	based on
Literature41		•						•			Rajotia et al. (1998)
Literature42			•	•				•	•		Bozer and Srinivasan (1992)

Table A.4: Applied data acquisition and treatment methods based on industry data

Layout ID	A_D based on					A_T based on			Coordinates	
	Distance matrix	Time matrix	Graph	Manhattan	Scaled plan	Job sequence	Job list	Transport matrix	given	assumed
Industry01					•		•			
Industry02				•	•			•		
Industry03				•	•			•		
Industry04				•	•			•		
Industry05				•	•			•		
Industry06	•							•	•	
Industry07	•						•			
Industry08					•		•			

Continued on next page

Layout ID	A_D based on					A_T based on			Coordinates	
	Distance matrix	Time matrix	Graph	Manhattan	Scaled plan	Job sequence	Job list	Transport matrix	given	assumed
Industry09	•							•		
Industry10	•							•		
Industry11	•					•				
Industry12					•	•				
Industry13	•						•			
Industry14	•						•			
Industry15	•						•			
Industry16	•						•			
Industry17	•						•			
Industry18	•						•			
Industry19	•						•			
Industry20	•						•			
Industry21	•						•			
Industry22	•						•			
Industry23	•						•			
Industry24	•						•			
Industry25	•						•			
Industry26					•		•		•	
Industry27					•		•		•	
Industry28					•		•		•	

Continued on next page

Layout ID	A_D based on					A_T based on			Coordinates	
	Distance matrix	Time matrix	Graph	Manhattan	Scaled plan	Job sequence	Job list	Transport matrix	given	assumed
Industry29					•		•		•	
Industry30					•		•		•	

A.2 ERM

Table A.5: Qualitative Process Analysis of Industrial AGVs

Nr	LHD	AGV Name	Process	PreDock		Dock	LH	Undock	PreDrive		Source
				Stop	init LHD				Stop	init LHD	
1	tug	Jungheinrich EZS 350a	lh^+	x	-	x	x	x	-	-	Jungheinrich AG (2021)
			lh^-	-	-	x	x	x	-	-	
2	fork-lift	Jungheinrich ERC 215a	lh^+,lh^-	x	x	x	x	x	x	x	Jungheinrich AG (2017)
3	fork-lift	Agilox One	lh^+,lh^-	x	-	x	x	x	x	-	CLS servizi e soluzioni in movimento (2020)
			charge	x	-	x	-	x	x	-	
4	fork-lift	Lmatic high-lift truck	lh^+,lh^-	x	x	x	x	x	-	-	Linde Material Handling (2021)
5	fork-lift	TÜNKERS STacker	lh^+	x	x	x	x	x	x	x	TÜNKERS Maschinenbau GmbH (2022)
6	fork-lift	K. Hartwall A-Mate	lh^+,lh^-	-	x	x	x	x	-	x	K. Hartwall (2021)
7	topload	Agilox ODM	lh^+	x	-	x	x	x	x	-	Agilox (2022)
			lh^-	x	x	x	x	x	x	-	
8	topload	MiR200	lh^+,lh^-	x	-	x	x	x	x	-	Mobile Industrial Robots (2019)
			park	x	-	x	-	x	x	-	
9	topload	Gebhardt Karis Custom	lh^+,lh^-	x	x	x	x	x	x	x	-
			charge	x	-	x	-	x	x	-	
10	topload	Jungheinrich AMR arculee S	lh^+,lh^-	x	-	x	x	x	x		Jungheinrich AG (2023)
11	topload	Idealworks iw.hub	lh^+,lh^-	x	-	x	x	x	x	-	idealworks (2021)

12	toplift	Milvus Robotics SEIT500	lh^+	x	-	x	x	x	x	x	Milvus Robotics (2021)
			lh^-	x	x	x	x	x	x	-	
13	toplift	Grenzebach L600-Li	lh^+,lh^-	x		x	x	x	x		STAPLERWORLD (2021)
14	toplift	Safelog X1	lh^+,lh^-	x	-	x	x	x	x	-	SAFELOG (2023)
15	toplift	Bosch Activeshuttle	lh^+,lh^-	x	x	x	x	x	x	x	Bosch Rexroth (2020)
16	passive	Mir 250	lh^+,lh^-	x	-	x	x	x	x	-	mR MOBILE ROBOTS (2021)
17	passive	SSI Schäfer Weasel Lite	lh^+,lh^-	-	-	-	-	-	x	-	SSI Schäfer Benelux (2016)
18	passive	SSI Schäfer Weasel	lh^+	x	-	-	-	-	-	-	SSI Schäfer D-A-CH (2016)
			lh^-	-	-	-	-	-	x	-	
19	passive	BITO FTS Leo	lh^+,lh^-	-	-	-	-	-	-	-	BITO-Lagertechnik (2021)
20	roller conveyor	DS Automation Sally	lh^+,lh^-	x	-	x	x	x	x	-	DS AUTOMOTION (2018)
21	roller conveyor	Carrybots Herbie	lh^+,lh^-	-	-	x	x	x	-	-	Carrybots GmbH (2022)
22	roller conveyor	SHERPA-B	lh^+,lh^-	-	-	x	x	x	-	-	SHERPA MOBILE ROBOTICS (2023)
23	roller conveyor	Omron LD-60,90	lh^+,lh^-	x	-	x	x	x	x	-	Omron Industrial Automation EMEA (2021)
24	roller conveyor	Gebhardt Karis Model 3	lh^+,lh^-	x	x	x	x	x	x	-	Gebhardt Intralogistics Group (2021)
25	customized lift	Gessbot Gb350	lh^-	x	x	x	x	x	x	x	W. Gessmann (2023)

Table A.6: Material Flow and Layout Description of the Experiments

ExpID	AGVID	Representation of Material Flow and Layout		Material Flow and Layout Classification		
		Layout	Material flow per hour	Flow path orientation	Layout topology	Task structure
01A 01B 01C 02	Weasel	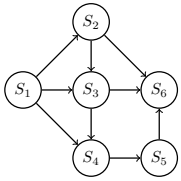	$A_{\mathrm{T},i}$	unidir.	multiloop	m:n
03 04 05 06 07 08 09 10	Weasel	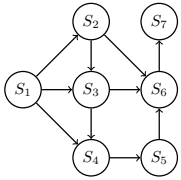	$A_{\mathrm{T},i}$	unidir.	multiloop	m:n
11 12	Karis	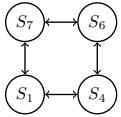	$J_{11} = 3 \cdot \left\{ \begin{array}{l} (S7 \rightarrow S6), (S4 \rightarrow S1), (S6 \rightarrow S4), \\ (S1 \rightarrow S7), (S7 \rightarrow S1), (S4 \rightarrow S6), \\ (S1 \rightarrow S4), (S6 \rightarrow S7) \end{array} \right\}$ $J_{12} = 3 \cdot \left\{ \begin{array}{l} (S7 \rightarrow S6), (S4 \rightarrow S1), (S6 \rightarrow S4), \\ (S1 \rightarrow S6), (S4 \rightarrow S1), (S6 \rightarrow S4), \\ (S1 \rightarrow S7) \end{array} \right\}$	bidir.	multiloop	m:n
13	Karis	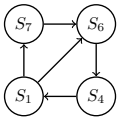	$J_{13} = 2 \cdot \left\{ \begin{array}{l} (S7 \rightarrow S6), (S4 \rightarrow S1), (S6 \rightarrow S4), \\ (S1 \rightarrow S6), (S4 \rightarrow S1), (S6 \rightarrow S4), \\ (S1 \rightarrow S6), (S4 \rightarrow S1), (S6 \rightarrow S4), \\ (S1 \rightarrow S6), (S4 \rightarrow S1), (S6 \rightarrow S4), \\ (S1 \rightarrow S7) \end{array} \right\}$	unidir.	multiloop	m:n

Table A.7: Technical Specifications of the AGVs

	Weasel	**Karis**
Manufacturer	SSI Schaefer	Gebhardt Fordertechnik
Mass (vehicle without load)	$\begin{cases} 40.1\text{kg}, & \text{for LA} \\ 39.0\text{kg}, & \text{for EDLC} \end{cases}$	95.0kg
Mass (load)	-	10.5kg, 20kg, 30kg
Dimensions (vehilce without load, l x w x h)	810mm x 420mm x 250mm	810mm x 420mm x 250mm
Nominal System Voltage	24V	24V, 48V
Battery	Lead-acid Battery, EDLC	Varta Easy Blade 48V

Table A.8: Technical Specifications of the used ESS

	Lead-acid battery	20S4P 400F EDLC	Easy Blade 48
Manufacturer	SSI Schaefer	Ansmann AG	Varta Storage GmbH
Version	1.0	1.0	56654 799 092
Cell type	2xYuasa NP12-12	80xDSF407Q3R0	14x N.A.
Mass	9.7kg	6.6kg	9.6kg
Dimensions (l x w x h)	317mm x 120mm x 104mm	315mm x 193mm x 140mm	330mm x 230mm x 80mm
Nominal Voltage	24.0V	60.0V	48.0V
Maximum Current	$\pm$3.0A	$\pm$18.9A ($\Delta T = 15.0°\text{K}$)	$\pm$31A
Nominal C-rate Charging	0.25C	14.2C	1.0C
Nominal E	288Wh	40Wh	1502Wh

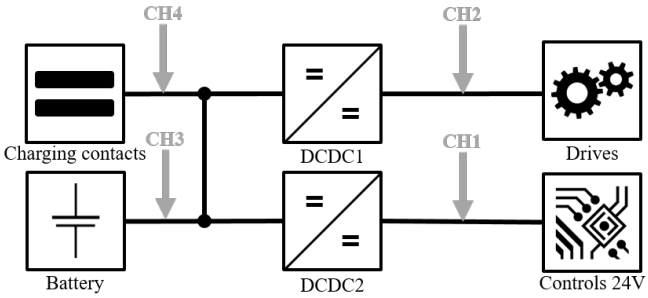

Figure A.1: AGV Weasel power consumption measurement concept

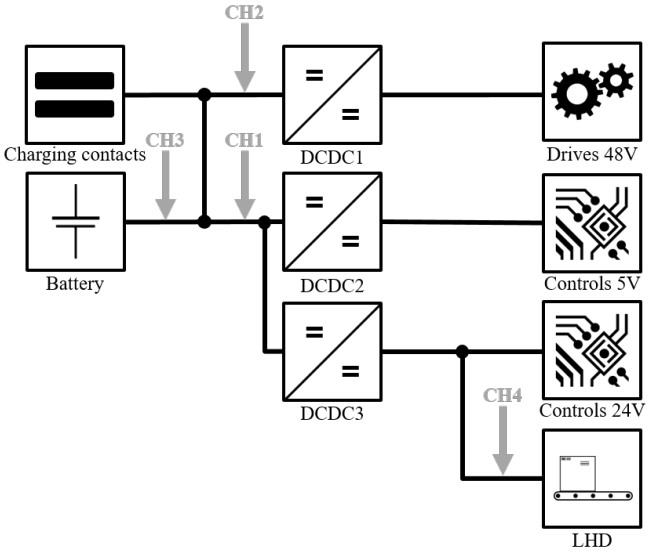

Figure A.2: AMR Karis power consumption measurement concept

Table A.9: Simulation parameter for model validation, based on measured experimental data

ExpID	Physics in $[\mathrm{m/s}, \mathrm{m/s^2}]$			Times in [s]					Powers in [W]										
									Charge	LHD		Controls		Drives					
	v	a_{acc}	a_{dec}	t_{lh}	t^{preDock}	t^{Dock}	t^{undock}	t^{preDrive}	P_{charge}	$P_{\mathrm{lh}}^{\pm}$	$P_{\mathrm{lh}}^{\mathrm{stby}}$	$P_{\mathrm{c}}^{\mathrm{active}}$	$P_{\mathrm{c}}^{\mathrm{stby}}$	$P_{\mathrm{d}}^{\mathrm{acc}}$	$P_{\mathrm{d}}^{\mathrm{d}}$	$P_{\mathrm{d}}^{\mathrm{dec}}$	$P_{\mathrm{d}}^{\mathrm{stby}}$	$P_{\mathrm{d}}^{\mathrm{dock}}$	$P_{\mathrm{d}}^{\mathrm{undock}}$
01A	1.0	1.0	1.0	5.0	-	-	-	-	-	-	-	7.480	5.480	39.179	12.478	-14.287	1.578	-	-
01B	0.5	1.0	1.0	5.0	-	-	-	-	-	-	-	7.414	5.476	26.747	6.204	-6.278	1.678	-	-
01C	0.7	1.0	1.0	5.0	-	-	-	-	-	-	-	7.245	5.469	30.405	8.451	-9.997	1.688	-	-
2	1.0	1.0	1.0	15.0	-	-	-	-	-	-	-	7.371	5.455	39.772	12.640	-14.384	1.644	-	-
3	1.0	1.0	1.0	10.0	-	-	-	-	75.591	-	-	7.430	5.457	40.080	13.008	-14.338	1.685	-	-
4	1.0	1.0	1.0	10.0	-	-	-	-	72.159	-	-	7.329	5.451	39.615	12.901	-14.284	1.601	-	-
5	1.0	1.0	1.0	10.0	-	-	-	-	65.292	-	-	7.492	5.459	40.822	13.380	-14.370	1.770	-	-
6	1.0	1.0	1.0	10.0	-	-	-	-	73.190	-	-	7.520	5.457	41.282	12.928	-13.931	1.629	-	-
7	1.0	1.0	1.0	10.0	-	-	-	-	92.626	-	-	7.363	5.480	38.175	12.756	-13.144	1.917	-	-
8	1.0	1.0	1.0	10.0	-	-	-	-	109.986	-	-	7.350	5.472	38.220	12.998	-13.136	1.884	-	-
9	1.0	1.0	1.0	10.0	-	-	-	-	52.696	-	-	7.338	5.477	38.987	13.103	-13.210	1.970	-	-
10	1.0	1.0	1.0	10.0	-	-	-	-	62.658	-	-	7.403	5.479	38.785	12.892	-13.212	1.954	-	-
11	0.25	0.4	1.0	10.735	3.664	17.626	9.356	0.924	1,415.0	52.254	7.339	62.961	57.271	-	36.021	-	10.797	17.625	17.986
12	0.27	0.4	1.0	9.330	3.580	18.202	9.951	0.795	1,415.0	54.511	7.455	62.920	55.814	-	37.614	-	10.913	18.160	18.488
13	0.28	0.4	1.0	8.667	3.436	15.708	9.693	0.870	1,365.0	54.716	7.504	63.193	55.152	-	37.897	-	11.651	18.067	18.235

Table A.10: System components energy requirement deviation between simulation and real experiments, presented as confidence intervals for specific siginificance levels α

ExpID	Max. rel. deviation controls				Max. rel. deviation drives				Max. rel. deviation LHD				Max. rel. deviation all components			
	$\alpha = 1\%$		$\alpha = 5\%$		$\alpha = 1\%$		$\alpha = 5\%$		$\alpha = 1\%$		$\alpha = 5\%$		$\alpha = 1\%$		$\alpha = 5\%$	
	Δ_{low}	Δ_{high}	Δ_{low}	Δ_{high}	Δ_{low}	Δ_{high}	Δ_{low}	Δ_{high}	Δ_{low}	Δ_{high}	Δ_{low}	Δ_{high}	Δ_{low}	Δ_{high}	Δ_{low}	Δ_{high}
01A	−0.06%	0.98%	0.08%	0.85%	0.61%	3.20%	0.94%	2.86%	-	-	-	-	0.38%	1.88%	0.57%	1.68%
01B	−1.14%	0.97%	−0.86%	0.69%	−2.16%	−0.02%	−1.88%	−0.30%	-	-	-	-	−1.39%	0.37%	−1.16%	0.14%
01C	−0.42%	0.33%	−0.32%	0.23%	−2.05%	−0.64%	−1.86%	−0.83%	-	-	-	-	−1.12%	−0.13%	−0.99%	−0.26%
02	−1.90%	−0.01%	−1.65%	−0.26%	−8.44%	−3.89%	−7.84%	−4.49%	-	-	-	-	−5.01%	−2.18%	−4.63%	−2.55%
03	−0.22%	0.48%	−0.13%	0.39%	−1.78%	0.39%	−1.49%	0.10%	-	-	-	-	−0.80%	0.32%	−0.65%	0.17%
04	−1.77%	−0.35%	−1.58%	−0.54%	−7.93%	−2.89%	−7.27%	−3.55%	-	-	-	-	−5.00%	−1.86%	−4.59%	−2.27%
05	−0.47%	0.60%	−0.33%	0.46%	−2.39%	0.20%	−2.05%	−0.14%	-	-	-	-	−1.16%	0.23%	−0.98%	0.04%
06	−3.81%	−1.54%	−3.51%	−1.84%	−9.47%	−6.50%	−9.08%	−6.89%	-	-	-	-	−6.67%	−4.38%	−6.37%	−4.68%
07	−1.00%	−0.06%	−0.88%	−0.18%	−3.66%	−2.03%	−3.45%	−2.25%	-	-	-	-	−1.97%	−1.07%	−1.86%	−1.19%
08	−1.74%	−0.28%	−1.55%	−0.47%	−3.89%	0.21%	−3.35%	−0.33%	-	-	-	-	−2.64%	−0.23%	−2.33%	−0.55%
09	−0.95%	−0.26%	−0.86%	−0.35%	−4.03%	−0.81%	−3.61%	−1.24%	-	-	-	-	−2.15%	−0.56%	−1.94%	−0.77%
10	−2.03%	−0.35%	−1.81%	−0.57%	−2.89%	0.13%	−2.49%	−0.27%	-	-	-	-	−2.19%	−0.38%	−1.95%	−0.62%
All Weasel	−0.82%	−0.37%	−0.76%	−0.43%	−2.98%	−1.84%	−2.85%	−1.98%	-	-	-	-	−1.86%	−1.14%	−1.77%	−1.22%
11	−0.09%	0.06%	−0.07%	0.04%	0.63%	1.17%	0.71%	1.10%	−2.05%	−1.62%	−2.00%	−1.67%	−0.10%	0.01%	−0.08%	0.00%
12	−0.48%	−0.40%	−0.47%	−0.41%	−0.05%	0.57%	0.04%	0.49%	−1.58%	−1.22%	−1.54%	−1.27%	−0.48%	−0.33%	−0.46%	−0.35%
13	−0.69%	−0.22%	−0.63%	−0.28%	−2.84%	−0.61%	−2.54%	−0.90%	−4.25%	−1.61%	−3.90%	−1.96%	−1.62%	−0.63%	−1.49%	−0.76%
All Karis	−0.40%	−0.20%	−0.37%	−0.22%	−0.68%	0.34%	−0.55%	0.21%	−2.51%	−1.60%	−2.39%	−1.71%	−0.73%	−0.31%	−0.68%	−0.36%

A.3 ESRM

Table A.11: DoE AGV type parameter set for ESRM Validation. pd:preDock, act:active

ID	v	$P_{\mathrm{c}}^{\mathrm{act}}$	$P_{\mathrm{c}}^{\mathrm{stby}}$	$P_{\mathrm{d}}^{\mathrm{act}}$	$P_{\mathrm{d}}^{\mathrm{stby}}$	$P_{\mathrm{LHD}}^{\mathrm{act}}$	$P_{\mathrm{LHD}}^{\mathrm{stby}}$	t_{lh}	t_{pd}	$c_{\mathrm{r}}^{\mathrm{I}}$	$c_{\mathrm{r}}^{\mathrm{O}}$
	[m/s]	[W]						[s]		[1/h]	
1	0.69	63.5	31.6	1498.5	192.3	1394.1	203.9	20.7	9.6	0.5	5
2	1.13	286	124.7	933.5	167.3	1361.7	239.1	17.5	7.2	0.35	3.5
3	0.73	8.1	1	1179	60.5	628.5	56.3	28.8	6.3	0.8	8
4	0.39	124	3.9	84	3.4	1313.1	50.7	6.7	8	0.75	7.5
5	1.04	185.7	59.1	1021.2	96.9	655.6	56.2	1.5	1.2	0.95	9.5
6	1.16	22.7	2.4	283.5	43.2	45.9	4.7	21.8	9.3	0.75	7.5
7	0.97	475.9	219.2	663.3	19.6	747.5	13.9	20.1	2.1	0.85	8.5
8	1.11	366.8	98.9	1283.3	181.1	896.9	27.6	6.4	7.8	0.25	2.5
9	0.65	333.2	140.7	479.6	56.4	384.5	49.8	4.9	1.1	0.7	7
10	0.57	291.7	68.5	758.6	41	1219.7	222.8	15.3	2.7	0.15	1.5
11	1.91	236.6	93.3	634.9	41.1	729.9	10	2.1	1.5	0.95	9.5
12	0.79	362.6	21.4	1442.9	236.3	811.1	71.6	24.2	4.9	0.3	3
13	1.86	160.3	53.2	613.7	50.3	1000.2	157.5	19.9	8.4	0.45	4.5
14	1.89	31.8	1.1	369.9	24.7	1295.2	107.4	7.6	7.9	0.6	6
15	1.22	88.2	29.2	454.1	51.8	268.2	25.6	12	6.1	0.9	9
16	1.08	351.3	89.4	1067.5	128.3	1495.8	216.4	9.4	5.6	0.15	1.5
17	1.94	194	23.7	728.9	25.2	609.2	77.7	9.1	5.7	0.6	6
18	1.43	390.6	76.4	1098.4	158.2	847.3	36.3	14.9	8.7	0.35	3.5
19	0.86	166.5	29.8	111.8	22	911.8	170.3	7	5.9	0.8	8
20	0.76	111.3	3.8	1260.9	229.6	703.4	121.1	29.7	9.8	0.65	6.5

Continued on next page

Table A.11 – Continued from previous page

ID	v	$P_{\mathrm{c}}^{\mathrm{act}}$	$P_{\mathrm{c}}^{\mathrm{stby}}$	$P_{\mathrm{d}}^{\mathrm{act}}$	$P_{\mathrm{d}}^{\mathrm{stby}}$	$P_{\mathrm{LHD}}^{\mathrm{act}}$	$P_{\mathrm{LHD}}^{\mathrm{stby}}$	t_{lh}	t_{pd}	$c_{\mathrm{r}}^{\mathrm{I}}$	$c_{\mathrm{r}}^{\mathrm{O}}$
21	1.4	172.5	22.5	466.2	80.5	436.6	85.5	12.2	7.6	0.25	2.5
22	0.42	298.9	11.9	38.2	1.3	1020.7	25.8	25	8.9	0.4	4
23	1.83	261.5	3.2	1159	55.3	1142.7	3.9	28.6	2.3	0.9	9
24	1.02	42.8	19.2	521.8	9.9	517.4	55	5.5	4.7	0.95	9.5
25	1.38	271.8	0.8	13.9	1.3	225.3	17.7	13.1	8.3	0.6	6
26	1.21	199.4	61.8	219.7	34.2	482.2	4.1	7.4	4.3	0.15	1.5
27	0.99	75.9	19.3	1347.3	226.1	576.5	72	11	8.1	0.3	3
28	1.32	385.6	116.9	1001.2	190.8	1077.8	148.8	1	9.2	0.5	5
29	1.36	95.9	43.5	349	36.7	140.8	17.1	18	2	0.85	8.5
30	0.63	302.7	125.5	821	12.4	686.3	79.8	15.8	7.5	0.4	4
31	1.77	130.8	6.6	1133.3	70.4	1124.8	159.2	18.2	2.3	0.85	8.5
32	0.9	428.8	87.1	1464.3	5.2	1053.4	58.1	25.5	1.9	0.3	3
33	0.83	437.9	57.2	567.1	7	65.4	3.9	19.4	9.7	0.8	8
34	1.64	310	155.3	1206.8	89.4	123.5	4	26.8	1.3	0.25	2.5
35	1.25	241.6	116.9	226.6	0.7	951.3	180.6	10.2	3.2	0.55	5.5
36	0.37	340.6	63	804.5	20.2	466.1	84	21.6	2.7	0.6	6
37	0.7	205.1	87.2	1359.2	156.1	213	20	18.5	9.1	0.55	5.5
38	1.97	451.5	215.4	1400.5	207.3	311.2	14.2	12.7	4.6	0.25	2.5
39	1.74	140.3	30.5	854.6	107.4	1045.4	157.6	5.9	9.4	0.2	2
40	1.28	470	24.1	873.4	38.2	426.4	71	16.1	9.9	0.85	8.5
41	1.49	250.9	93.9	1237.3	137.2	362.1	72.1	27.8	1.7	0.75	7.5
42	0.52	279.9	102.6	1434	283.3	594.9	67.2	22.9	4	0.55	5.5
43	0.35	399.9	158.2	1199.5	202.3	1189.2	184.2	23.4	1.4	0.15	1.5
44	0.56	97.6	34.8	1317.6	130.3	1376.4	29.4	23.1	3.3	0.65	6.5

Continued on next page

Table A.11 – Continued from previous page

ID	v	$P_{\mathrm{c}}^{\mathrm{act}}$	$P_{\mathrm{c}}^{\mathrm{stby}}$	$P_{\mathrm{d}}^{\mathrm{act}}$	$P_{\mathrm{d}}^{\mathrm{stby}}$	$P_{\mathrm{LHD}}^{\mathrm{act}}$	$P_{\mathrm{LHD}}^{\mathrm{stby}}$	t_{lh}	t_{pd}	$c_{\mathrm{r}}^{\mathrm{I}}$	$c_{\mathrm{r}}^{\mathrm{O}}$
45	1.63	434.9	33.4	595.3	79.6	1435.6	193	11.4	8.5	0.55	5.5
46	0.95	226.5	79.4	1384.9	130.4	789	134.9	4.3	6.9	1	10
47	0.59	48.6	14	1051.7	107	535.5	85.9	26.1	2.5	0.45	4.5
48	0.92	321.1	52.6	1306.8	241.6	189	0.6	3.3	2.9	0.7	7
49	0.47	175.5	79.8	965.1	131.6	109.7	4.1	8.7	7.2	0.4	4
50	0.43	325.9	33	907.7	97.1	1344.8	93.8	10.7	4.7	1	10
51	1.3	376.4	177.6	710.9	6.9	875.3	143.9	3.5	5.2	0.35	3.5
52	0.78	446.1	130.4	899.8	64.3	974.6	25.3	24.3	5	0.2	2
53	0.47	36.8	9.4	149.4	11.8	1465.2	143.5	13.5	4.4	0.8	8
54	1.66	353.1	59.9	180.5	10.7	560.6	38.2	2.3	3.8	0.9	9
55	1.8	252.7	86.2	676.9	60.8	165	12.1	8.1	3.6	0.45	4.5
56	0.51	480.1	51.1	298.4	12.6	1275.1	68.7	16.7	3.5	0.3	3
57	1.55	58.5	9.1	1094.2	30.2	393.4	47.3	26.4	6.5	0.35	3.5
58	1.18	406	120.7	315.9	23.9	78	15.1	2.9	7.3	0.1	1
59	1.47	133.7	51.4	69.9	13.2	1248.5	95.8	24.6	8.7	0.5	5
60	1.59	153.2	29.3	562.1	90.7	1107.9	67.2	27.3	2.9	0.2	2
61	1.53	74.5	11.9	504.5	43.7	926.9	142.9	21.3	5.5	0.9	9
62	1.7	221.5	20.4	260.9	14.7	770.6	81	29.5	6.7	0.5	5
63	1.57	409.3	45.7	378.7	2.6	1160.6	59.2	28.3	3.9	0.45	4.5
64	1.48	13.9	4.5	738.5	128.9	1224.2	133.5	22.2	7	0.7	7
65	1.06	417.8	170.4	973	127.1	344.3	63.7	4.2	4.2	0.65	6.5
66	1.99	216.1	48.2	416.3	80.9	819.6	52.6	18.8	5.4	0.4	4
67	0.32	486.4	68.8	161.1	25.7	288.8	13.6	14.1	5.8	0.65	6.5
68	1.72	461	166.9	785.1	109.3	26.9	0.4	16.9	3.3	0.7	7

Continued on next page

Table A.11 – Continued from previous page

ID	v	$P_{\mathrm{c}}^{\mathrm{act}}$	$P_{\mathrm{c}}^{\mathrm{stby}}$	$P_{\mathrm{d}}^{\mathrm{act}}$	$P_{\mathrm{d}}^{\mathrm{stby}}$	$P_{\mathrm{LHD}}^{\mathrm{act}}$	$P_{\mathrm{LHD}}^{\mathrm{stby}}$	t_{lh}	t_{pd}	$c_{\mathrm{r}}^{\mathrm{I}}$	$c_{\mathrm{r}}^{\mathrm{O}}$
69	1.85	495.4	130.3	128.2	2.9	1441.2	189.8	10	6.3	0.75	7.5
70	0.86	104.3	24.3	396.5	59.2	256.3	4	14.4	6.6	0.1	1

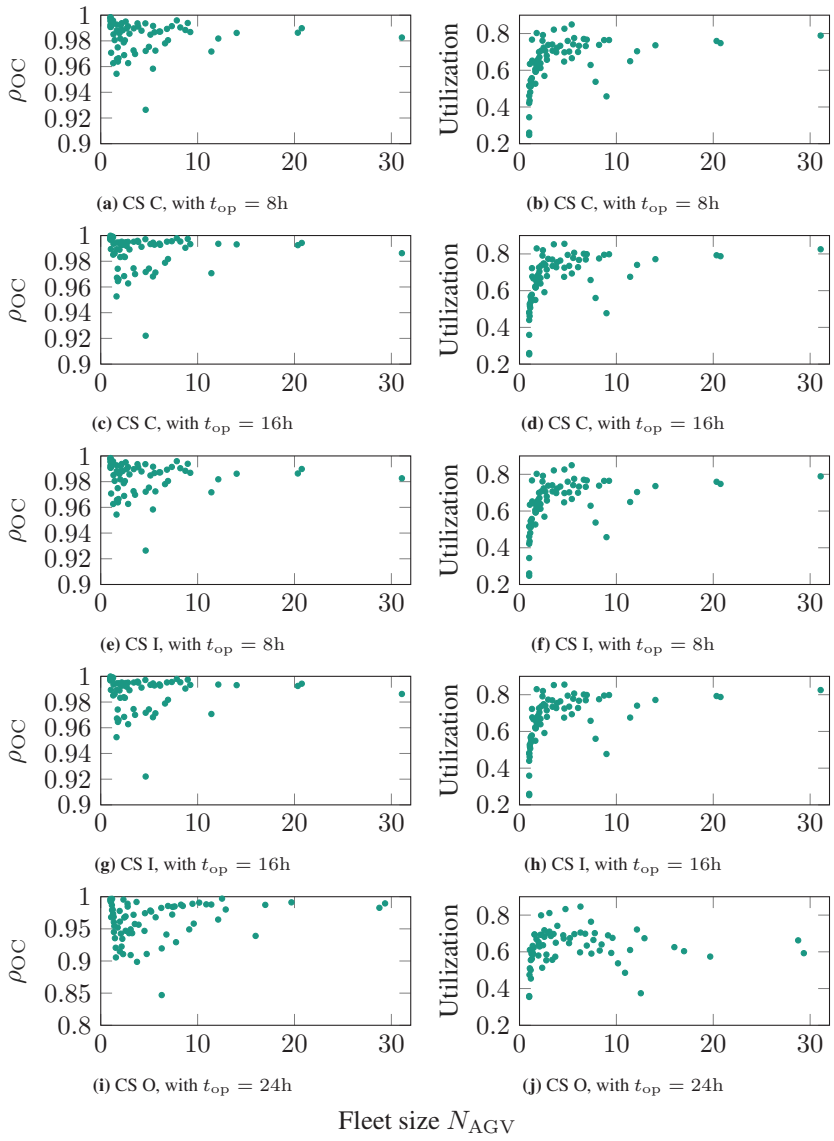

(a) CS C, with $t_{op} = 8h$ **(b)** CS C, with $t_{op} = 8h$

(c) CS C, with $t_{op} = 16h$ **(d)** CS C, with $t_{op} = 16h$

(e) CS I, with $t_{op} = 8h$ **(f)** CS I, with $t_{op} = 8h$

(g) CS I, with $t_{op} = 16h$ **(h)** CS I, with $t_{op} = 16h$

(i) CS O, with $t_{op} = 24h$ **(j)** CS O, with $t_{op} = 24h$

Figure A.3: Fleet size model analysis with linear data interpolation for different CS, analysis based on Eq. 5.49

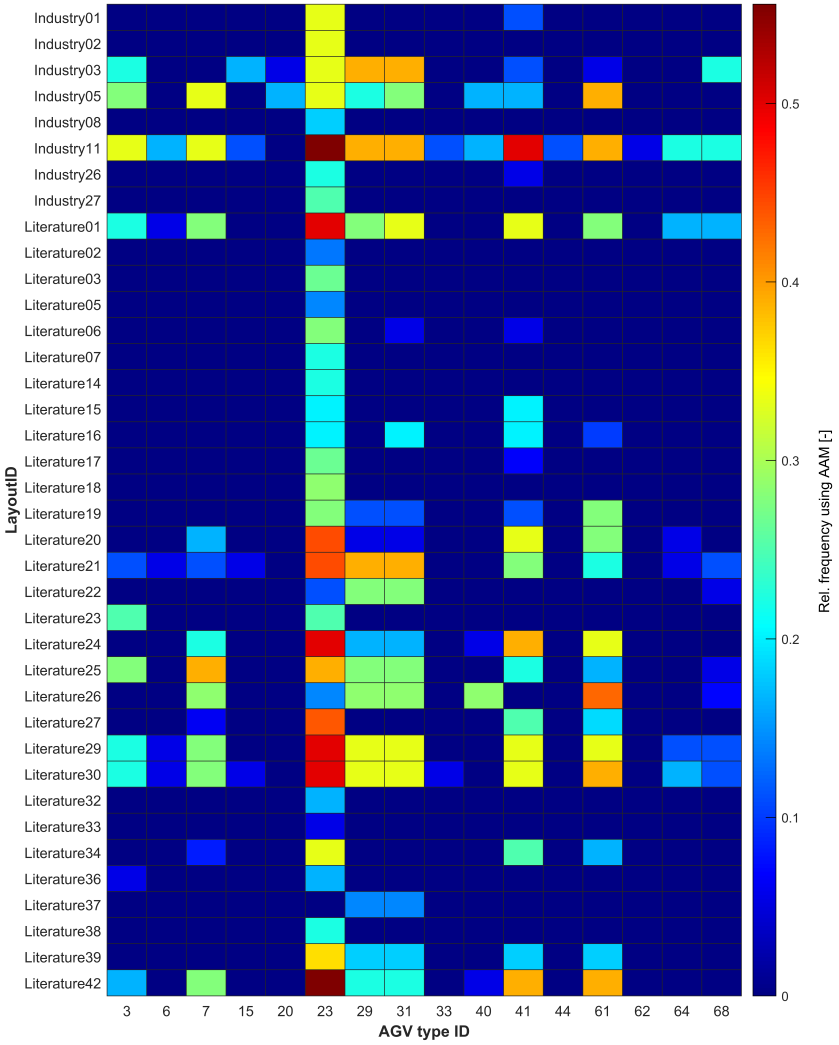

Figure A.4: Relative frequency of using AAM for CS I with $t_{\mathrm{op}} = 16\mathrm{h}$, analysis based on Equation 5.47

Table A.12: One-tailed z_{CI} -values for standard normal distribution

z_{CI}	.00	.01	.02	.03	.04	.05	.06	.07	.08	.09
0.0	.50000	.50399	.50798	.51197	.51595	.51994	.52392	.52790	.53188	.53586
0.1	.53983	.54380	.54776	.55172	.55567	.55962	.56356	.56749	.57142	.57535
0.2	.57926	.58317	.58706	.59095	.59483	.59871	.60257	.60642	.61026	.61409
0.3	.61791	.62172	.62552	.62930	.63307	.63683	.64058	.64431	.64803	.65173
0.4	.65542	.65910	.66276	.66640	.67003	.67364	.67724	.68082	.68439	.68793
0.5	.69146	.69497	.69847	.70194	.70540	.70884	.71226	.71566	.71904	.72240
0.6	.72575	.72907	.73237	.73565	.73891	.74215	.74537	.74857	.75175	.75490
0.7	.75804	.76115	.76424	.76730	.77035	.77337	.77637	.77935	.78230	.78524
0.8	.78814	.79103	.79389	.79673	.79955	.80234	.80511	.80785	.81057	.81327
0.9	.81594	.81859	.82121	.82381	.82639	.82894	.83147	.83398	.83646	.83891
1.0	.84134	.84375	.84614	.84849	.85083	.85314	.85543	.85769	.85993	.86214
1.1	.86433	.86650	.86864	.87076	.87286	.87493	.87698	.87900	.88100	.88298
1.2	.88493	.88686	.88877	.89065	.89251	.89435	.89617	.89796	.89973	.90147
1.3	.90320	.90490	.90658	.90824	.90988	.91149	.91309	.91466	.91621	.91774
1.4	.91924	.92073	.92220	.92364	.92507	.92647	.92785	.92922	.93056	.93189
1.5	.93319	.93448	.93574	.93699	.93822	.93943	.94062	.94179	.94295	.94408
1.6	.94520	.94630	.94738	.94845	.94950	.95053	.95154	.95254	.95352	.95449
1.7	.95543	.95637	.95728	.95818	.95907	.95994	.96080	.96164	.96246	.96327
1.8	.96407	.96485	.96562	.96638	.96712	.96784	.96856	.96926	.96995	.97062
1.9	.97128	.97193	.97257	.97320	.97381	.97441	.97500	.97558	.97615	.97670
2.0	.97725	.97778	.97831	.97882	.97932	.97982	.98030	.98077	.98124	.98169
2.1	.98214	.98257	.98300	.98341	.98382	.98422	.98461	.98500	.98537	.98574
2.2	.98610	.98645	.98679	.98713	.98745	.98778	.98809	.98840	.98870	.98899
2.3	.98928	.98956	.98983	.99010	.99036	.99061	.99086	.99111	.99134	.99158
2.4	.99180	.99202	.99224	.99245	.99266	.99286	.99305	.99324	.99343	.99361
2.5	.99379	.99396	.99413	.99430	.99446	.99461	.99477	.99492	.99506	.99520
2.6	.99534	.99547	.99560	.99573	.99585	.99598	.99609	.99621	.99632	.99643
2.7	.99653	.99664	.99674	.99683	.99693	.99702	.99711	.99720	.99728	.99736
2.8	.99744	.99752	.99760	.99767	.99774	.99781	.99788	.99795	.99801	.99807
2.9	.99813	.99819	.99825	.99831	.99836	.99841	.99846	.99851	.99856	.99861
3.0	.99865	.99869	.99874	.99878	.99882	.99886	.99889	.99893	.99896	.99900
3.1	.99903	.99906	.99910	.99913	.99916	.99918	.99921	.99924	.99926	.99929
3.2	.99931	.99934	.99936	.99938	.99940	.99942	.99944	.99946	.99948	.99950
3.3	.99952	.99953	.99955	.99957	.99958	.99960	.99961	.99962	.99964	.99965
3.4	.99966	.99968	.99969	.99970	.99971	.99972	.99973	.99974	.99975	.99976
3.5	.99977	.99978	.99978	.99979	.99980	.99981	.99981	.99982	.99983	.99983
3.6	.99984	.99985	.99985	.99986	.99986	.99987	.99987	.99988	.99988	.99989
3.7	.99989	.99990	.99990	.99990	.99991	.99991	.99992	.99992	.99992	.99992
3.8	.99993	.99993	.99993	.99994	.99994	.99994	.99994	.99995	.99995	.99995
3.9	.99995	.99995	.99996	.99996	.99996	.99996	.99996	.99996	.99997	.99997
3.8	.99993	.99993	.99993	.99994	.99994	.99994	.99994	.99995	.99995	.99995
3.9	.99995	.99995	.99996	.99996	.99996	.99996	.99996	.99996	.99997	.99997

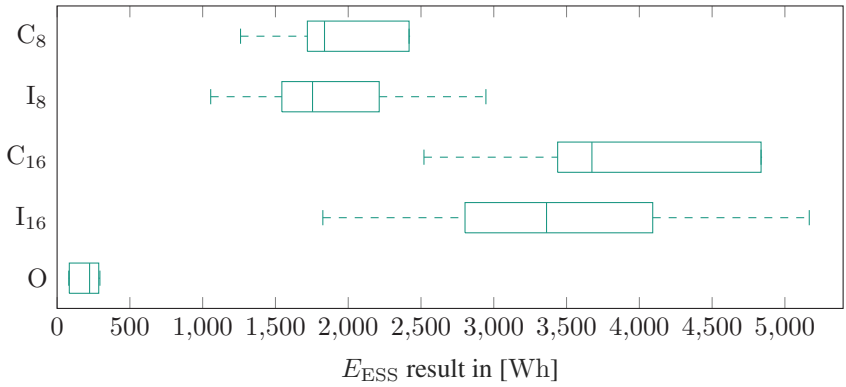

Figure A.5: Comparison of total ESR of the different CS, analysis based on Equation 5.47 with AGV type IDs 4, 6, 22, 25, 29 (cf. Appendix A.9)

List of Figures

List of Tables

List of Video Material

Agilox (2022). Agilox odm product demonstration. https://www.youtube.com/watch?v=6lzsqsnp04o. Online; accessed 03 January 2024.

BITO-Lagertechnik (2021). Fts leo - automatische übergabestationen. https://www.youtube.com/watch?v=hoeWz2ftIu8. Online; accessed 03 January 2024.

Bosch Rexroth (2020). Intralogistics solution with autonomous transport system and production assistants. https://www.youtube.com/watch?v=Y-m3YcmCAVg. Online; accessed 03 January 2024.

Carrybots GmbH (2022). Herbie: Das fahrerlose transportsystem (fts) der carrybots gmbh. https://www.youtube.com/watch?v=MqnBsURV6tY. Online; accessed 03 January 2024.

CLS servizi e soluzioni in movimento (2020). Agilox - intelligent guided vehicle. https://www.youtube.com/watch?v=F5DoflSjiWQ. Online; accessed 03 January 2024.

DS AUTOMOTION (2018). Sally automatisierte lastübergabe - automated load handling. https://www.youtube.com/watch?v=SqjsVQU5TXA. Online; accessed 03 January 2024.

Gebhardt Intralogistics Group (2021). Mobile verkettung von end-of-line solutions durch das gebhardt karis fts. https://www.youtube.com/watch?v=Z4adQ2YGQyo. Online; accessed 03 January 2024.

idealworks (2021). Anyfleet x iw.hub. https://www.youtube.com/watch?v=iu625kWJtUA. Online; accessed 03 January 2024.

Jungheinrich AG (2017). Fahrerlose transportsysteme von jungheinrich im einsatz bei bmw group. https://www.youtube.com/watch?v=4TInapyb3-8. Online; accessed 03 January 2024.

Jungheinrich AG (2021). Der automatisierte schlepper zur effizienten produktionsversorgung: Jungheinrich ezsa. https://www.youtube.com/watch?v=NBEKhpSZ7j4. Online; accessed 03 January 2024.

Jungheinrich AG (2023). Amr arculee s - jungheinrich autonoous mobile robots. https://www.youtube.com/watch?v=ShJPbAe6Vu8&list=PLq4j2kMTCkn0jzxcpsBToOurZol8IDMwL. Online; accessed 03 January 2024.

K. Hartwall (2021). A-mate mobile robot. https://www.youtube.com/watch?v=r_yMB66FCNA. Online; accessed 03 January 2024.

Linde Material Handling (2021). Two value-adding industrial trucks at full speed | linde material handling. https://www.youtube.com/watch?v=4fzakJh2MyY. Online; accessed 03 January 2024.

Milvus Robotics (2021). A fleet of seit500 autonomous mobile robots operating at unilver konya hpc factory. https://www.youtube.com/watch?v=4FKv-7OfK70. Online; accessed 03 January 2024.

Mobile Industrial Robots (2019). A fleet of mir200 robots boosts productivity at whirlpool. https://www.youtube.com/watch?v=hGOLQXaFCXQ. Online; accessed 03 January 2024.

mR MOBILE ROBOTS (2021). Autonomous intralogistics with mobile robots: Mir 250 with body for conveyor belt connection. https://www.youtube.com/watch?v=PDpJo00-a84. Online; accessed 03 January 2024.

Omron Industrial Automation EMEA (2021). Material handling solutions with autonomous mobile robots. https://www.youtube.com/watch?v=03ODgmLZTVU. Online; accessed 03 January 2024.

SAFELOG (2023). Mobile transport robot - safelog agv x1 tt. https://www.youtube.com/watch?v=sAPg9B-Ar2U. Online; accessed 03 January 2024.

SHERPA MOBILE ROBOTICS (2023). 2023 sherpa industrie caoutchouc. https://www.youtube.com/watch?v=-_HQAETfJUQ. Online; accessed 03 January 2024.

SSI Schäfer Benelux (2016). Agv-systeem weasel, productielogistiek bij bachmann forming ag. https://www.youtube.com/watch?v=UOScoyjt4oA. Online; accessed 03 January 2024.

SSI Schäfer D-A-CH (2016). Fahrerloses transportsystem weasel für hermes fulfilment gmbh: Ssi schäfer. https://www.youtube.com/watch?v=Qhp9BwxZT80. Online; accessed 03 January 2024.

STAPLERWORLD (2021). Grenzebach kompakt fts im messedemo-einsatz. https://www.youtube.com/watch?v=DGKbD4sETEo. Online; accessed 03 January 2024.

TÜNKERS Maschinenbau GmbH (2022). Tünkers stacker. https://www.youtube.com/watch?v=8oGxvqBVKs8. Online; accessed 03 January 2024.

W. Gessmann (2023). Gessbot gb 350 mit systemaufbau. https://www.youtube.com/watch?v=FlfVExG52C4. Online; accessed 03 January 2024.

List of Publications

Denkena, B., D. Arnold, and M. Sperling (2019). Perspektiven vernetzter systeme für die intralogistik. *Logistics Journal : nicht referierte Veröffentlichungen 2019*(10).

Enke, C., J.-F. Klein, M. Sperling, B. Zhou, and K. Furmans (2022). Development of an experimental environment to study the challenges in cyber-physical intralogistics systems [entwicklung einer versuchsumgebung zur untersuchung der herausforderungen in cyber-physischen intralogistiksystemen]. *Logistics Journal 2022*(18).

Eschenweck, R., M. Sperling, and M. Leunissen (2024). Hybrid energy storage solutions – das beste aus zwei welten. *Elektronik 73*(08), 23–27.

Kivelä, T., M. Sperling, M. Abdelawwad, M. Drabesch, M. Schwarz, J. Börcsök, and K. Furmans (2022). Development of a safe charging infrastructure system: Requirements, design, verification and validation. In *Smart Cities, Green Technologies, and Intelligent Transport Systems : 10th International Conference, SMARTGREENS 2021, and 7th International Conference, VEHITS 2021, Virtual Event, April 28–30, 2021, Revised Selected Papers. Ed.: C. Klein*, Volume 1612 of *Communications in Computer and Information Science*, pp. 412–434. Springer International Publishing.

Kivelä., T., M. Abdelawwad., M. Sperling., M. Drabesch., M. Schwarz., J. Börcsök., and K. Furmans. (2021). Functional safety and electric vehicle charging: Requirements analysis and design for a safe charging infrastructure system. In *Proceedings of the 7th International Conference on Vehicle Technology and Intelligent Transport Systems - VEHITS*, pp. 317–324. INSTICC: SciTePress.

Kivelä, T. and M. Sperling (2021). Sicheres ladeinfrastruktursystem für elektrofahrzeuge - silis; teilprojekt: Überwachung eines elektroauto-ladevorgangs mit vermeidung und erkennung externer ungewollter angriffe : Schlussbericht. Technical report, Karlsruher Institut für Technologie (KIT).

Sperling, M. and K. Furmans (2024). Energy requirement modeling for automated guided vehicles considering material flow and layout data. *Designs 8*(3).

Sperling, M. and T. Kivelä (2022). Concept of a dual energy storage system for sustainable energy supply of automated guided vehicles. *Energies 15*(2), 479.

Sperling, M., T. Kurschilgen, and P. Schumacher (2024). Concept of a peripheral-free electrified monorail system (pems) for flexible material handling in intralogistics. *Inventions 9*(3).

Sperling, M., B. Schulz, C. Enke, D. Giebels, and K. Furmans (2023). Classified agv material flow and layout data set for multidisciplinary investigation. *IEEE Access 11*, 94992–95007.

Bibliography

Abderrahim, M., A. Bekrar, D. Trentesaux, N. Aissani, and K. Bouamrane (2020). Manufacturing 4.0 operations scheduling with agv battery management constraints. *Energies 13*(18), 4948.

Aiello, G., M. Enea, and G. Galante (2002). An integrated approach to the facilities and material handling system design. *International Journal of Production Research 40*(15), 4007–4017.

Arbetter, B., R. Erickson, and D. Maksimovic (1995). Dc-dc converter design for battery-operated systems. In *Proceedings of PESC '95 - Power Electronics Specialist Conference*, pp. 103–109. IEEE.

Arnold, D. and K. Furmans (2019). *Materialfluss in Logistiksystemen*. Berlin, Heidelberg: Springer Berlin Heidelberg.

Asef-Vaziri, A. and G. Laporte (2005). Loop based facility planning and material handling. *European Journal of Operational Research 164*, 1–11.

Berlinger, M. (2021). *A Methodology to Model the Statistical Fracture Behavior of Acrylic Glasses for Stochastic Simulation*, Volume 59. Wiesbaden: Springer Fachmedien Wiesbaden.

Bozer, Y. A. and M. M. Srinivasan (1991). Tandem configurations for automated guided vehicle systems and the analysis of single vehicle loops. *IIE Transactions 23*(1), 72–82.

Bozer, Y. A. and M. M. Srinivasan (1992). Tandem agv systems: A partitioning algorithm and performance comparison with conventional agv systems. *European Journal of Operational Research 63*(2), 173–191.

Bruno, G., G. Ghiani, and G. Improta (2000). Dynamic positioning of idle automated guided vehicles. *Journal of Intelligent Manufacturing 11*(2), 209–215.

Cavazzuti, M. (2013). Design of experiments. In M. Cavazzuti (Ed.), *Optimization Methods*, pp. 13–42. Berlin, Heidelberg: Springer Berlin Heidelberg.

Cebrian, J. M. and L. Natvig (2013). Temperature effects on on-chip energy measurements. In *2013 International Green Computing Conference Proceedings*, pp. 1–6. IEEE.

Colling, D., J. Oehler, and K. Furmans (2019). Battery charging strategies for agv systems. *Logistics Journal 2019*, 1–8.

de Ryck, M., D. Pissoort, T. Holvoet, and E. Demeester (2021). Decentral task allocation for industrial agv-systems with resource constraints. *Journal of Manufacturing Systems 59*, 310–319.

de Ryck, M., D. Pissoort, T. Holvoet, and E. Demeester (2022). Decentral task allocation for industrial agv-systems with routing constraints. *Journal of Manufacturing Systems 62*, 135–144.

DeGroot, M. H. and M. J. Schervish (2012). *Probability and statistics* (4. ed. ed.). Boston, Mass.: Addison-Wesley.

Dehnavi-Arani, S., A. Sabaghian, and M. Fazli (2019). A job shop scheduling and location of battery charging storage for the automated guided vehicles (agvs). *Journal of Optimization in Industrial Engineering 12*(2), 121–129.

Devillers, N., S. Jemei, M.-C. Péra, D. Bienaimé, and F. Gustin (2014). Review of characterization methods for supercapacitor modelling. *Journal of Power Sources 246*, 596–608.

Dodge, Y. (2008). Anderson–darling test. In *The Concise Encyclopedia of Statistics*, pp. 12–14. New York, NY: Springer New York.

Ebben, M. (2001). *Logistic control in automated transportation networks*. Enschede: Twente Univ. Press.

Egbelu, P. J. (1993). Positioning of automated guided vehicles in a loop layout to improve response time. *European Journal of Operational Research 71*(1), 32–44.

Flake, S. (2003). *UML-based specification of state oriented real time properties: Zugl.: Paderborn, Univ., Diss, 2003*, Volume 16 of *C-LAB publication*. Aachen: Shaker.

Fottner, J., S. Galka, S. Habenicht, E. Klenk, I. Meinhardt, and T. Schmidt (2022). *Planung von innerbetrieblichen Transportsystemen*. Berlin, Heidelberg: Springer Berlin Heidelberg.

Fragapane, G., R. de Koster, F. Sgarbossa, and J. O. Strandhagen (2021). Planning and control of autonomous mobile robots for intralogistics: Literature review and research agenda. *European Journal of Operational Research 294*(2), 405–426.

Freis, J. and W. A. Günthner (2016). A systemic approach to analysing interactions and impacts of alternative design options on the total energy balance of distribution warehouses. *Logistics Journal Volume 2016*, 1–16.

Gao, Z., H. Xie, X. Yang, W. Niu, S. Li, and S. Chen (2022). The dilemma of c-rate and cycle life for lithium-ion batteries under low temperature fast charging. *Batteries 8*(11), 234.

Gen, M., W. Zhang, L. Lin, and Y. Yun (2017). Recent advances in hybrid evolutionary algorithms for multiobjective manufacturing scheduling. *Computers & Industrial Engineering 112*, 616–633.

Gourgand, M., X.-C. Sun, and N. Tchernev (1995). Choice of the guide path layout for an agv based material handling system. In *Proceedings 1995 INRIA/IEEE Symposium on Emerging Technologies and Factory Automation. ETFA'95*, pp. 475–483. IEEE Comput. Soc. Press.

Großeschallau, W. (1984). *Materialflußrechnung: Modelle und Verfahren zur Analyse und Berechnung von Materialflußsystemen: Zugl.: Dortmund, Univ.,*

Habil.-Schr. Logistik in Industrie, Handel und Dienstleistungen. Berlin and Heidelberg: Springer.

Hamdy, A. (2019). *Optimization of Automated Guided Vehicles (AGV) Fleet Size With Incorporation of Battery Management*. Ph. D. thesis, Old Dominion University Libraries.

Hanschek, A. J., Y. E. Bouvier, E. Jesacher, and P. J. Grbovic (2021). Analysis of power distribution systems based on low-voltage dc/dc power supplies for automated guided vehicles (agv). In *2021 21st International Symposium on Power Electronics (Ee)*, pp. 1–6. IEEE.

Horn, M., J. MacLeod, M. Liu, J. Webb, and N. Motta (2019). Supercapacitors: A new source of power for electric cars? *Economic Analysis and Policy Volume 61*(61), 93–103.

Hou, L., L. Zhang, and J. Kim (2019). Energy modeling and power measurement for mobile robots. *Energies 12*(1), 27.

Hu, X., Le Xu, X. Lin, and M. Pecht (2020). Battery lifetime prognostics. *Joule 4*(2), 310–346.

International Electrotechnical Commission (2013). Iec 62264-1:2013 enterprise-control system integration - part 1: Models and terminology.

Jodejko-Pietruczuk, A. and S. Werbinska-Wojciechowska (2021). Availability assessment for a multi-agv system based on simulation modeling approach. In *2021 International Conference on Electrical, Computer, Communications and Mechatronics Engineering (ICECCME)*, pp. 1–6. IEEE.

Jones, D. R., M. Schonlau, and W. J. Welch (1998). Efficient global optimization of expensive black-box functions. *Journal of Global Optimization 13*(4), 455–492.

Kabir, Q. S. and Y. Suzuki (2019). Comparative analysis of different routing heuristics for the battery management of automated guided vehicles. *International Journal of Production Research 57*(2), 624–641.

Kaspi, M., U. Kesselman, and J. M. A. Tanchoco (2002). Optimal solution for the flow path design problem of a balanced unidirectional agv system. *International Journal of Production Research 40*(2), 389–401.

Kaspi, M. and J. M. A. Tanchoco (1990). Optimal flow path design of unidirectional agv systems. *International Journal of Production Research 28*(6), 1023–1030.

Kim, C. H. and B. K. Kim (2007). Minimum-energy translational trajectory generation for differential-driven wheeled mobile robots. *Journal of Intelligent and Robotic Systems 49*(4), 367–383.

Kim, H. and B.-K. Kim (2008). Minimum-energy translational trajectory planning for battery-powered three-wheeled omni-directional mobile robots. In *2008 10th International Conference on Control, Automation, Robotics and Vision*, pp. 1730–1735. IEEE.

Komma, V. R., P. K. Jain, and N. K. Mehta (2012). Simulation of agv system – a multi agent approach. In B. Katalinic (Ed.), *DAAAM INTERNATIONAL SCIENTIFIC BOOK 2012*. DAAAM International Vienna.

Leuchter, J. and P. Bauer (2015). Capacity of power-batteries versus temperature. In *2015 17th European Conference on Power Electronics and Applications (EPE'15 ECCE-Europe)*, pp. 1–8. IEEE.

Liu, S. and D. Sun (2014). Minimizing energy consumption of wheeled mobile robots via optimal motion planning. *IEEE/ASME Transactions on Mechatronics 19*(2), 401–411.

Maxwell, W. L. and J. A. Muckstadt (1982). Design of automatic guided vehicle systems. *A I I E Transactions 14*(2), 114–124.

McHaney, R. (1995). Modelling battery constraints in discrete event automated guided vehicle simulations. *International Journal of Production Research 33*(11), 3023–3040.

Mei, Y., Y.-H. Lu, Y. C. Hu, and C. Lee (2006). Deployment of mobile robots with energy and timing constraints. *IEEE Transactions on Robotics 22*(3), 507–522.

Meißner, M. and L. Massalski (2020). Modeling the electrical power and energy consumption of automated guided vehicles to improve the energy efficiency of production systems. *The International Journal of Advanced Manufacturing Technology 110*(1-2), 481–498.

Müller, C. (2020). *World Robotics: Service Robots 2020*. Frankfurt am Main, Germany: IFR Statistical Department, VDMA Services GmbH.

Müller, C. (2021). *World Robotics: Service Robots 2021*. Frankfurt am Main, Germany: IFR Statistical Department, VDMA Services GmbH.

Müller, C. (2022). *World Robotics: Service Robots 2022*. Frankfurt am Main, Germany: IFR Statistical Department, VDMA Services GmbH.

Müller, C. (2023). *World Robotics: Service Robots 2023*. Frankfurt am Main, Germany: IFR Statistical Department, VDMA Services GmbH.

Müller, E., H. Hopf, and M. Krones (2013). Analyzing energy consumption for factory and logistics planning processes. In C. Emmanouilidis, M. Taisch, and D. Kiritsis (Eds.), *Advances in Production Management Systems. Competitive Manufacturing for Innovative Products and Services*, Volume 397 of *IFIP Advances in Information and Communication Technology*, pp. 49–56. Berlin, Heidelberg: Springer Berlin Heidelberg.

Niestrój, R., T. Rogala, and W. Skarka (2020). An energy consumption model for designing an agv energy storage system with a pemfc stack. *Energies 13*(13), 3435.

Pacheco, D. S., L. González, J. L. Espinoza, and C. Campoverde (2019). Energy consumption of an electric forklift truck: Alternative with fuel cell and supercapacitor. In *2019 IEEE International Autumn Meeting on Power, Electronics and Computing (ROPEC)*, pp. 1–6.

Plaue, M. (2023). *Data Science: An Introduction to Statistics and Machine Learning* (1st ed. 2023 ed.). Berlin, Heidelberg: Springer Berlin Heidelberg and Imprint Springer.

Qiu, L., J. Wang, W. Chen, and H. Wang (2015). Heterogeneous agv routing problem considering energy consumption. In *2015 IEEE International Conference on Robotics and Biomimetics (ROBIO)*, pp. 1894–1899. IEEE.

Quadrini, W., E. Negri, and L. Fumagalli (2020). Open interfaces for connecting automated guided vehicles to a fleet management system. *Procedia Manufacturing 42*, 406–413.

Rahimikelarijani, B., H. Fazlollahtabar, and S. Nayeri (2020). Multi-objective multi-load tandem autonomous guided vehicle for robust workload balance and material handling optimization. *SN Applied Sciences 2*(7), 1–11.

Rajotia, S., K. Shanker, and J. L. Batra (1998). Determination of optimal agv fleet size for an fms. *International Journal of Production Research 36*(5), 1177–1198.

Reddy, B. S. P. and C. S. P. Rao (2006). A hybrid multi-objective ga for simultaneous scheduling of machines and agvs in fms. *The International Journal of Advanced Manufacturing Technology 31*(5-6), 602–613.

Roy, D., R. de Koster, and R. Bekker (2020). Modeling and design of container terminal operations. *Operations Research 68*(3), 686–715.

Saldaña, G., J. I. San Martín, I. Zamora, F. J. Asensio, and O. Oñederra (2019). Analysis of the current electric battery models for electric vehicle simulation. *Energies 12*(14), 2750.

Salehipour, A. and M. M. Sepehri (2014). Optimal location of workstations in tandem automated-guided vehicle systems. *The International Journal of Advanced Manufacturing Technology 72*, 1429–1438.

Schiefer, H. and F. Schiefer (2021). *Statistics for engineers: An introduction with examples from practice*. Wiesbaden and Heidelberg: Springer.

Schrecker, A. (2000). *Planung und Steuerung Fahrerloser Transportsysteme*. Wiesbaden: Deutscher Universitätsverlag.

Singh, N., Q.-V. Dang, A. Akcay, I. Adan, and T. Martagan (2022). A matheuristic for agv scheduling with battery constraints. *European Journal of Operational Research 298*(3), 855–873.

Singh, N., P. V. Sarngadharan, and P. K. Pal (2011). Agv scheduling for automated material distribution: a case study. *Journal of Intelligent Manufacturing 22*(2), 219–228.

Sinriech, D., J. Tanchoco, and Y. T. Herer (1996). The segmented bidirectional single-loop topology for material flow systems. *IIE Transactions 28*(1), 40–54.

Sinriech, D. and J. M. A. Tanchoco (1993). Solution methods for the mathematical models of single-loop agv systems. *International Journal of Production Research 31*(3), 705–725.

Sinriech, D. and J. M. A. Tanchoco (1994). Sft — segmented flow topology. In J. M. A. Tanchoco (Ed.), *Material Flow Systems in Manufacturing*, pp. 200–235. Boston, MA: Springer US.

Sinriech, D. and J. M. A. Tanchoco (1995). An introduction to the segmented flow approach for discrete material flow systems. *International Journal of Production Research 33*(12), 3381–3410.

Srinivasan, M. M., Y. A. Bozer, and M. Cho (1994). Trip-based material handling systems: Throughput capacity analysis. *IIE Transactions 26*(1), 70–89.

Stampa, M., C. Rohrig, F. Kunemund, and D. Hes (2015). Estimation of energy consumption on arbitrary trajectories of an omnidirectional automated guided vehicle. In *2015 IEEE 8th International Conference on Intelligent Data Acquisition and Advanced Computing Systems: Technology and Applications (IDAACS)*, pp. 873–878. IEEE.

Stroe, A.-I., D.-L. Stroe, V. Knap, M. Swierczynski, and R. Teodorescu (2018). Accelerated lifetime testing of high power lithium titanate oxide batteries. In

2018 IEEE Energy Conversion Congress and Exposition (ECCE), pp. 3857–3863. IEEE.

The MathWorks Inc. (2024a). lhsdesign – latin hypercube sample. `https://de.mathworks.com/help/stats/lhsdesign.html`. Online; accessed 03 January 2024.

The MathWorks Inc. (2024b). polyfit - polynomiale kurvenanpassung. `https://de.mathworks.com/help/matlab/ref/polyfit.html`. Online; accessed 03 January 2024.

Ullrich, G. and T. Albrecht (2023). *Automated Guided Vehicle Systems*. Wiesbaden: Springer Fachmedien Wiesbaden.

Uttendorf, S. and L. Overmeyer (2015). Fuzzy-enhanced path-finding algorithm for agv roadmaps. In *Proceedings of the 2015 Conference of the International Fuzzy Systems Association and the European Society for Fuzzy Logic and Technology*, Advances in Intelligent Systems Research. Atlantis PressParis, France.

VDI Society Production and Logistics (2000). Compatibility of automated guided vehicle systems (agvs) - power supply and charging technology.

VDI Society Production and Logistics (2022). Automated guided vehicle systems (agvs) - power supply and charging technology.

Ventura, J. A., S. Pazhani, and A. Mendoza (2015). Finding optimal dwell points for automated guided vehicles in general guide-path layouts. *International Journal of Production Economics 170*, 850–861.

Ventura, J. A. and B. Q. Rieksts (2009). Optimal location of dwell points in a single loop agv system with time restrictions on vehicle availability. *European Journal of Operational Research 192*(1), 93–104.

Vidal, C., O. Gross, R. Gu, P. Kollmeyer, and A. Emadi (2019). xev li-ion battery low-temperature effects—review. *IEEE Transactions on Vehicular Technology 68*(5), 4560–4572.

Vivaldini, K. C. T., L. F. Rocha, M. Becker, and A. P. Moreira (2015). Comprehensive review of the dispatching, scheduling and routing of agvs. In A. P. Moreira, A. Matos, and G. Veiga (Eds.), *CONTROLO'2014 – Proceedings of the 11th Portuguese Conference on Automatic Control*, Volume 321 of *Lecture Notes in Electrical Engineering*, pp. 505–514. Cham: Springer International Publishing.

Wood, E., M. Alexander, and T. H. Bradley (2011). Investigation of battery end-of-life conditions for plug-in hybrid electric vehicles. *Journal of Power Sources 196*(11), 5147–5154.

Xu, C., Q. Dai, L. Gaines, M. Hu, A. Tukker, and B. Steubing (2020). Future material demand for automotive lithium-based batteries. *Communications Materials 1*(1), 1–10.

Yan, R., S. J. Dunnett, and L. M. Jackson (2022). Model-based research for aiding decision-making during the design and operation of multi-load automated guided vehicle systems. *Reliability Engineering & System Safety 219*, 108264.

Yang, H. (2020). Effects of aging and temperature on supercapacitor charge capacity. In *2020 IEEE Power & Energy Society General Meeting (PESGM)*, pp. 1–5. IEEE.

Yang, X.-G. and C.-Y. Wang (2018). Understanding the trilemma of fast charging, energy density and cycle life of lithium-ion batteries. *Journal of Power Sources 402*, 489–498.

Yao, Y., T. van Woensel, L. P. Veelenturf, and P. Mo (2021). The consistent vehicle routing problem considering path consistency in a road network. *Transportation Research Part B: Methodological 153*, 21–44.

Yu, W. and P. J. Egbelu (2001). Design of a variable path tandem layout for automated guided vehicle systems. *Journal of Manufacturing Systems 20*(5), 305–319.

Zamiri Marvizadeh, S. and F. F. Choobineh (2014). Entropy-based dispatching for automatic guided vehicles. *International Journal of Production Research 52*(11), 3303–3316.

Zhai, N., Y. Yao, D. Zhang, and D. Xu (2006). Design and optimization for a supercapacitor application system. In *2006 International Conference on Power System Technology*, pp. 1–4. IEEE.

Zhan, X., L. Xu, J. Zhang, and A. Li (2019). Study on agvs battery charging strategy for improving utilization. *Procedia CIRP 81*, 558–563.

Zhang, Z., J. Chen, W. Zhao, and Q. Guo (2021). A least-energy-cost agvs scheduling for rasterized warehouse environments. In *2021 IEEE International Conference on Systems, Man, and Cybernetics (SMC)*, pp. 2888–2893. IEEE.

Zou, B., R. de Koster, Y. Gong, X. Xu, and G. Shen (2021). Robotic sorting systems: Performance estimation and operating policies analysis. *Transportation Science 55*(6), 1430–1455.